CORA Cork Open Research Archive
Cartlann Taighde Oscailte Chorcaí

Title	Feasibility study of reusing concrete gravity-based foundations designed for tidal energy converters
Authors	Dineen, Kate
Publication date	2022
Original Citation	Dineen, K. 2022. Feasibility study of reusing concrete gravity-based foundations designed for tidal energy converters. MSc Thesis, University College Cork.
Type of publication	Masters thesis (Research)
Rights	© 2022, Kate Dineen. - https://creativecommons.org/licenses/by-nc-nd/4.0/
Download date	2026-11-02 17:34:37
Item downloaded from	https://hdl.handle.net/10468/14499



UCC
University College Cork, Ireland
Coláiste na hOllscoile Corcaigh

Ollscoil na hÉireann, Corcaigh

National University of Ireland, Cork



Feasibility Study of Reusing Concrete Gravity-Based Foundations Designed for Tidal Energy Converters

Thesis presented by

Kate Dineen, BE(Civil)

for the degree of

Master of Engineering Science (Civil)

University College Cork

School of Engineering

Head of School/Department: Prof Jorge Oliveira

Supervisors: Dr Zili Li & Dr Paraic Ryan

2022

Table of Contents

Table of Figures iv
Table of Tables vi
Declaration vii
Acknowledgements viii
Abstract ix
1. Introduction 2
1.1 Background 2
1.2 Research Aims and Objectives 3
1.3 Thesis Layout 4
2. Literature Review 7
2.1 Background 7
2.2 Gravity-Based Foundations 9
2.3 Tidal Turbine Projects 10
2.4 Novel Concrete Gravity-Based Foundation Concepts 12
2.5 Decommissioning of Offshore Concrete Structures 17
2.6 Geotechnical Hazards 19
2.7 Concrete Degradation in Marine Environments 21
2.8 Conclusion 24
3. Design of Concrete Gravity-Based Foundation 26
3.1 Design Guidance 26
3.2 Design and Analysis Tools 30
3.2.1 DTOcean 30
3.2.2 Selkie's Foundation and Mooring Decision Support Model 31
3.3 Finalised Gravity-Based Foundation Design 38
4. Barrier 1: Geotechnical Hazards 41
4.1 Methodology 41
4.1.1 Case 1 41
4.1.2 Case 2 44
4.2 Results 47
4.2.1 Short Term Settlement 55
4.2.2 Long Term Settlement 60
4.3 Discussion 64
5. Barrier 2: Degradation of GBF 69
5.1 Chloride Ingress 70

5.1.1 Methodology 71
5.1.2 Results and Discussion 75
5.2 Oxygen Availability and Water Saturation Degree 79
5.2.1 Oxygen Transport 79
5.2.2 Oxygen Availability as a Function of Water Saturation Degree 80
5.2.3 Concrete Drying Models 81
5.2.4 Summary 83
6. Conclusions 86
6.1 Introduction 86
6.2 Conclusions from Geotechnical Analysis 86
6.3 Conclusions from Concrete Degradation Analysis 87
6.4 Overall Recommendations and Future Work 88
References 91
Appendices 108
Appendix A 109
Appendix B 111
Appendix C 113
Appendix D 115
Appendix E 121
Project dimensions 121
Soils mode 121
Structures mode 124
Mesh mode 126
Staged construction mode 127
Appendix F 130

Table of Figures

Figure 2-1: The primary categories of tidal energy converters: (a) horizontal axis turbine, (b) vertical axis turbine, (c) oscillating hydrofoils, (d) ducted turbine or enclosed tips (e) Archimedes screw (f) tidal kite. Source: (Nachtane et al., 2020) 8
Figure 2-2: AR1500 tidal turbine supported on a steel tripod gravity-based foundation installed during the MeyGen project (Phase 1A). Source: (Rajgor, 2016) 10
Figure 2-3: Sabella's tidal turbine supported on a steel tripod gravity-based structure. Source: (Slama et al., 2021) 11
Figure 2-4: The evolution of concrete gravity-based foundations. Source: (Esteban et al., 2015) 13
Figure 2-5: The ballasting process of a novel concrete GBF. Source: (Esteban et al., 2015) 14
Figure 2-6: BAMs concrete GBFs prior to installation on Blyth wind farm. Source: (Esteban et al., 2015) 15
Figure 2-7: Left: Vici Ventus concrete GBF concept. Source: (Mathern, von der Haar and Marx, 2021). Right: Seatower cranefree concrete GBF concept. Source: (Esteban, López-Gutiérrez and Negro, 2019) 15
Figure 2-8: Stages of steel corrosion in concrete where t_0 is the time at which corrosion initiates due to the chloride ion concentration at the steel surface surpassing the critical chrloide concentration threshold . Source:(Xia et al., 2019) 22
Figure 3-1: Direction of load and moment acting on the centre of the foundation (generated in Plaxis 3D geotechnical software) 35
Figure 3-2: Gravity-based foundation dimensions (drawing created in AutoCAD) 38
Figure 4-1: Case 1 Plaxis 3D model 42
Figure 4-2: Case 2 Plaxis 3D model 45
Figure 4-3: Cross section A-A* 47
Figure 4-4: Vertical displacements under cross section A-A* for Case 1 sandy soil model 48
Figure 4-5: Vertical displacements under cross section A-A* for Case 2 clayey soil model 49
Figure 4-6: Excess pore water pressure under cross section A-A* for Case 2 (clay) 52
Figure 4-7: Plan view of model with the reference points labelled 53
Figure 4-8: Case 1 settlement vs time 54
Figure 4-9: Case 2 settlement vs time 54
Figure 4-10: Case 1 (sand) short term settlement-time curve 56
Figure 4-11: Case 2 (clay) short term settlement-time curve 57
Figure 4-12: Case 1 (sand). Phase 2: Activate loads settlement-time curve 58
Figure 4-13: Case 2 (clay). Phase 3: Activate loads settlement-time curve 59
Figure 4-14: Case 1 (sand). Phases 3-7 settlement-time curve 61
Figure 4-15: Case 2 (clay). Phases 4-8 settlement-time curve 61
Figure 4-16: Bar chart displaying the differential settlement results associated with increased turbine loads to determine at what load level would the tilt threshold become unsatisfactory 64

Figure 5-1: The varying concentrations of contaminants in the concrete over the life cycle of the GBF 70
Figure 5-2: Chloride concentration profiles comparing three sets of long-term exposure chloride ingress parameters after 25 years. These profiles were developed in MATLAB using Fick's second law of diffusion. 77
Figure 5-3: Chloride concentration profiles comparing three sets of long-term exposure chloride ingress parameters after 25 years with modified parameters to account for water pressure 78
Figure A-1: Project properties window 121
Figure A-2: Modify soil layers window 122
Figure A-3: Sand_1 general soil properties 122
Figure A-4: Sand_1 parameters 123
Figure A-5: Sand_1 groundwater properties 123
Figure A-6: Polycurve shape designer 124
Figure A-7: Plate properties 125
Figure A-8: Load settings 125
Figure A-9: Finalised Plaxis 3D model 126
Figure A-10: Finite element mesh settings 126
Figure A-11: Finalised mesh model (pre-calculation) 127
Figure A-12: Calculation phases 128
Figure A-13: Phase 1 - Activate foundation phase settings 128
Figure A-14: Phase 3 - Year 1-5 phase settings 129

Table of Tables

Table 3-1: Guidelines, specifications, and standards referred to for the concrete gravity-based foundation design 27
Table 3-2: Target safety levels for the certification of tidal energy converters (DNV-OSS-312, 2008; DNVGL-ST-0164, 2015) 29
Table 3-3: Geotechnical parameters used for representative GBF design 33
Table 3-4: Input parameters for GBF sizing calculations 34
Table 3-5: Gravity-based foundation characteristics 39
Table 4-1: Calculation phases as specified in staged construction mode for Case 1 model analysis 43
Table 4-2: Case 2 geotechnical parameters 44
Table 4-3: Calculation phases as specified in staged construction mode for Case 2 model analysis 46
Table 4-4: Case 1 (sand) differential settlement calculation 62
Table 4-5: Case 2 (clay) differential settlement calculation 63
Table 5-1: Values for the surface chloride concentration and apparent diffusion coefficient from the literature 73
Table 5-2: Modified values for surface chloride concentration and apparent diffusion coefficient accounting for hydrostatic pressure 75
Table 5-3: Comparison of modified and unmodified chloride concentration values at a depth of 50mm and a time of 25 years 78

Declaration

This is to certify that the work I am submitting is my own and has not been submitted for another degree, either at University College Cork or elsewhere. All external references and sources are clearly acknowledged and identified within the contents. I have read and understood the regulations of University College Cork concerning plagiarism and intellectual property.

Signature of the candidate: 

Date: 07/10/2022

Acknowledgements

I would like to take this opportunity to express my gratitude to the following people who have supported me over the course of this Masters.

Firstly, I would like to extend my sincere thanks to Dr Zili Li and Dr Paraic Ryan for their continued guidance and support throughout this project. I am grateful to all from the Selkie project who have offered advice, with special thanks to Paul Bonar, TJ Horgan, and Majid Hussain. For their role as industry support, I would like to express my gratitude to Cian Desmond, Satish Jawalageri, Saroosh Jalilvand, and Louis Lapastoure in GDG.

I would also like to show my appreciation to my family for their continuous encouragement. Finally, I would be remiss not to thank Eileen, my aunt, for all she has done to support me throughout this project.

Abstract

Tidal energy converter devices have been developed to capture the enormous energy potential of the tides. These devices rely on robust mooring and foundation systems to ensure efficient energy extraction in operational conditions, and stability in extreme environmental conditions. Gravity-based foundations (GBF) are currently the most commonly used foundation type within the tidal energy industry. While tidal turbines are typically supported using bespoke carbon-steel tripod structures, concrete gravity-based foundations have been put forward by a number of studies as an alternative support solution. Several novel concrete GBF concepts exist and the developers of such concrete structures state that these foundations may be reused or relocated following decommissioning. Reuse of these massive concrete structures would greatly reduce construction and demolition (C&D) waste, and the need for new concrete GBFs for future devices, thus contributing significantly to the sustainability of the tidal energy industry. However, the concept of reusing concrete gravity-based foundations following long periods of deployment underwater has not been tested in real-world scenarios due to the nascent nature of the industry and long commissioning time periods.

As highlighted from a related concept in the oil and gas industry, several safety issues may arise from reusing and relocating concrete GBFs, including geotechnical hazards and concrete degradation due to corrosion. Therefore, this study assessed the practicalities of reusing concrete foundations following decommissioning by designing a concrete GBF from first principles to be used for further analysis. This representative GBF was then extensively tested using Plaxis geotechnical software to investigate soil subsidence and differential settlement, assessing their impact on GBF relocation feasibility. Subsequently, the risk of corrosion to the steel reinforcement in the GBF was examined by, firstly, modelling the chloride concentration profile of the concrete, and secondly, investigating the interrelationship between oxygen availability and water saturation level. Thorough investigation into these study considerations can significantly contribute to the determination of whether it is practicable to reuse or relocate concrete gravity-based foundations in the tidal industry.

The findings from the geotechnical analysis supports the possibility of reusing and relocating concrete GBFs for tidal turbines as both the total settlement and the tilt were significantly less than the allowable total settlement and tilt tolerance in a deployment site for which the GBF was designed and a contrasting site for which it was not. However, the findings from the concrete degradation analysis does not support the feasibility of reusing concrete GBFs. A chloride ingress analysis encapsulating three datasets indicated that the critical chloride threshold would be surpassed during a GBFs deployment period, meaning that the protective passive layer on the steel would be compromised leaving it vulnerable to corrosion should sufficient oxygen and water be present.

CHAPTER 1

INTRODUCTION

1. Introduction

1.1 Background

There is a growing demand for clean, renewable energy sources in today's world. Tidal energy converters offer huge potential for predictable, reliable energy extraction (Mendoza *et al.*, 2019). The fixed horizontal axis tidal turbine is the most cutting-edge tidal energy technology available today (Shiekh Elsouk, Santa Cruz and Guillou, 2018). These turbines require robust support structures that can withstand extreme forces generated by the hostile environments in which they are deployed. Steel-based, tripod, gravity-based foundations (GBFs) are the most prevalent support structure type employed in major tidal projects worldwide. However, concrete GBFs could provide an alternative, with developers of novel concrete GBFs claiming that their foundations are suitable for reuse or relocation following the end of a turbine's serviceability life (Vici Ventus, 2010; Jackson, Duff and Taylor, 2012; Mathern, von der Haar and Marx, 2021). If feasible, the concept of reusing these massive concrete structures would hugely elevate the sustainability of the offshore renewable energy industry. However, due to the nascent stage of the industry coupled with deployment periods of up to 25 years, there is no practical evidence of concrete GBF reuse or relocation (Weller *et al.*, 2018; Lande-Sudall, Stallard and Stansby, 2019). Therefore, it is the role of academic research to investigate the practicalities of reuse.

A similar concept in the offshore oil and gas industry, coined "life-extension", examines the safety issues associated with prolonging the serviceability life of obsolete oil and gas (O&G) concrete platforms for varying purposes (Leporini *et al.*, 2019; Capobianco *et al.*, 2021; Zagonari, 2021). Two major safety issues have been identified in the industry, namely, hazardous geotechnical behaviour, and concrete degradation due to corrosion (Ersdal and Hörnlund, 2008; PlaCE, 2019; McKenna, D'Andrea and González, 2021). Intuitively, it can be assumed that these safety issues could similarly affect concrete GBFs that have been reused or relocated. However, to the best of the authors knowledge, these safety hazards have not been studied in the literature for tidal turbine GBFs, meaning a gap in knowledge exists which urgently needs to be addressed to help increase the sustainability of the energy industry.

In this study, it was necessary to obtain the design of a concrete gravity-based foundation for further analysis. However, due to the competitive nature of the tidal

industry, there is an understandable reluctance within the industry to disclose detailed loading information for confidentiality reasons. Furthermore, commercial sensitivities dictated that the detailed design data of GBFs required to comprehensively assess geotechnical and deterioration concerns were unavailable, despite active collaboration with an industry partner involved in the project. In order to overcome this issue, the design of a concrete GBF from first principles was conducted as part of this research, with subsequent assessment of the identified geotechnical and concrete deterioration concerns.

1.2 Research Aims and Objectives

It is important to note that the aim of this thesis was not to select the best support structure option for tidal turbines but instead wanted to focus on the feasibility of reusing and relocating tidal turbine support structures at the end of a turbines service life. To the best of the authors knowledge, concrete gravity-based foundations are the only support structures where developers actively claim that reuse and relocation is possible, although there has been no practical evidence of such coupled with a paucity of relevant research into the area. Similarly the possibility of reusing or relocating micropiles or other offshore support structures has also not been studied meaning this could also be an interesting area for future work. Nevertheless, the overarching aim of this research was to address the knowledge gap pertaining to safety issues caused by reusing or relocating concrete gravity-based foundations designed for tidal turbines. Specific objectives included the following:

(i) **Designing a concrete gravity-based foundation from first principles for further analysis.**

A concrete GBF was designed in accordance with internationally recognised design guidance and standards using real-world geotechnical data and loading conditions.

(ii) **Examining geotechnical hazards which could potentially limit GBF reuse using Plaxis FEA geotechnical analysis software.**

Plaxis FEA software was employed to assess the settlement behaviour of the GBF in a different soil profile than the one for which it was initially designed.

(iii) Investigating the risk of concrete degradation of the case-study GBF due to chloride-induced corrosion.

Chloride ingress modelling was utilised to determine whether the critical chloride threshold of concrete was likely to be breached over intended service life. Subsequently, the relationship between oxygen availability and water saturation levels was explored through literature review to provide insight into the risk of corrosion in chloride-contaminated concrete situated on a dry-dock following decommissioning.

1.3 Thesis Layout

This thesis consists of six chapters and five appendices. An introduction to the issue of reusing concrete GBFs in the tidal turbine industry along with the significant shortcomings in knowledge in this area are presented in Chapter 1. This chapter also summarises the shortcomings selected for further study in this thesis and, finally, an overview of the thesis structure is outlined in this subsection.

Chapter 2 presents the relevant background information relating to concrete gravity-based foundations in the tidal industry and two potential barriers to their reuse and relocation, namely geotechnical hazards, and concrete degradation. The literature review also presents current state-of-the-art methodologies employed to examine these barriers in the context of reusability.

A representative concrete GBF is designed in Chapter 3 in order to study the selected barriers to reuse. The design methodology employed is presented and shown to be in accordance with international standards and design guidance, as well as design and analysis tools. Geotechnical parameters and loading conditions are obtained from real-life data. This chapter culminates in the design and sizing of a tidal turbine concrete gravity-based foundation that is used for further analysis in Chapter 4 and Chapter 5.

Chapter 4 presents the methodology, results, and findings from geotechnically analysing the representative concrete GBF. Using Plaxis 3D finite element analysis

software, geotechnical hazards, namely soil subsidence and differential settlement, were numerically analysed to determine the feasibility of reusing and relocating concrete GBFs in a different deployment environment.

Concrete degradation, the second barrier to concrete GBF reuse examined herein, is discussed in Chapter 5. The feasibility of reusing concrete GBFs following deployment is closely linked to the initiation and propagation of corrosion products within the reinforced structure caused by the presence of chlorides, water, and oxygen at the steel reinforcement surface. Therefore, this chapter presents a chloride ingress analysis using data and methods from the literature before discussing the interrelationship between water saturation degree and oxygen availability.

The thesis is concluded in Chapter 6 where the main findings pertaining to the feasibility of reusing and relocating concrete GBFs are presented, along with recommendations for future work and research implications.

CHAPTER 2

LITERATURE REVIEW

2. Literature Review

2.1 Background

As population numbers rise (United Nations, Department of Economic and Social Affairs, and Population Division, 2019), fossil fuel reserves deplete (Bentley, 2002), and the climate crisis worsens, there is an ever-increasing need for clean, non-fossil energy sources in the world today (Intergovernmental Panel on Climate Change, 2015; Thomsen, 2017; Zhou *et al.*, 2017). This creates new challenges, as well as opportunities, in the renewable energy sector, as increased public environmental awareness has led to a push to implement energy solutions that are environmentally conscious, sustainable, and low carbon (European Commission, 2017; O'Rourke, Boyle and Reynolds, 2010; Dai and Zhang, 2017). As part of the UN Sustainable Development Goals, Goal 7 (Affordable and Clean Energy) aims to considerably increase the contribution of renewable energy to the global energy mix by 2030 (United Nations, 2020), and, more locally, the Irish government's Climate Action Plan includes a target to increase the proportion of renewable electricity to up to 80% by 2030 (Government of Ireland, 2021). With further development, marine renewable energy technologies could factor significantly in meeting this global energy demand (Frid *et al.*, 2012).

Although offshore wind energy is the most technologically advanced component of marine renewable energy (Raoux *et al.*, 2020), tidal energy has enormous potential for energy capture (Segura *et al.*, 2017; Mendoza *et al.*, 2019; Nachtane *et al.*, 2020). Tidal Energy Converters are nascent-stage technologies that require further research and development in order to reach commercial viability (Mofor, Goldsmith and Jones, 2014; Weller *et al.*, 2018). Tidal Energy Converters (TEC) capture the kinetic energy of currents flowing in and out of tidal areas. As tides can be forecasted years in advance, it is an extremely predictable and consistent form of energy (Guillou, Chapalain and Neill, 2016; Mestres *et al.*, 2016; Burić *et al.*, 2021; Simonsen and Niclasen, 2021). This reliability factor is compounded by the fact that tidal stream energy is unaffected by weather (Wani, Dong and Polinder, 2020). Tidal energy extraction methodologies have evolved from large tidal range impoundment plants (Cochet and Lambert, 2017; Breeze, 2019) to the more commercial tidal stream energy converters (Mendi, Rao and Seelam, 2016).

A diverse range of Tidal Energy Converter devices exist in the world today, with development of both fixed and floating TEC occurring at a rapid rate (Zhou *et al.*, 2017). Tidal-stream energy converters generally fall under one of the following categories; horizontal axis turbines, vertical axis turbines, oscillating hydrofoils, ducted turbines or enclosed tips, archimedes screws, and tidal kites (Neill and Hashemi, 2018; Nachtane *et al.*, 2020). Please refer to Figure 2-1 for illustrations of these turbine categories. Depending on the device, tidal energy converters are at technology readiness levels (TRL) 6 or 7 with the fixed horizontal axis tidal turbine being the most developed tidal stream device (Starling and Scott, 2009; Uihlein and Magagna, 2016; Shiekh Elsouk, Santa Cruz and Guillou, 2018). These devices are often deployed in aggressive marine environments and therefore require robust support structures to resist both cyclical and extreme loading conditions caused by wind, wave, and tidal forces. Whilst floating devices come with their own range of mooring configurations and anchor options, support structures for fixed devices can be in the form of gravity-based foundations, piled foundations or suction piles (Weller, Hardwick and Johanning, 2014).

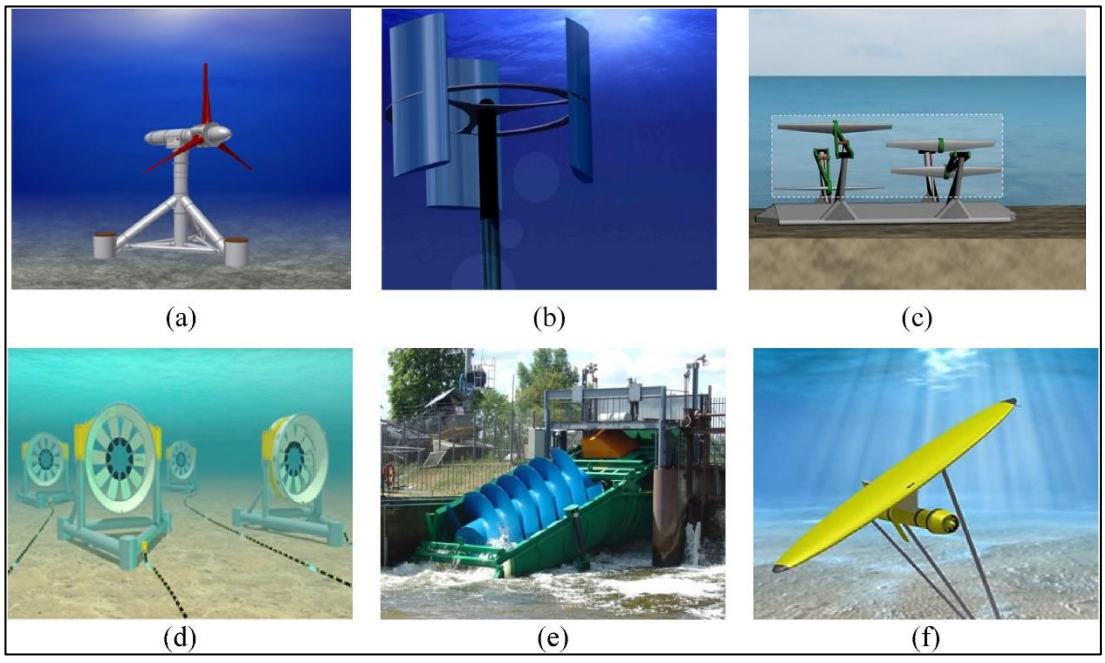


Figure 2-1: *The primary categories of tidal energy converters: (a) horizontal axis turbine, (b) vertical axis turbine, (c) oscillating hydrofoils, (d) ducted turbine or enclosed tips (e) Archimedes screw (f) tidal kite. Source: (Nachtane* et al.*, 2020)*

2.2 Gravity-Based Foundations

Current state-of-the-art tidal turbines are generally fixed to the seabed using gravity-based foundations. Initially used in the oil and gas sector, gravity-based foundations (GBF) are fast becoming recognised as one of the more advantageous anchoring solutions for offshore renewable energy (Esteban, López-Gutiérrez and Negro, 2019). Resting on the seabed, gravity-based foundations utilise a combination of their own self-weight and soil friction in order to resist both vertical and horizontal loads, and provide stability to offshore structures (Smith, Hytiris and Mickovski, 2015; Ikhennicheu *et al.*, 2020; Owen, 2020). GBFs are customisable depending on the loadings they are subjected to in their deployment environment. For instance, the addition of ballasts to a GBF is common practice to increase the overall weight of the foundation on the seabed and thus improve the foundations resistance to uplift, overturning and other forces on the foundation. Or, for increased lateral resistance and reduced dragging, GBFs can be fitted with foundation skirts, shear keys or pin-piles (Whitehouse, Sutherland and Harris, 2011; Han *et al.*, 2018).

GBFs are versatile in terms of deployment location; they may be installed in a large range of water depths, they are suited for deployment in complex geological environments where piling may not be possible and, unlike piled foundations, the structure remains visible throughout service lift for inspection (Attari, Prendergast and Gavin, 2016; Esteban, López-Gutiérrez and Negro, 2019). However, the slope of the seafloor influences the functionality of a GBF making them an unsuitable option for steeply sloping deployment sites (Sound and Sea Technology, 2009). While other commonly used offshore support structures require pile-driving, which may cause disruptive noise and vibrations with negative environmental repercussions (Bailey *et al.*, 2010; Hernandez C *et al.*, 2021), GBFs simply rest on the seabed surface eliminating the issue of noise pollution. This also means that at the end of service life, GBFs can easily be decommissioned, leaving no remnants in the deployment site. Deployment of gravity-based foundations do however present significant logistical challenges. Onshore production infrastructure with adequate bearing capacity and space is required for construction and storage of these massive structures which can be inhibitive (Mathern, von der Haar and Marx, 2021). Although gravity-based foundations may come with certain limitations, they are by far the most prevalent

foundation type used worldwide for ongoing and previous tidal projects as discussed in the following section.

2.3 Tidal Turbine Projects

The MeyGen tidal turbine project, in operation since March 2018, uses GBFs to stabilise four 1.5MW tidal turbines off the coast of Pentland Firth, Scotland (MeyGen, 2021). Each steel tripod structure (please refer to Figure 2-2) weighs between 250 to 350 tonnes with 6 ballast blocks providing a further 1200 tonnes of deadweight (MeyGen, 2021). These turbines and attached GBFs are located at water depths of 31.5m to 38m (MeyGen, 2020). Two types of turbines are employed as part of this project: the Andritz Hydro Hammerfest AH1000 MK1 and the Atlantis Resources AR1500 turbine. In 2015, Sabella's D10 tidal turbine became the first tidal turbine to connect to the grid in France (Sabella, 2018). This 1MW turbine is also supported on a steel tripod structure (please refer to Figure 2-3) deployed at a 55m water depth. The European Marine Energy Centre (EMEC) has facilitated the testing of numerous tidal turbines in recent years including Atlantis Resources AR1000 turbine, Andritz Hydro Hammerfest's HS1000 turbine, and Alstom's 1MW turbine, all of which were tested on steel tripod gravity-based structures (EMEC, 2021). From studying current, state-of-the-art tidal projects, it is evident that gravity-based foundations in the form of carbon steel tripod structures are the preferred support structure for tidal turbines.



Figure 2-2: *AR1500 tidal turbine supported on a steel tripod gravity-based foundation installed during the MeyGen project (Phase 1A). Source: (Rajgor, 2016)*

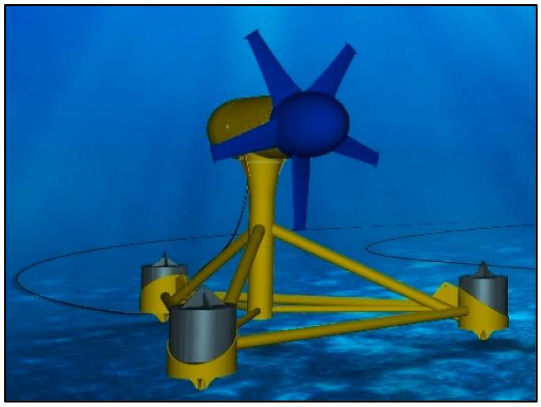


Figure 2-3: *Sabella's tidal turbine supported on a steel tripod gravity-based structure. Source: (Slama* et al.*, 2021)*

The steel tripod GBF concept favoured by tidal turbine projects is recognised as a well-established foundation solution, and, due to the nascent stage of the tidal industry, many developers focus on reliable, well-tested foundations rather than novel foundation concepts. In fact, a technology roadmap, published by the UK Energy Research Centre, identified reliability as one of the main challenges to commercial deployment within the wave and tidal energy community (Mueller and Jeffrey, 2008). To be perceived as 'reliable' is of utmost importance for developing ocean energy conversion technologies in order to stimulate industry investment, traverse the "valley of death", and reach commercial viability (Weller *et al.*, 2015). Furthermore, development of new and novel foundations is cost and time prohibitive for an industry in such early stages. Hence, the industry-wide use of the tried-and-tested steel tripod GBF concept. However, the high cost of steel structure fabrication could prove prohibitive to future tidal turbine development specifically in the case of tidal farms where hundreds of support structures would be required. The cost of transporting the structures from steel fabrication plants to deployment areas could also prove expensive and unenticing to investors and developers, thus hindering technology progress. Therefore, it is the role of academic research to explore and investigate alternative support structures for tidal turbines and provide guidance to industry based on research results. Furthermore, the tidal industry is uniquely placed to learn from the further developed and mature offshore wind turbine industry, which has a comparable working principle to tidal turbines (Dai *et al.*, 2015; Nachtane *et al.*, 2020). The following section outlines the current developments in support structures in the offshore wind industry, from which the tidal industry can learn.

2.4 Novel Concrete Gravity-Based Foundation Concepts

Steel monopiles are the primary foundation type used for offshore wind turbines (OWT), with an estimated 71% of deployed wind turbines supported on monopile foundations as of March 2018 (Li, Zeng and Wang, 2020). Monopiles have high capacity to resist uplift and overturning (Doherty and Gavin, 2011) while also being reliable, simplistic, and economical (Wang *et al.*, 2018; Sunday and Brennan, 2021). However, advances in OWT technology has led to larger turbines of increased generation capacity situated in deeper water which has, in turn, has led to greater structural demand on monopiles (Sunday and Brennan, 2021). Simply increasing monopile diameters in tandem with increasing structural requirements can lead to prohibitive material and installation costs (Chen *et al.*, 2020). Therefore, the opportunity to satisfy these increased demands has led to rapid development of alternative novel foundations solutions.

There have been many studies into new and novel foundation concepts for OWTs namely, hybrid-monopile foundations (Chen *et al.*, 2020; Li, Zeng and Wang, 2020; Ma and Yang, 2020; Trojnar, 2021), suction bucket foundations (Ding *et al.*, 2015; Faizi *et al.*, 2019; Lian *et al.*, 2021), and concrete gravity-based foundations. Concrete GBFs themselves are not novel offshore support structures having been widely employed as support structures in the oil & gas industry and for early-stage offshore wind farms. In fact, GBFs were used in the world's first offshore wind farm at Vindeby, Denmark in 1991 (Russell, 2020). Since then, concrete GBFs have evolved from first-generation reinforced slabs to hollow RC structures in conical form (Futai, Haigh and Madabhushi, 2021). This evolutionary process is described in detail by Esteban, López-Gutiérrez and Negro (2019) and is summarised in Figure 2-4. In the quest to find alternative support solutions to monopile foundations, there has been huge industry interest in the design of these third-generation concrete GBFs.

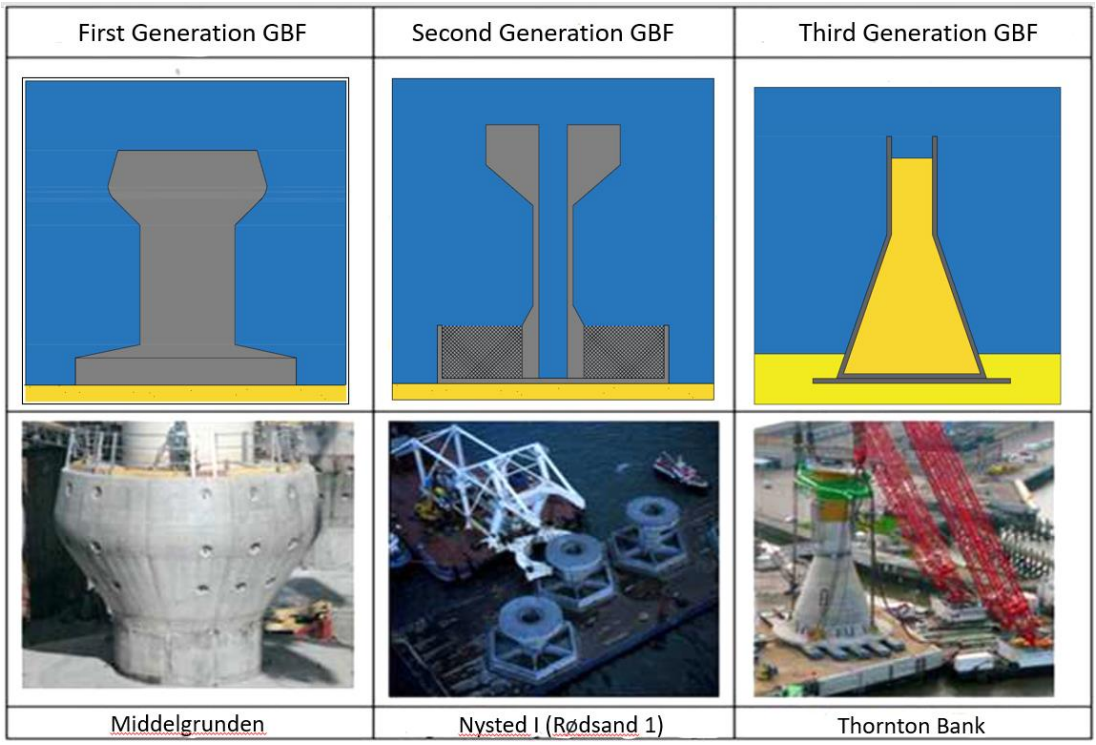


Figure 2-4: *The evolution of concrete gravity-based foundations. Source: (Esteban* et al., *2015)*

As several novel-concept GBFs are hollow and thus semi-submersible, they reduce the need for expensive heavy-lifting vessels during the installation process by using the F2F (floated to fixed) installation concept. This means the semi-buoyant GBF is floated to its deployment using standard tugboats before being ballasted with seawater firstly, to 'sink' the foundation to the seabed, and sand/aggregate secondly to stabilise the foundation and ensure load resistance requirements are met (McAuliffe and Norbeck, 2017; Esteban, López-Gutiérrez and Negro, 2019). Please refer to Figure 2-5 to see this ballasting method represented pictorially. Although there has been no practical evidence of decommissioning yet (as discussed in Section 2.5), theoretically the process of decommissioning these foundations is simply a reversal of the installation process. This innovative installation/decommissioning technique reduces equipment costs while concurrently increasing the installation weather window by avoiding the need for weather-sensitive equipment. There are numerous concrete GBF designs that operate using this semi-submersible principle. Thornton Bank wind farm first demonstrated the use of innovative, third generation GBFs which consists of a vertical shaft atop a conical structure. Six GBFs were commissioned in 2009 as part

of this project, with heights ranging from 38.5m to 44m (Peire, Nonnneman and Bosschem, 2009). Five of BAMs concrete GBFs (please refer to Figure 2-6) are currently installed at Blyth offshore demonstrator wind farm in the UK (BAM, 2018). Operational since 2017, each of these reinforced concrete structures contains roughly 1,800 cubic meters of concrete and weigh approximately 15,000 tonnes when fully submerged (BAM, 2017). Previous to this, in 2015, the first Seatower Cranefree Gravity foundation (please refer to Figure 2-7) was installed at the Fécamp offshore wind farm site at a water depth of 27m (Weston, 2015). Using just two tugboats for installation, the Seatower technology ensures minimal noise disruption to the marine environment (Seatower, no date). Similar concepts which have not yet been deployed are ARUPs Gravitas and Vici Ventus' GBF concepts (please refer to Figure 2-7) (Vici Ventus, 2010; Jackson, Duff and Taylor, 2012). Specifically developed for deep water, the Vici Ventus concrete GBF is suitable for water depths of 30-100m (Kim and Kim, 2018) while the Gravitas GBF can be deployed in water depths up to 60m (Esteban, López-Gutiérrez and Negro, 2019).

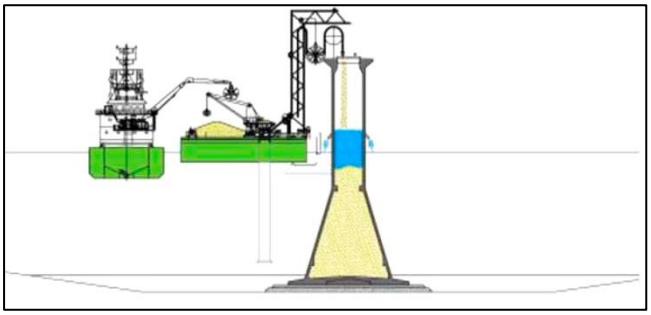


Figure 2-5: *The ballasting process of a novel concrete GBF. Source: (Esteban* et al.*, 2015)*



Figure 2-6: *BAMs concrete GBFs prior to installation on Blyth wind farm. Source: (Esteban* et al.*, 2015)*

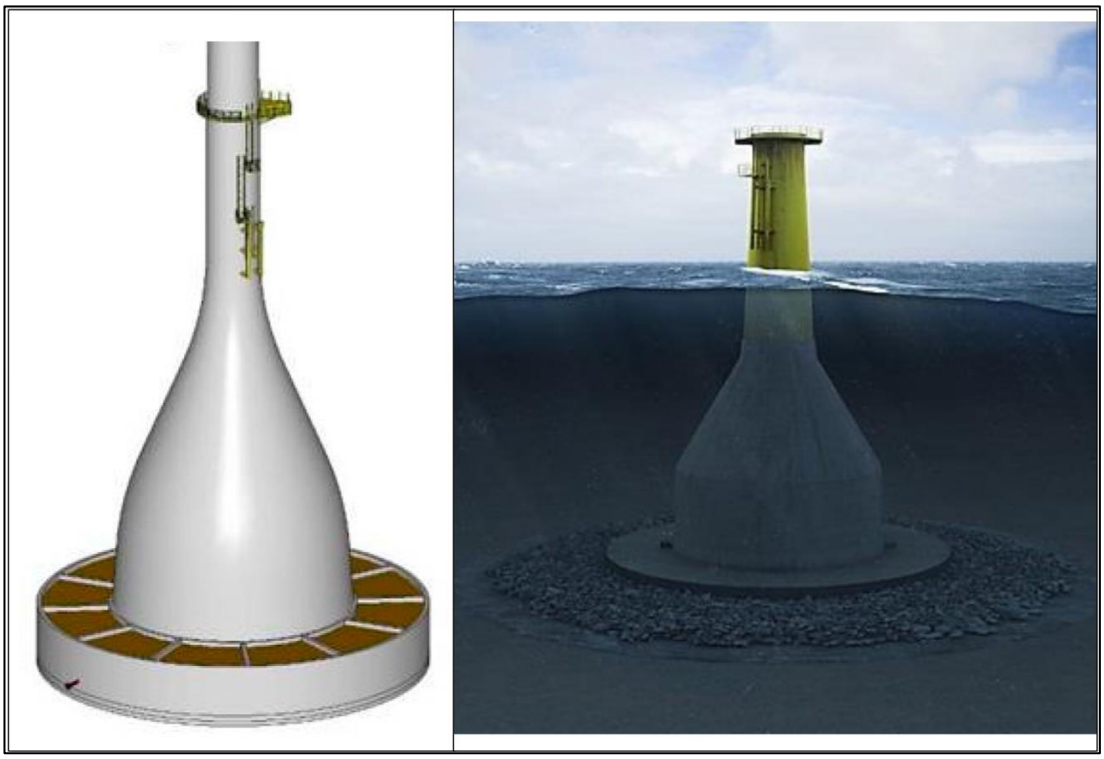


Figure 2-7: *Left: Vici Ventus concrete GBF concept. Source: (Mathern, von der Haar and Marx, 2021). Right: Seatower cranefree concrete GBF concept. Source: (Esteban, López-Gutiérrez and Negro, 2019)*

The aforementioned novel GBFs are constructed primarily of concrete whose production is much less carbon intensive than other commonly used building materials such as steel (Jones and Hammond, 2008; Adesina, 2020). However, although concrete is an ecologically favourable option when compared to steel, the widespread usage of concrete as a building material has outweighed its environmental advantage (Adesina, 2020). Concrete accounts for more than 50% of construction and demolition (C&D) waste worldwide, with up to 13 billion tons consumed per annum (Xia, Ding and Xiao, 2020). Concrete manufacturing mostly uses non-renewable raw materials, namely, cement and aggregate, whose energy-consuming production accounts for more CO_2 emissions than can be offset by the three trillion trees on the earth's surface (Brito and Kurda, 2021). In fact, it is estimated that the cement production industry is responsible for 5% of global CO_2 emissions, ranking it third in CO_2 emitting industries, behind only power plants and the iron and steel industry (Benhelal, Shamsaei and Rashid, 2021).

However, several novel GBF developers have addressed the possibility of reusing and relocating concrete GBFs at the end of a turbine's service life (Vici Ventus, 2010; Jackson, Duff and Taylor, 2012; Mathern, von der Haar and Marx, 2021). The Gravitas brochure specifically states that the foundation can be "re-located, re-powered, and removed at the end of its operational life", and "the durability of the concrete gravity foundations could allow developers to re-deploy them in different locations with new turbines fitted" (Jackson, Duff and Taylor, 2012). Similarly, Vici Ventus, when listing the main features of their GBF, state that it is "simple to remove/decommission or reuse at suitable location" (Vici Ventus, 2010). It is clear that reusing these massive concrete support structures would increase the sustainability of offshore renewable energy industries by reducing the significant environmental impact required for both their construction and disposal. Furthermore, if reuse and relocation proved viable, this would limit capital expenditure on support structures for future tidal stream projects and reduce the levelised cost of energy over its lifespan.

Clearly, reusing or relocating concrete GBFs would provide numerous advantages that, if viable, could make concrete GBFs a sustainable, practical support structure solution in the tidal industry. However, there has been little research into the feasibility of this concept, and absolutely no practical evidence of reuse or relocation to show that this is a tenable option in offshore renewable energy industries. Hence, the

primary goal of this research is to investigate barriers that may impede the reuse or relocation of concrete GBFs in order to determine whether it is a practical solution in the tidal energy sector. Therefore, the remainder of the literature review will explore not only barriers to reuse and relocation but also current decommissioning practices that may inform research into said barriers.

2.5 Decommissioning of Offshore Concrete Structures

Due to the nascent stage of the novel concrete GBF concepts and long deployment periods, decommissioning has yet to be demonstrated and subsequently there is no evidence of third generation GBF reuse or relocation to the best of the author's knowledge. In fact, there is a paucity of offshore renewable decommissioning experience for concrete gravity-based foundations in general, with even first and second generation GBFs still in operation. For instance, the second generation foundations for the Nysted project (see Figure 2-4), which was completed in 2003, were anticipated to last fifty years (Topham *et al.*, 2019). One of the few examples of concrete GBF decommissioning in the offshore renewable energy sector comes from the experience of the world's first wind farm in Vindeby, commissioned in 1991. Vindeby wind farm consisted of eleven 450kW wind turbines with concrete gravity-based foundations (Topham and McMillan, 2017). During decommissioning, the foundations were broken down using hydraulic hammers, hydraulic scissors, and rocks wheels. The remaining rubble was then collected and transported offsite to be used as new building material (Lempriere, 2017).

Looking beyond the marine renewable energy industry, the offshore oil and gas industry has a wealth of experience in using and decommissioning concrete gravity-based foundations. The first concrete gravity-based platforms were deployed in the UK North Sea in 1973 with around 50 major concrete gravity structures erected since then (Smith *et al.*, 2016). There are four types of oil and gas platform decommissioning options: complete removal, partial removal, toppling and leave-in-place (Lakhal, Khan and Islam, 2009). The chosen category depends on the weight and geometry of the structure, the deployment location, and the deployment depth. With many gravity-based structures weighing hundreds of thousands of tonnes, the structures were not initially designed to be removed and disposed of (Techera and Chandler, 2015). Thus, many large gravity-based structures are left in place, such as the Hazel Platform,

whose removal would create unacceptable disruption to the seafloor due to its excessive weight (Bull and Love, 2019).

Thousands of oil and gas (O&G) platforms are expected to become obsolete in the coming decades, triggering mass commercial and environmental interest in decommissioning processes and alternatives (Fowler *et al.*, 2018; Leporini *et al.*, 2019; Capobianco *et al.*, 2021). Recently, studies have been conducted into sustainable decommissioning of platforms, and more specifically the conversion of oil and gas platforms into renewable energy production sites (Leporini *et al.*, 2019; Capobianco *et al.*, 2021; Zagonari, 2021) using the concept of "life-extension" for existing oil and gas infrastructure. Extending the life of O&G platforms and reusing them has come to the forefront as a decommissioning option, ushering in issues and safety concerns associated with extending a structure beyond its design life (Ersdal and Hörnlund, 2008; McKenna, D'Andrea and González, 2021). One study, commissioned by the Petroleum Safety Authority, identified several components of aging that could compromise the safety of structures, namely, fatigue, corrosion, degradation of foundation capacity, seabed subsidence, and differential settlement (Galbraith and Sharp, 2007). Corrosion and concrete degradation is another concern that could affect an aging structure (PlaCE, 2019) with studies dedicated to protecting aging platforms against corrosion using mineral accretion technology (Margheritini *et al.*, 2020). These obstacles to O&G platform life-extension could be applied to the reuse and relocation of concrete GBFs in the marine renewable energy sector considering the similarities in principle.

Therefore, while there are discrepancies between massive oil and gas platforms and relatively small tidal turbine gravity-based foundations, comparisons can be drawn when it comes to barriers that may impede reuse, or the "second-life", of a concrete gravity-based structure, specifically the issues of concrete degradation due to corrosion, and geotechnical hazards, namely, subsidence and differential settlement (Galbraith and Sharp, 2007; Ersdal and Hörnlund, 2008; PlaCE, 2019; Margheritini *et al.*, 2020). While these barriers have not yet been studied in the literature in the context of tidal turbine GBF reuse, there is ample research in these areas that can be applied to this specific issue. The following sections of the literature review will specifically focus on the impact geotechnical hazards and corrosion may have on concrete gravity-based foundation reuse in the tidal energy sector.

2.6 Geotechnical Hazards

Soil subsidence and differential settlement have been identified as safety hazards associated with offshore structural design life extension (Galbraith and Sharp, 2007; Ersdal and Hörnlund, 2008). Therefore, it is reasonable to anticipate that similar risks would be applicable to tidal turbine support structures undergoing redeployment and relocation. Structural design typically takes place using specified environmental parameters, which, in the case of tidal turbine support structures, would include the geotechnical profile of the deployment site. Problems may arise if a structure is relocated to a deployment location for which it was not designed as the geotechnical strength parameters could differ. For instance, the behavioural properties of pure clay and pure sand stand at the opposite extremes of the soil spectrum (Subramanian, Khan and Ku, 2020). Soil settlement behaviour also depends on the soil type with three categories of settlement, namely, elastic or immediate settlement, primary consolidation settlement, and secondary consolidation settlement. Permeable sandy soils experience elastic settlement and consolidation settlement simultaneously, in contrast to a clayey soil where the consolidation settlement may be much greater than the elastic settlement (Das and Sobhan, 2016). Clearly, the soil type and associated parameters have great bearing on soil deformation, and in turn, soil subsidence and differential settlement. To the best of the author's knowledge, the concept of relocating a GBF to a deployment site for which it was not initially designed has not been studied, however, there exists vast knowledge on the best methods for the prediction of soil settlement which can be modified and used in this study.

Soil deformation has long been studied in the literature using a variety of methods including traditional analytical methods and modern numerical modelling methods. Das and Sivakugan (2007) discussed several analytical settlement prediction methods including Terzaghi and Peck (1948), Schmertmann (1970), and Burland and Burbidge (1985), and found that in general settlements were overestimated while allowable pressures were underestimated. They also found that more recent prediction methods, namely, Berardi and Lancellotta (1991) and Mayne and Poulos (1999), provided more accurate estimations. However, as computational ability has improved, the development and application of numerical techniques in geotechnical engineering have grown in popularity. Finite Element Analysis (FEA) has long been used in geotechnical engineering for its numerous advantages as outlined by Radhakrishnan

and Reese (1970) who stated that "the method can handle complicated, realistic geometries; layered isotropic and anisotropic materials with linear, nonlinear or viscous properties; mixed boundary conditions; and constructional sequences in earth building operations". Many commercial software tools have been developed to perform geotechnical predictions using FEA, including Plaxis (Bentley, 2022), Abaqus (Smith, 2009),and Oasys (Oasys Ltd, 2014). Although FEA is the most widely used numerical modelling technique for geotechnical analysis, there are various alternative techniques and analysis software available as well. Fast Lagrangian Analysis of Continua (FLAC) is a geotechnical software that utilises Finite Difference Method (Itasca, 2015). LimitState:GEO, a tool for the expeditious computation of limit state analysis, employs Discontinuity Layout Optimisation (DLO) (LimitState Ltd, 2021).

Smith, Hytiris and Mickovski (2015) analysed the immediate, consolidation, and overall settlement of a concrete GBF for a wind turbine using analytical methods, namely, Schmertmann's method, De Beer and Marten's method, and Meyhof's method, as well as numerical modelling tools including Plaxis and Oasys. They found that there were high levels of compliance demonstrated between the traditional analytical methods and the numerical modelling techniques, with Plaxis geotechnical software in particular exhibiting great potential for highly realistic settlement modelling. Additional examples in the literature demonstrate the aptitude of Plaxis software for settlement prediction and bearing capacity analysis of footings (Naderi and Hataf, 2014; Russell, 2020; Abdullah, 2022).

From Section 2.5, it is clear that geotechnical hazards including soil subsidence and differential settlement pose a threat to redeploying or relocating concrete GBFs. These safety issues may be exacerbated by placing a concrete GBF on a deployment site for which it was not designed, considering the strength parameters and settlement patterns of soil types differ. While this specific issue has not been studied in the literature so far, methodologies for predicting soil settlement have, with finite element analysis, and particularly Plaxis FEA software, proven to be a reliable, state-of-the-art methodology for the prediction of soil behaviour and soil-structural interaction. Therefore, this methodology is employed in this study to examine the geotechnical hazard of soil subsidence and differential settlement of a concrete GBF under different

deployment conditions to examine the feasibility of relocating concrete GBFs in the tidal turbine industry.

2.7 Concrete Degradation in Marine Environments

Although rebar corrosion has not yet been addressed in the literature in the context of offshore concrete structure reuse, it is reasonable to acknowledge that the deterioration of a structures reinforcement steel due to corrosion is a major factor that can affect the durability of offshore concrete structures, and thus affects the feasibility of reusing such structures. Corrosion of rebar within concrete structures could significantly shorten the service life of concrete structures, especially those exposed to marine environments (Xu and Jin, 2018; Li, Wang and Li, 2019). The consequences of corrosion on the degradation of concrete structures are twofold. Firstly, the formation of products of corrosion, which are larger in volume than the original reinforcing steel, induce tensile stresses on the concrete encompassing it (Rossi *et al.*, 2021). This results in the cracking, delamination or spalling of the concrete over time (Neville, 1995; Shi *et al.*, 2012; Šavija and Schlangen, 2012). Furthermore, the cross-sectional area of rebar steel is reduced during corrosion, inhibiting its load-carrying capacity (Neville, 1995; Fu *et al.*, 2021; Qiu *et al.*, 2021). The serious structural implications and variabilities caused to reinforced concrete structures due to corrosion have triggered extensive studies on the prediction, and prevention, of steel corrosion (Macdonald *et al.*, 2021).

Steel rebar inside concrete structures are protected by a passive film on its surface that develops gradually due to the natural alkalinity of concrete (Ming, Wu and Shi, 2021). This oxide layer protects the reinforcement by obstructing the movement of corroding ions between the steel and concrete (Goyal *et al.*, 2018). However, over time, chloride ions ingress into the concrete pore structure and build up on the protective layer eventually crossing a critical chloride threshold. At this threshold, the passive oxide film is damaged which is considered stage one, or ‘initiation’, of corrosion (Khatami, Hajilar and Shafei, 2021).

The second stage, or ‘propagation,’ of corrosion is the production and propagation of corrosion products, namely, iron oxide more commonly known as rust. Both oxygen and water are required, along with chloride ions, for the formation of rust. Therefore,

for concrete durability studies it is also important to investigate the ingress and availability of oxygen and water in different environments, much like what is done for chloride ingress. The availability of oxygen and the saturation levels of concrete are interrelated, such that when concrete is fully submerged there is reduced corrosion due to the paucity of oxygen at the steel-concrete interface, and when concrete is dry (relative humidity < 60%) there is reduced corrosion due to lack of moisture (Neville, 1995).

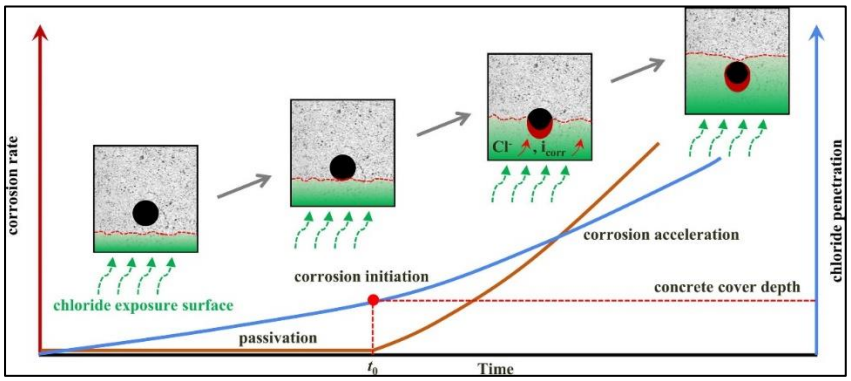


Figure 2-8: *Stages of steel corrosion in concrete where t_0 is the time at which corrosion initiates due to the chloride ion concentration at the steel surface surpassing the critical chrloide concentration threshold . Source:(Xia* et al.*, 2019)*

Chloride ions can penetrate concrete via several transport systems, namely, diffusion, convection, electrical migration, and ionic movement due to interactions between ions (Shakouri and Trejo, 2018). The transport mechanism of chloride ions depends on whether the surrounding marine environment is atmospheric, splash, tidal, or submerged (Ju *et al.*, 2021). Structures located in splash and tidal zones are subject to aggressive chloride ingress rates as cyclical wetting and drying promotes various chloride ion transport mechanisms (Balestra, Reichert and Savaris, 2019). In submerged zones, diffusion is considered to be the predominant transport mechanism of chloride ions (Yu *et al.*, 2015; Shakouri and Trejo, 2018). There have been extensive studies dedicated to the development of experimental methods and mathematical models for the prediction of chloride ion diffusion through concrete.

Statistical methods such as linear and non-linear regression have been widely used to model chloride penetration in concrete using Fick's second law of diffusion. However, significant attempts have recently been made to model chloride ingress using an

artificial neural network (ANN) technique (Najimi, Ghafoori and Nikoo, 2019; Cai *et al.*, 2020; Liu *et al.*, 2020; Al-Sodani *et al.*, 2022). In experiment, chloride ingress prediction has evolved from natural long-term exposure methods to bulk diffusion tests (NT Build 433, 1995; ASTM C1556, 2016) to rapid chloride migration tests (NT Build 492, 1999, p. 492; ASTM C1202, 2010).

As well as chloride ions, corrosion propagation requires the presence of oxygen and water at the steel-concrete interface. While an initial supply of oxygen is present in the micro- and nano-pores of the concrete, this reserve is quickly depleted when corrosion commences (Khatami, Hajilar and Shafei, 2021). A continuous supply of oxygen is required for the propagation of corrosion, prompting the development of mathematical models and experiments that examine the transport and availability of oxygen in concrete. One of the first physical-mathematical models to examine the transport of oxygen through concrete exposed to seawater was outlined by Bažant (1979), and has since been adopted as a basis for several studies. Yoon (2018) proposed a formulation for calculation of the apparent oxygen diffusivity of concrete based on diffusivity parameters, namely, diffusivity in air, tortuosity, cement micro-structural properties, and aggregate properties. Khatami, Hajilar and Shafei (2021) modelled the oxygen diffusion into concrete using cellular automaton framework to solve a time-dependent formulation based on the mass conservation equation coupled with Fick's second law of diffusion. Yu *et al.* (2021) considered the impact of both moisture level and oxygen transportation on both corrosion initiation and propagation through the development of a time-dependent numerical framework.

Of course, the ingress and availability of oxygen and water are linked, such that when concrete is fully submerged there is reduced corrosion due to a paucity of oxygen. This is because the pores of the concrete are blocked with moisture, limiting the connectivity required to transport oxygen from the environment to the steel surface (Hussain and Ishida, 2010). Similarly, when concrete is dry (relative humidity < 60%) there is reduced corrosion due to lack of moisture (Neville, 1995). Raupach (1996b, 1996a) expanded on this relationship by investigating the influence of oxygen diffusivity on corrosion in concrete under various exposure conditions namely, constantly dry, short-term wetting, long-term wetting, and constantly water saturated. It was found that in the latter case corrosion rates are negligible due to the high resistance to oxygen diffusion. Huet *et al.* (2007) treated oxygen as a function of water

saturation degree when developing a mathematical model based on Fick's second law of diffusion to examine whether oxygen diffusion should be accounted for during reinforcement corrosion modelling in various water saturation scenarios. The authors found that for water saturation degree of greater than 0.9, the concrete is at low risk of corrosion. Hussain (2011), when examining the effects of moisture on the oxygen consumption rate, found that reinforced concrete must be either completely saturated (RH = 100%) or in a high humidity environment (RH = 95%) with a low water-cement ratio and a thick concrete cover for oxygen to be a significant limiting factor for corrosion. It is generally agreed that a 90-95% relative humidity or cyclical wetting-drying conditions are the most favourable conditions for corrosion (Angst *et al.*, 2009).

2.8 Conclusion

Novel concrete gravity-based foundations are gaining popularity in offshore applications with numerous technology developers claiming that they can be reused and relocated following decommissioning. This would be a major environmental and economic advantage to the tidal industry should this concept prove practicable. However, due to the nascent stage of the industry, coupled with long deployment periods, there is no evidence or research into the feasibility of reusing or relocating concrete GBFs. A thorough search of decommissioning literature yielded a related concept known as "life-extension" in the offshore oil and gas sector, which identified two major safety issues associated with extending the life of concrete platforms, namely geotechnical hazards, and corrosion. Inferentially, it can be assumed that these safety concerns could affect the reusability of concrete GBFs. Therefore, this study aims to bridge the current knowledge gap on the feasibility of reuse and relocation of concrete GBFs in the tidal industry through examination of these safety issues. Although there is a wealth of research on both geotechnical risks and concrete degradation due to corrosion, neither of these topics have been examined in the context of reuse, adding to the novelty of this work.

CHAPTER 3

DESIGN OF CONCRETE GRAVITY-BASED FOUNDATION

3. Design of Concrete Gravity-Based Foundation

To examine the feasibility of reusing concrete GBFs, it was first necessary to design a representative concrete GBF for further analysis. Due to the scarcity of design data in the tidal turbine industry, it was not feasible to conduct a detailed design. Therefore, the design of the representative concrete GBF was done from first principles. The GBF design was based on realistic loading and deployment conditions and adhered to global offshore design standards. Chapter 3 will discuss the methodologies the design process followed, as set out by global standardisation agencies, the software tools employed to accelerate the foundation sizing calculation, and the loadings and environmental conditions with which the concrete GBF was designed. The final section of this chapter will then give an overview of all relevant characteristics of the representative GBF that were required for further analysis.

3.1 Design Guidance

Design guidance for tidal turbine support structures are heavily based on an extensive catalogue of offshore design standards, specifications and guidelines that have been issued by numerous classification bodies due to long-running commercial activities across the hydrocarbon industry, the fish farm industry and the offshore wind industry (PCCI, 2009; Weller, Hardwick and Johanning, 2014). A detailed list of such relevant standards and guidelines are compiled in Appendix A, adapted from similar tables that can be found in Sound and Sea Technology (2009) and Weller, Hardwick and Johanning (2014). Table 3-1 contains a condensed list of standards used for the design of the GBF. From Table 3-1 there are two documents specifically created for the tidal industry: DNVGL's Standard "Tidal Turbines" (DNVGL-ST-0164, 2015) and Bureau Veritas' Guidance note 'Current and Tidal Turbines' (NI 603 DT R01 E, 2015). These standards and the associated documents they refer to were extensively consulted throughout the design of the representative gravity-based foundation.

Table 3-1: *Guidelines, specifications, and standards referred to for the concrete gravity-based foundation design*

Title	Identifier	Current version
Det Norske Veritas & Germanischer Lloyd		
1. DNVGL Offshore Service Specification: Certification of Tidal and Wave Energy Converters	DNV-OSS-312	October 2008
2. DNVGL Standard: Tidal Turbines	DNVGL-ST-0164	October 2015
3. DNVGL Standard: Offshore Concrete Structures	DNVGL-ST-C502	February 2018
4. DNVGL Standard: Support Structures for Wind Turbines	DNVGL-ST-0126	July 2018
5. DNVGL Offshore Standard: Position Mooring	DNVGL-OS-E301	July 2020
6. DNVGL Recommended Practice: Environmental Conditions and Environmental Loads	DNVGL-RP-C205	December 2020
International Organisation for Standardisation		
7. ISO: Petroleum and natural gas industries – Concrete offshore structures	ISO 19903:2019	2019
European Committee for Standardisation (CEN)		
8. Eurocode 2: Design of Concrete Structures – Part 1-1: General rules and rules for buildings	EN1992-1-1	2004
9. Eurocode 7: Geotechnical Design – Part 1: General rules	EN1997-1	2004
10. Concrete – Part 1: Specification, performance, production, and conformity	EN206-1	2000
11. Cement – Part 1: Composition, specifications and conformity criteria for common cements	EN197-1	2000
Bureau Veritas		
12. Bureau Veritas Guidance Note: Current and Tidal Turbines	NI 603 DT R01 E	May 2015

DNVGL's design standard "Tidal Turbines" (DNVGL-ST-0164, 2015) advises using the limit state method for gravity base foundation design. Limit state design, also known as Load and Resistance Factor Design (LRFD), is a method for predicting

structural reliability. Structural reliability analysis is concerned with the prediction of the probability of structural failure or 'limit state violation' (Melchers and Beck, 2017). At the most basic level, a limit state violation occurs when the load effect on the structure is greater than the resistance of the structure, as shown in the following equation:

$$p_f = P(R \leq S) \tag{3-1}$$

where p_f is the probability of failure/probability of limit state violation, R is the resistance of the structure, and S is the load effect on the structure.

Tidal energy converters require long-term foundation systems and therefore, it is essential that the system meet a series of limit state criteria, namely ultimate limit state (ULS), accidental limit state (ALS), serviceability limit state (SLS), and fatigue limit state (FLS). These design criteria, as outlined by DNVGL-ST-0164 (2015) ensure that the foundation system has the capacity to withstand various load cases throughout its operational life without experiencing structural failure. There are several modes of structural failure that may occur over the lifetime of a foundation system, namely, bearing failure, sliding, overturning, or large settlements and displacements. Within limit state design, partial safety factors are employed to ensure a target safety level is obtained (please refer to Table 3-2 for target safety levels). Partial factors are commonly utilised in offshore engineering as they allow a certain level of variability. For example, a load of greater uncertainty can be subject to a larger safety factor than a load that may be well represented with a lesser uncertainty (Melchers and Beck, 2017). In this study, the partial safety factors as set out in Section 6, Table 6-1 of DNVGL's "Tidal Turbines" standard for safety level low were used for the ultimate limit state design. This standard also refers its reader to DNV-OS-J101 (currently superseded by DNVGL-ST-0126), DNV's "Support structures for wind turbines". Material factors, as outlined in Section 10 of this standard, were also applied to soil shear strength characteristics during the GBF design calculations.

Table 3-2: *Target safety levels for the certification of tidal energy converters (DNV-OSS-312, 2008; DNVGL-ST-0164, 2015)*

Consequence Class	**Description**	**Target Annual Probability of Failure**
Safety Level Low	Where failure implies low risk of human injury and minor environmental and economic consequences	10^{-3}
Safety Level Normal	For temporary conditions where failure implies risk of human injury, significant environmental pollution or very high economic or political consequences	10^{-4}
Safety Level High	For operating conditions where failure implies high risk of human injury, significant environmental pollution or very high economic or political consequences	10^{-5}

Bureau Veritas' Guidance note 'Current and Tidal Turbines' (NI 603 DT R01 E, 2015) refers to Eurocode 2 (EN1992-1-1, 2004) for supplementary information on concrete design. The Eurocode structural design standards were consulted for recommendations on exposure classes and concrete strength classes. For permanently submerged concrete with risk of corrosion induced by chlorides from seawater, the exposure class designation is XS2 which equates to 50mm concrete cover in the representative GBF. This exposure class also indicates that the concrete should have a maximum water-cement ratio of 0.45, and a minimum concrete strength class is C35/45 (EN 206-1, 2000). The chosen concrete type for this study was OPC (Ordinary Portland Cement).

This section discussed the standards and methodologies followed during the design of the GBF. Compliance with the global safety standards was hugely important to ensure that the gravity-based foundation was representative of a typical concrete GBF design method. The following sections will describe the design process in detail.

3.2 Design and Analysis Tools

To accelerate the foundation design process, there are several open-source design and analysis tools available. This section will discuss the use of two of these software applications, both of which employ the above methodologies described by the global offshore design standards for analysis.

3.2.1 DTOcean

The DTOcean (Optimal Design Tools for Ocean Energy Arrays) project facilitated the creation of an open-source, rapid mooring and foundation design tool. This tool was designed to assist in the initial selection of mooring and foundation systems for marine renewable energy devices by essentially eliminating unsuitable mooring and foundation configurations (Heath *et al.*, 2014; Weller *et al.*, 2018). This subsequently minimises the number of design permutations that may be subjected to further dynamic analysis, although exhaustive analysis is still necessary before physical implementation of a mooring system (Weller *et al.*, 2018).

At the beginning of this project DTOcean software was utilised in an attempt to design a gravity-based foundation. However, for a variety of reasons the tool was not suitable for this particular study. Although this tool is considered a preliminary design tool, a significant amount of input data was required prior to running a simulation, including sophisticated bathymetry and loading data that far exceeded what was accessible during this study. Furthermore, knowledge of various software packages such as pgAdmin and PostgresQL were necessary to upload said data. Additionally, the software did not contain sufficient details in the calculation steps, particularly being opaque regarding the selection process of the GBF. Reliability was also based on the statistical ‘bottoms-up’ reliability method which was not suitable for this project. It was thus concluded that this software was not suitable for this early-stage, high-level design.

However, there are many positives associated with the software too. Unlike other commercial analysis tools available, the DTOcean+ offers a complete mooring system analysis, inclusive of flexible mooring lines, anchors, and foundations, making it suitable for both fixed and floating devices. Furthermore, it does this whilst taking cost and environmental impact into account (Topper, Olson and Roberts, 2020). Currently, this tool is being further developed by the DTOcean+ project (Luxcey *et al.*, 2020).

3.2.2 Selkie's Foundation and Mooring Decision Support Model

The second foundation design tool used in this study was Selkie's Foundation and Mooring Decision Support Model, hereafter referred to as Selkies F&M design tool. This tool was built for early-stage foundation sizing and therefore requires minimal user-input making it suitable for the design of a high-level representative GBF. Although it is an early-stage model, the tool adheres to the limit state design methodology and uses GBF sizing formulae recommended by offshore design guidance. The Selkie F&M tool utilises quasi-static analysis which is an iterative process that substitutes complex dynamic forces on a mooring system with safety factors and coefficients. Because of the limited timeframe of this study, the GBF design procedure described in this section is very high-level, necessitating several simplifying assumptions regarding design loadings and output. The following sections will describe the source and characterisation of the input data, the design procedure, and the finalised GBF design that will be further analysed in Chapter 4 and Chapter 5.

Input data

Selkie's F&M tool requires geotechnical and loading input data in order to permute a design iteration for ULS analysis. The source and characterisation of the input data are described in this section, along with the safety and material factors applied to the data to ensure adherence to international design standards.

Geotechnical Parameters

This section describes the geotechnical soil parameters that were used for the representative GBF design. The soil parameters were based on open-source site investigation data combined with empirical values and assumptions. Currently, the Netherlands Enterprise Agency (RVO) is assessing and developing multiple offshore wind turbine deployment sites. One such site, located off the west coast of the Netherlands is the Hollandse Kust West Wind Farm Zone (HKW WFZ). As part of this project the RVO commissioned extensive geotechnical site investigations and laboratory testing to determine the geotechnical data associated with the site. The site investigation and accompanying laboratory testing were completed according to procedures advised by Eurocode 7 EN 1997-1:2004. This data is freely available for use and was employed in this study to create a soil model based on realistic and quantifiable geotechnical data.

Due to its large size, the land area of the HKW site is disaggregated into various provinces (Fugro, 2020). The data associated with soil province five were used in this study and are described in detail in this section. Within province five, this study focussed on the geotechnical parameters in HKW117-PCPT. This data set is available for download from Netherlands Enterprise Agency (2021) with screenshots of the data compiled in Appendix B.

For the purpose of the foundation sizing calculations and, later, Plaxis modelling, it was necessary to apply the following assumptions to the soil model:

- All sand layers are in a drained condition
- Poisson's ratio has a value of 0.2 for all sand layers i.e., v = 0.2
- All sand layers are cohesionless i.e., c = 0 kN/m^2
- The seabed slope is 0^o

The following empirical formulae were employed to convert some of the given HKW geotechnical parameters into input values for the Selkie foundation design tool and later, the Plaxis soil model.

The value of Young's modulus, E, was derived from the HKW data using Equation 3-2:

$$G = \frac{E}{2(1+v)}$$

(3-2)

where G is the shear modulus at small strain (MPa), E is Young's modulus (MPa), and v is Poisson's ratio.

The dilatancy angle was derived from the friction angle using Equation 3-3:

$$\psi = \varphi - 25^o$$

(3-3)

The final geotechnical parameters used for the representative foundation design calculations and subsequently for the Plaxis soil model are summarized in Table 3-3.

Table 3-3: *Geotechnical parameters used for representative GBF design*

Soil layer	Depth below seafloor	Bulk unit weight	Shear modulus	Young's modulus	Friction angle	Dilatancy angle	Coefficient of permeability
-	-	γ_{sat}	G	E'	φ'	ψ'	k_c
-	[m]	kN/m^3	MPa	MPa	^{o}	^{o}	m/day
Sand_1	0.0-2.0	20	52.5	126	39	14	1.037
Sand_2	2.0-8.2	20	80	192	38	13	1.037
Sand_3	8.2-15.2	20	100	240	37	12	1.037
Sand_4	15.2-20.0	19.5	150	360	33.5	8.5	0.041
Sand_5	20.0-24.9	19.5	150	360	33.5	8.5	0.041
Sand_6	24.9-33.3	19.5	105	252	31	6	0.041

Loading on GBF

The design loads used for the foundation sizing calculation were based on the AR1500 tidal turbine specifications (Atlantis Resources, 2016), and DNVGL's Tidal Turbine Standard. Ultimate limit state design ensures that the structure can withstand extreme loads and, in the case of tidal turbines, governing extreme loads will be produced at operational conditions during power production (DNVGL-ST-0164, 2015, sec. 5).

The AR1500 brochure specifies a rated operational velocity of 3.0m/s at a turbine height of 15m above the seabed. This was converted to a thrust force of 500kN which, assuming the turbine and foundation behave like a fixed-end cantilever, generated a resultant horizontal force of 500kN on the base of the foundation and an overturning moment of 7500kNm. The downwards vertical force on the foundation consisted of structural loads from the buoyant weight of the tidal turbine and the environmental load from the seawater. The AR1500 brochure specifies the turbine dimensions and weight in air giving a downwards buoyant force of 925kN. The calculation of these forces are shown in Appendix C.

Safety Factors

In compliance with offshore design standards, safety factors were applied to the geotechnical shear strength parameters, the loads on the GBF, and the ULS checks. A

safety factor of 1.25 was applied to loadings on the GBF in accordance with DNVGL-ST-0164 (2015, sec. 6). For the characteristic soil shear strength parameters, a material factor of 1.25 was applied to the cohesion and the friction angle of the soil in conformity with DNVGL-ST-0126 (2018). Conformance to international offshore design standards ensured that a realistic methodology was followed during the representative GBF design giving a high-level, conservative output suitable for further analysis.

Input

Table 3-4 shows a comprehensive list of the inputs used for the representative GBF design. The direction of the loads and overturning moment acting on the centre of the foundation are shown in Figure 3-1.

Table 3-4: *Input parameters for GBF sizing calculations*

Inputs			
	Symbol	Value	Unit
Geotechnical parameters			
Soil type	-	Sand	-
Seabed slope	β	0	^{o}
Friction angle	φ	39	^{o}
Cohesion	c_d	0	kN/m^2
Bulk unit weight of soil	γ_d	20	kN/m^3
Foundation characteristics			
Unit weight of concrete	γ_{conc}	24	kN/m^3
Loads			
Moment	M_{uls}	7,500	kNm
Vertical load	V_{uls}	925	kN
Horizontal load	H_{uls}	500	kN
Safety factors			
Geotechnical parameters	-	1.25	-
Loads	-	1.25	-
Bearing capacity	-	1.5	-
Sliding	-	1.5	-
Overturning moment	-	1.5	-

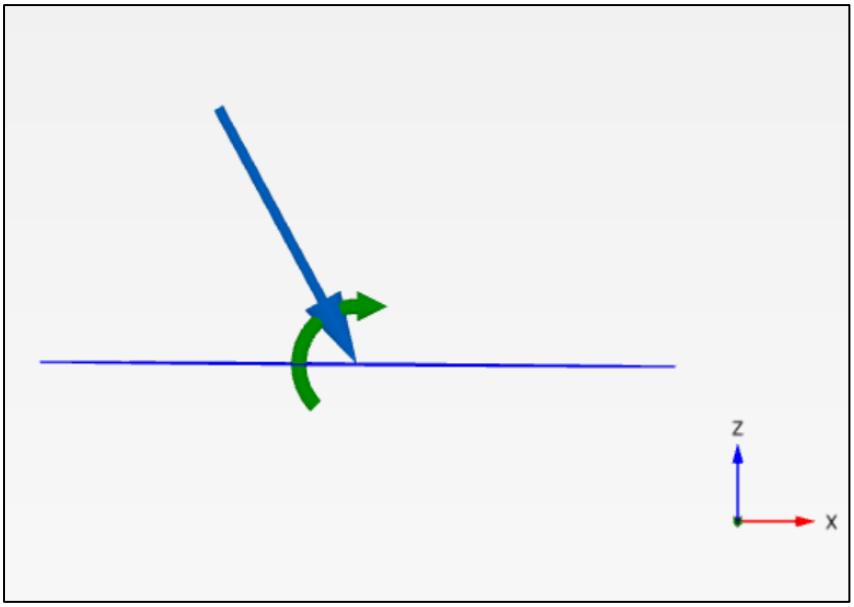


Figure 3-1: *Direction of load and moment acting on the centre of the foundation (generated in Plaxis 3D geotechnical software)*

Calculations

As the Selkie Foundation and Mooring Decision Support Model was in the 'pre-alpha' software stage during this project, a modified Microsoft Excel spreadsheet was created to execute iterative foundation design calculations based on the format demonstrated by the Selkie F&M design tool. The calculation methodology was also based on procedures endorsed by offshore design standards and guidelines. This methodology is broadly outlined in this section. Please also refer to Appendix D where the Microsoft Excel spreadsheet is available to view.

The minimum foundation dimensions were determined by the load eccentricity (e_r). Eccentricity is a function of the overturning moment and the total vertical load (where W_b is the buoyant weight of a pre-sized GBF):

$$e_r = \frac{M_{uls}}{V_{uls} + W_b}$$

(3-4)

To prevent loads that are excessively eccentric, the minimum radius (r_{min}) should, as a rule, be greater than or equal to 6 times the eccentricity (e_r), or greater than the radius of the structure connecting the tidal device to the GBF (device r):

$$r_{min} = MAX(6e_r, device\ r)$$

(3-5)

Prior to performing the ULS checks, it was necessary to calculate the effective area (A') of the foundation:

$$A' = 2\left[r^2 arccos\left(\frac{e_r}{r}\right) - e_r\sqrt{r^2 - {e_r}^2}\right]$$

(3-6)

A rectangle of length L' and breadth B' was determined from the effective area (where b_e is the effective breadth and l_e is the effective length) using the following formulae. It was necessary to compute a representative rectangle from the effective area of the circular GBF for use in the ULS bearing capacity check.

$$b_e = 2(r - e)$$

(3-7)

$$l_e = 2r\sqrt{1 - \left(1 - \frac{B'}{2r}\right)^2}$$

(3-8)

$$L' = \sqrt{A'\frac{l_e}{b_e}}$$

(3-9)

$$B' = \frac{L'}{l_e}b_e$$

(3-10)

The Selkie F&M tool performs three ULS checks for each design iteration: a bearing capacity check, a sliding resistance check, and an overturning check. If a GBF design fails to pass any of these checks, the radius of the GBF is increased by an increment

value set by the user and the effective area is recalculated to pass through the checks again. This process iterates with the radius increasing in increments until a design permutation passes all ULS checks.

Bearing Capacity Check

The stability of the GBF is ascertained in the bearing capacity check.

$$\frac{Q_u}{SF} > (V_{uls} + W_b)(cos\beta + H_{uls} sin\beta)$$

(3-11)

Where:

- Q_u: bearing capacity, based on Terzaghi's bearing capacity equation
- SF: safety factor
- W_b: the buoyant weight of the foundation (N)

Sliding Resistance Check

The sliding check ensures that the GBF's lateral resistance is greater than the maximum applied horizontal load.

$$\frac{H_u}{SF} > (V_{uls} + W_b) sin\beta + (H_{uls} cos\beta)$$

(3-12)

Overturning Moment Check

The purpose of the overturning moment check is to verify that the GBF's stability moment is greater than overturning moments induced by environmental loads.

$$\frac{(V_{uls} + W_b) cos\beta \; x \; r}{SF} > \; M_{uls} + (H_{uls} \cdot z_{ap})$$

(3-13)

Where:

- z_{ap}: the vertical distance between the seabed and the point where the maximum horizontal load is applied (m)

Output

Following the iterative design process outlined in the previous section, it was determined that a circular concrete foundation of 8m radius and 2.4m thickness was appropriate as per the input geological and loading conditions (please refer to Figure 3-2). Due to time restraints, the design presented here is relatively high-level necessitating a number of simplifying assumptions and omissions, namely, the reinforcement steel design. The addition of steel for tensile strength is common practice in concrete structures, however, rebar design can be time consuming, and, in the case of this study, it was only necessary to determine the rough size and weight of the GBF for geotechnical analysis. Therefore, while it was assumed that rebar steel was present in the concrete GBF, the detailed design of the reinforcement was not necessary nor feasible.

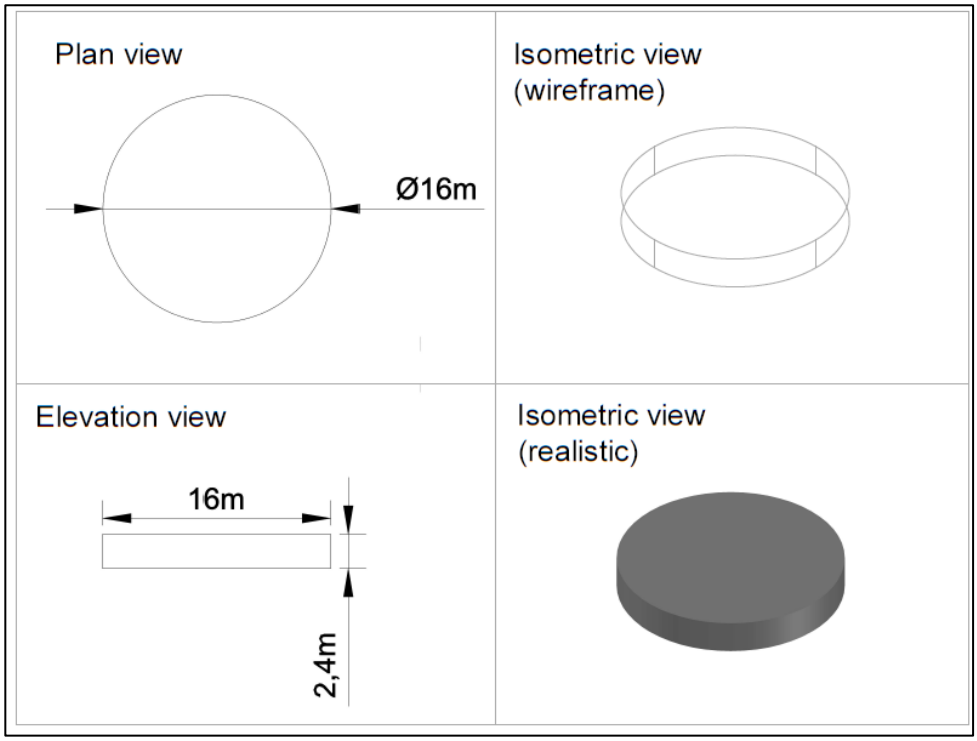


Figure 3-2: *Gravity-based foundation dimensions (drawing created in AutoCAD)*

3.3 Finalised Gravity-Based Foundation Design

The characteristics of the finalised representative GBF are outlined in Table 3-5. The Selkie F&M tool determined the geometry of the GBF, and the concrete exposure class

and associated cover were determined from EN1992-1-1 (2004). The concrete is assumed to be Ordinary Portland cement (OPC) with a maximum water-binder ratio of 0.45 and a minimum strength class of C35/45. This finalised GBF design was used to analyse the feasibility of reusing concrete GBFs in Chapter 4 and Chapter 5.

Table 3-5: *Gravity-based foundation characteristics*

Gravity-Based Foundation Characteristics			
	Symbol	Value	Unit
Foundation Geometry			
Radius	r	8	m
Thickness	t	2.4	m
Area	A	201	m^2
Volume	V	482.4	m^3
Weight	W	11,581	kN
Buoyant Weight	W_b	6,736	kN
Corrosion protection			
Concrete exposure class	-	XS2	-
Concrete cover	-	50	mm

CHAPTER 4

BARRIER 1: GEOTECHNICAL HAZARDS

4. Barrier 1: Geotechnical Hazards

Plaxis 3D FEA geotechnical analysis tool was used to numerically analyse the representative gravity-based foundation in order to gather results on soil subsidence and differential settlement, two parameters which could impact the decommissioning and reuse of concrete GBFs. To do this, a model of the GBF was developed in Plaxis 3D, using the output data described in Chapter 3, to simulate initial and long-term soil-structure interaction. Further to this, a second model was built in Plaxis 3D to demonstrate the soil-structure interaction should a GBF be placed on a seabed stratum for which it is not designed. Finally, the GBF model was subjected to increased loading conditions to simulate the tilt behaviour of the GBF should a greater load be placed on it than what it was designed to support. This chapter describes the Plaxis analysis methodology and discusses the feasibility of reusing concrete GBFs with regards to geotechnical hazards from the results of this analysis.

4.1 Methodology

Plaxis 3D finite element analysis software was employed to examine the feasibility of reusing concrete gravity-based foundations from a geotechnical standpoint. This section will discuss the methods employed in Plaxis 3D software for this analysis. Two Plaxis models were developed in order to study the settlement patterns of the foundation and soil in two cases, differentiated as follows:

- Case 1 – Sandy soil with 1.5MW turbine loads (GBF design case)
- Case 2 – Clayey soil over sand with 1.5MW turbine loads

The methods employed for building 3D Plaxis models for each of these cases are described in the following sections.

4.1.1 Case 1

The Case 1 model was developed to analyse the soil-structure interaction of the representative GBF under the geotechnical and loading conditions for which it was designed. A 100m x 100m soil model was developed to satisfy the rule-of-thumb which advises a soil model of at least five times greater than the footprint of the structure. The soil model consisted of six layers, whose geotechnical parameters can be found in Table 3-3. The GBF was modelled as a stiff plate of 8m radius and 2.4m

thickness as per the output of the Selkie tool design calculations (please refer to Table 3-5 and Figure 3-2). A description of the step-by-step development of the model for Case 1 conditions is provided in Appendix E. The finalised Case 1 model is shown in Figure 4-1.

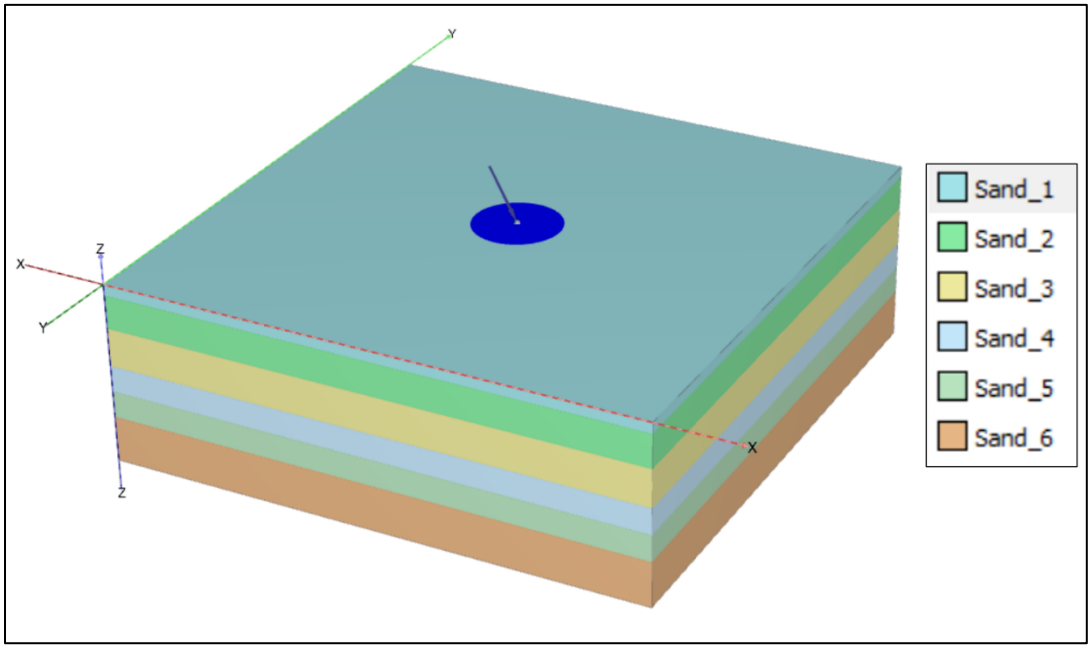


Figure 4-1: *Case 1 Plaxis 3D model*

Following the development of the model, it entered 'staged construction' mode. This allowed for the definition of different calculation phases. For sandy soil, plastic analysis was suitable to calculate the immediate soil displacement following firstly, the placement of the GBF which was represented using a plate, and secondly, the placement of the turbine which was represented using a points load and overturning moment as outlined in Table 3-4. Following this, a time-dependent analysis of soil deformation was defined using a fully-coupled flow deformation calculation type for a 25-year turbine service life in 5-year intervals. This staged construction process is also outlined in Table 4-1. The results from the FEA analysis of this model are presented in Section 4.2.(Kumar, Toan and Vahedifard, 2021)

Table 4-1: *Calculation phases as specified in staged construction mode for Case 1 model analysis*

Phase	Description	Calculation type	Time interval (days)	End time (days)
Initial	Calculation of initial stresses, pore pressures and state parameters; No structures/loads active	K0 procedure	-	-
1: Activate foundation	GBF plate activated	Plastic	1	1
2: Activate loads	GBF active; Turbine loads and moment activated	Plastic	1	2
3: Year 1-5	GBF active; Turbines loads and moment active	Fully-coupled flow deformation	1,825	1,827
4: Year 6-10	GBF active; Turbines loads and moment active	Fully-coupled flow deformation	1,825	3,652
5: Year 11-15	GBF active; Turbines loads and moment active	Fully-coupled flow deformation	1,825	5,477
6: Year 16-20	GBF active; Turbines loads and moment active	Fully-coupled flow deformation	1,825	7,302
7: Year 21-25	GBF active; Turbines loads and moment active	Fully-coupled flow deformation	1,825	9,127

4.1.2 Case 2

Case 2 was used to examine the geotechnical performance of the design GBF on an alternative soil type. As discussed in Section 2.4, several concrete GBF manufacturers state the possibility of relocation following the end of a turbine's operational life. Therefore, this case examined the feasibility of relocating the design GBF by replacing the first 8.2m of sand with clayey soil of similar stiffness. To provide a contrast to the drained, cohesionless sandy soil in Case 1, an undrained, cohesive clayey soil was selected as the alternative soil type. Again, the clayey soil parameters are based on real-life soil examples from the open-source HKW geotechnical data (Netherlands Enterprise Agency, 2021). The data for Clay_1 and Clay_2 was obtained from province 4 HKW082 and from province 8 HKW065 respectively (Please refer to Appendix B for the HKW province data). Table 4-2 details the characteristic values of the clayey soil layers. The bottom four sand layers from 8.2-33.3m below the seabed remain unchanged from Case 1, as do the turbine loads. Please refer to Figure 4-2 to view the finalised Case 2 model.

Table 4-2: *Case 2 geotechnical parameters*

Soil layer	**Depth below seafloor**	**Bulk unit weight**	**Shear modulus**	**Young's modulus**	**Undrained shear strength**
-	-	γ_{sat}	G	E	$s_{u,k1}$
-	[m]	kN/m^3	kN/m^2	kN/m^2	kN/m^2
Clay_1	0.0-2.0	19	45	126	15
Clay_2	2.0-8.2	19.5	70	196	75

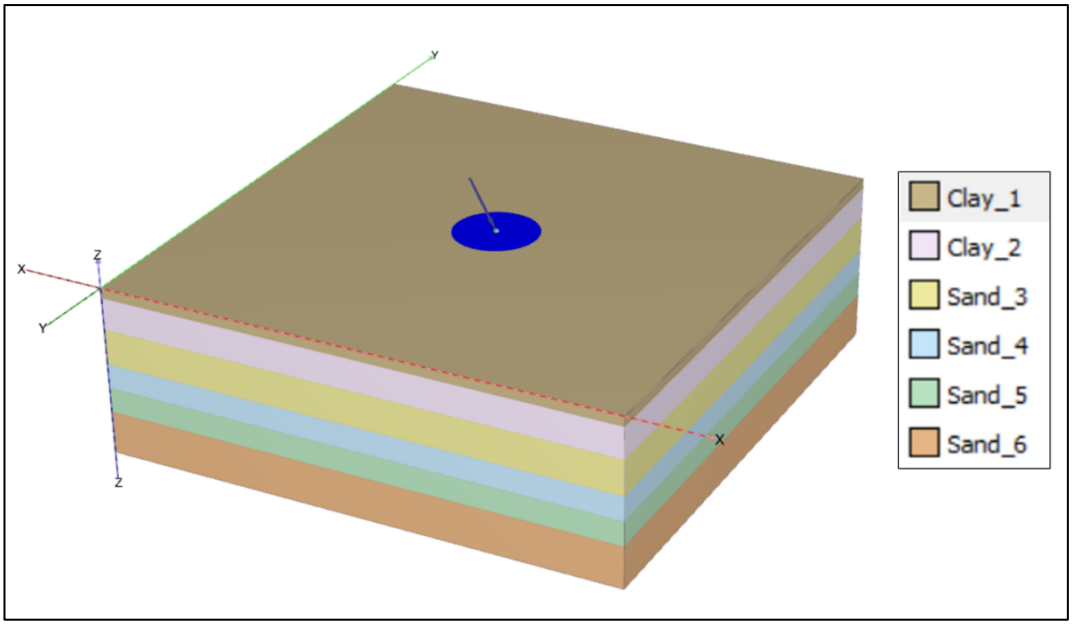


Figure 4-2: *Case 2 Plaxis 3D model*

The staged construction for Case 2 differed from Case 1 due to the presence of clay soil layers. Due to the finite hydraulic conductivity of clay, consolidation analysis was required to model the behaviour of the soil realistically. Plastic analysis does not consider consolidation and therefore was not utilised in Case 2. The consolidation calculation type was selected for all phases in this analysis as it conducts a time-dependent analysis of deformations and excess pore pressures. Furthermore, it was necessary to allow a 30-day consolidation time period after the placement of the foundation plate to emulate realistic building conditions. Again, the long-term soil settlement was analysed for a 25-year turbine operation period in 5-year intervals. Table 4-3 contains a summary of the calculation phases for Case 2.

Table 4-3: *Calculation phases as specified in staged construction mode for Case 2 model analysis*

Phase	Description	Calculation type	Time interval (days)	End time (days)
Initial	Calculation of initial stresses, pore pressures and state parameters; No structures/loads active	K0 procedure	-	-
1: Activate foundation	GBF plate activated	Consolidation	1	1
2: 30-day consolidation	30-day consolidation period	Consolidation	30	31
3: Activate loads	GBF active; Turbine loads and moment activated	Consolidation	1	32
4: Year 1-5	GBF active; Turbines loads and moment active	Consolidation	1,825	1,857
5: Year 6-10	GBF active; Turbines loads and moment active	Consolidation	1,825	3,682
6: Year 11-15	GBF active; Turbines loads and moment active	Consolidation	1,825	5,507
7: Year 16-20	GBF active; Turbines loads and moment active	Consolidation	1,825	7,332
8: Year 21-25	GBF active; Turbines loads and moment active	Consolidation	1,825	9,157

4.2 Results

The results of the Plaxis 3D analysis pertaining to the feasibility of reusing concrete gravity-based foundations in different soil conditions for which it was designed are presented in the following section. The soil settlement behaviour and foundation tilt are the focus of this section. There is also a brief analysis of the effects of increased loading on the soil-structure behaviour.

To view the settlement activity of the soil under the foundation, a cross-section A-A* was taken directly through the centre of the model as shown in Figure 4-3. Figures 4-4 and 4-5 show the phase-by-phase settlement of the soil for Case 1 and Case 2 respectively at the A-A* cross-section.

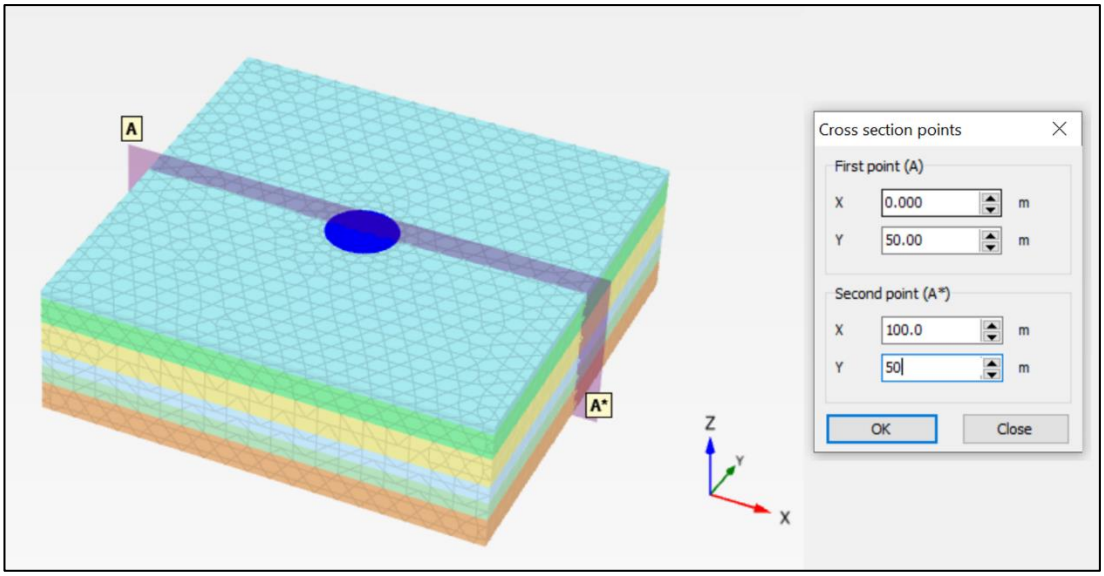


Figure 4-3: *Cross section A-A**

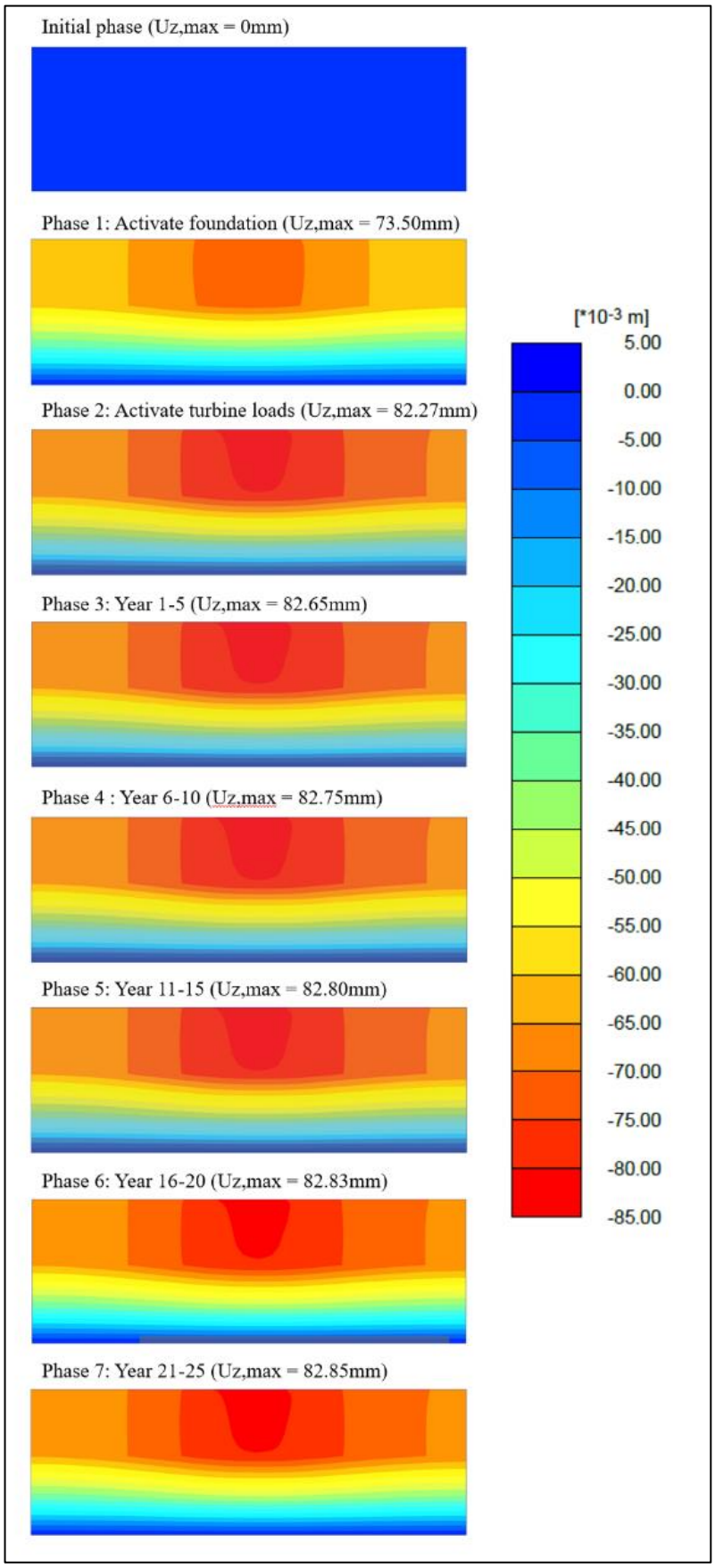


Figure 4-4: *Vertical displacements under cross section A-A* for Case 1 sandy soil model*

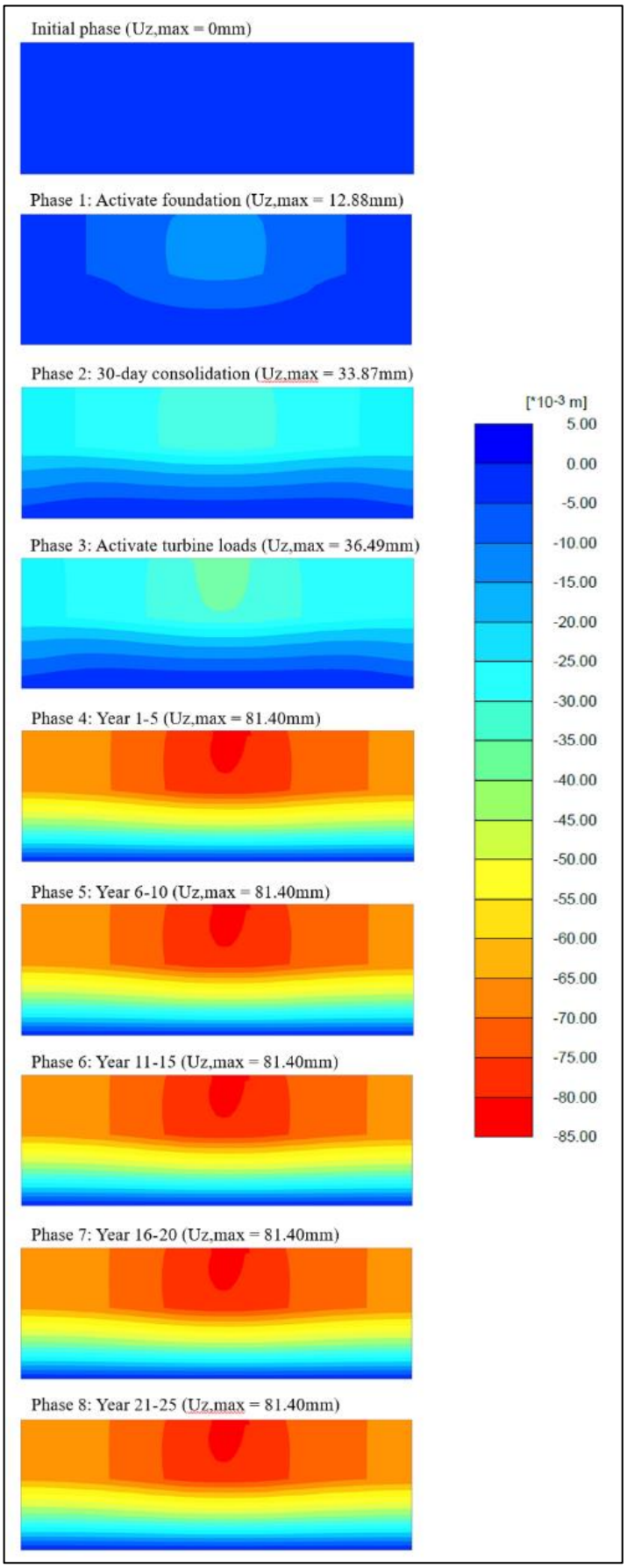


Figure 4-5: *Vertical displacements under cross section A-A* for Case 2 clayey soil model*

Figure 4-4 demonstrates the vertical displacement of the Case 1 soil at the cross-section A-A*. During phase 1 the soil settlement was symmetrical about the centre of the foundation, however, once the turbine loading was applied in phase 2 there was greater settlement on the right-hand side of the foundation. This is due to the application of the turbine loads which included a horizontal load and an overturning moment. As expected, the vertical displacement of the soil decreased as the depth below the seabed increased, so that the bottom soil layers experienced less disturbances than the top soil layers. These statements also hold true for the Case 2 model, as shown in Figure 4-5.

However, there are differences in the soil settlement between Case 1 and Case 2. In Case 1, the sandy soil experienced immediate settlement after placing the foundation, and again after placing the turbine. From phase 2 to phase 7 the vertical displacement profile remains similar, albeit with a minor increase in the maximum vertical displacement during the service life of the turbine. Overall, the max displacement increased by a further 0.58mm over the 25-year service life following an immediate settlement of 73.50mm and 8.77mm after activating the foundation and activating the turbine loads, respectively.

Case 2 demonstrated a different phase-by-phase settlement process to Case 1. Following the placement of the foundation, the maximum vertical displacement was 12.88mm in Case 2, compared to 73.50mm in Case 1. The Case 2 model then underwent a 30-day consolidation period, as is required for clayey soil conditions, before finally reaching a maximum settlement of 33.87mm. This is still less than half the vertical displacement that was caused by the foundation placement in Case 1. This consolidation behaviour was repeated following the turbine load activation. The immediate maximum settlement of the soil was 20.99mm, which interestingly is greater than the immediate settlement following turbine load activation in Case 1 (8.77mm). This is due to the continued consolidation caused by the weight of the foundation, as consolidation phase was completed at the end of a 30-day time-period rather than at the minimum excess pore pressure. Therefore, it is not known what proportion of the 20.99mm settlement was caused by the foundation weight and what proportion was caused by the turbine loads. Following phase 3 in Case 2, the model entered the turbine serviceability lifetime phases spanning 25 years. Again, there are discrepancies between the Case 1 and Case 2 models. As can be seen in Figure 4-5,

the maximum vertical displacement increased from 36.49mm to 81.40mm in the first 5 years of service life. This 44.91mm settlement was the most significant vertical displacement that took place in Case 2, however, unlike Case 1 where there was continuous minor displacement throughout the 25-year service life, there was no more displacement following this. The final maximum GBF settlement was 82.85mm in Case 1 and 81.40mm in Case 2. This is only a difference of 1.45mm between the sand model and the clay model, which is relatively small, considering the span of the foundation is 16m. This maximum displacement coincided with the dissipation of the excess pore pressure within the soil as can be seen in Figure 4-6.

Figure 4-6 demonstrates the excess pore water pressure responses in Case 2 throughout cross section A-A*. It is evident that excess pore water pressures were generated in the clayey soil surrounding the GBF following the activation of the foundation. This is due to the pore water pressure compensating for the change in total stress of the soil. As Case 2 went through the 30-day consolidation phase, the excess pore water pressure dissipated, although not completely. The dissipation signifies that during this phase soil compression occurred (incurring GBF settlement), effective stress increased, and the excess pore water pressure decreased, although not fully back to the static pore water pressure due to the limit on consolidation time. In Phase 3, the excess pore water pressure increased again due to the activation of the turbine loads. While these loads incurred excess pore water pressure, it was to a lesser extent than Phase 1. Again, over time in Phase 4 the excess pore water pressure dissipated, and further compression of the soil took place, causing settlement of the GBF. Although the static pore water pressure was not reached until Phase 6, the excess pore water pressures are negligible at the end of Phase 4 and throughout Phase 5. The dissipation patterns shown in Figure 4-6 coincide with the settlement patterns described in Figure 4-5, as is expected due to the intrinsic relationship between excess pore water pressure and soil compression.

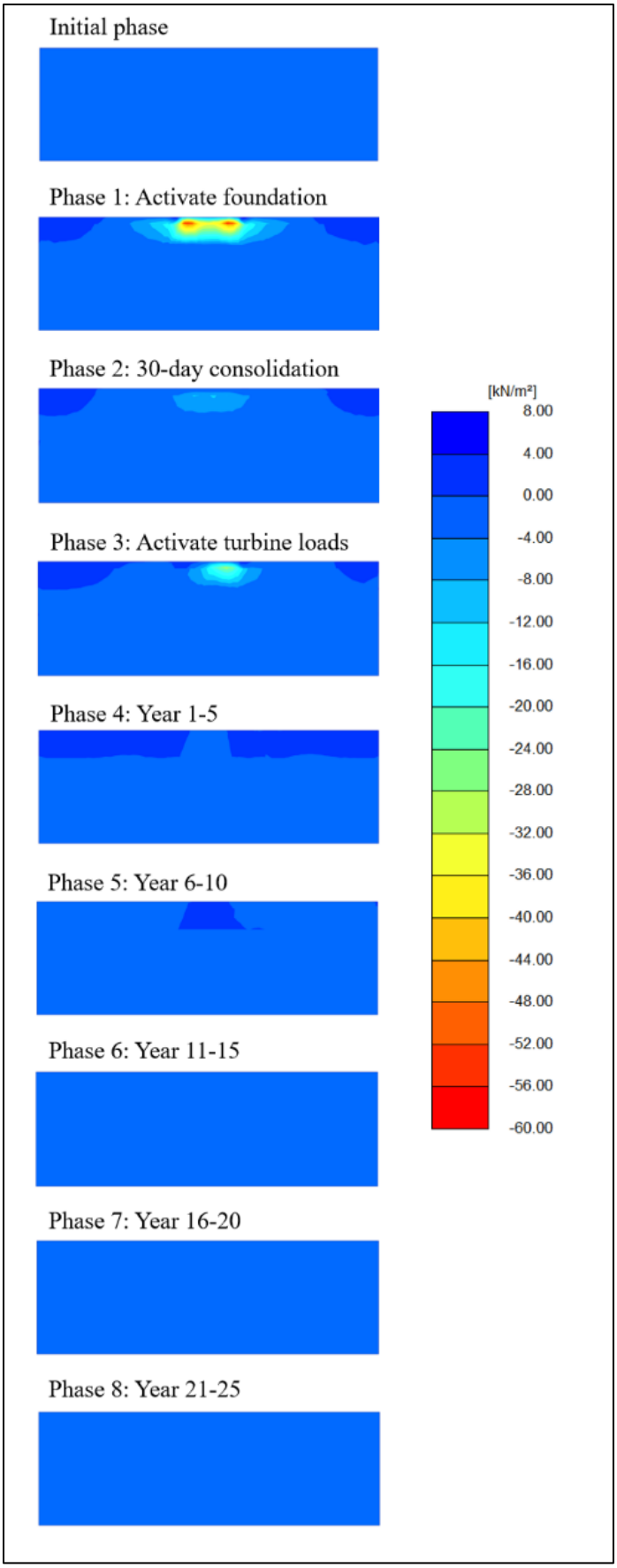


Figure 4-6: *Excess pore water pressure under cross section A-A* for Case 2 (clay)*

For offshore turbines, it is imperative that the foundation does not exceed a 0.25 degree tilt tolerance in order to maintain serviceability (Smith, Hytiris and Mickovski, 2015). The tilt of the foundation was examined over the lifetime of the turbine for both Case 1 and Case 2. Several points along the perimeter of the foundation as well as the center point were selected as reference points for this purpose of analysing the tilt of the foundation over time. These points were (50,50,0), (42,50,0), (58,50,0), (50,42,0), and (50,58,0) as shown in Figure 4-7. These points are highlighted in blue, red, pink, orange, and green respectively and these colours are assigned to these points for all graphical illustrations henceforth to ensure clarity.

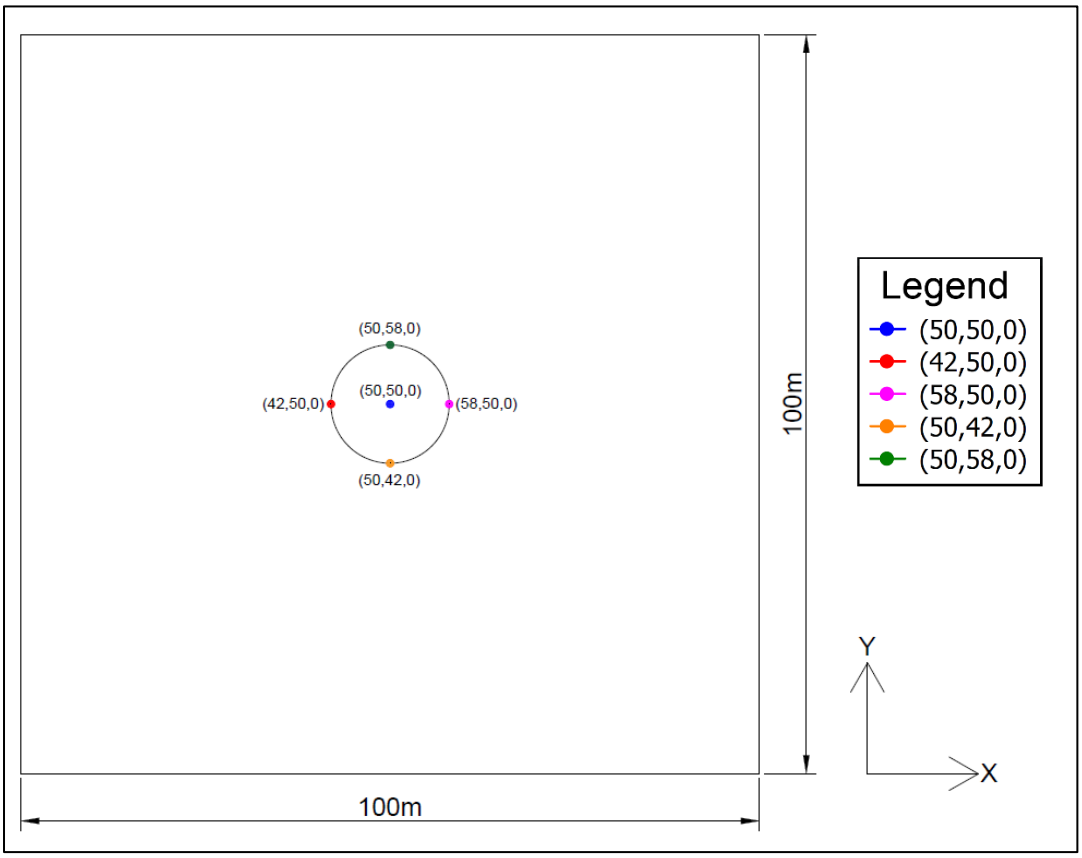


Figure 4-7: *Plan view of model with the reference points labelled*

The settlement curves of these points were generated using Plaxis 3D software and are shown in Figures 4-8 and 4-9 for Case 1 and Case 2 respectively. These curves show the vertical displacement (U_z) of the selected foundation points over the complete serviceability life. The points outlined in black represent the start of each new calculation phase. These settlement curves reiterate the differences in settlement

between the Case 1 sand model and Case 2 clay model. For instance, it is clear that all the majority of the settlement in Case 1 takes place immediately, with very little settlement occuring after day 2. This can be compared to Case 2 where the majority of the settlement occurs between days 32 and 1857 (which is Phase 4: year 1-5). It can also be observed how the total settlements are similar for both Cases, with the total settlement for all foundation points being between 75mm-85mm.

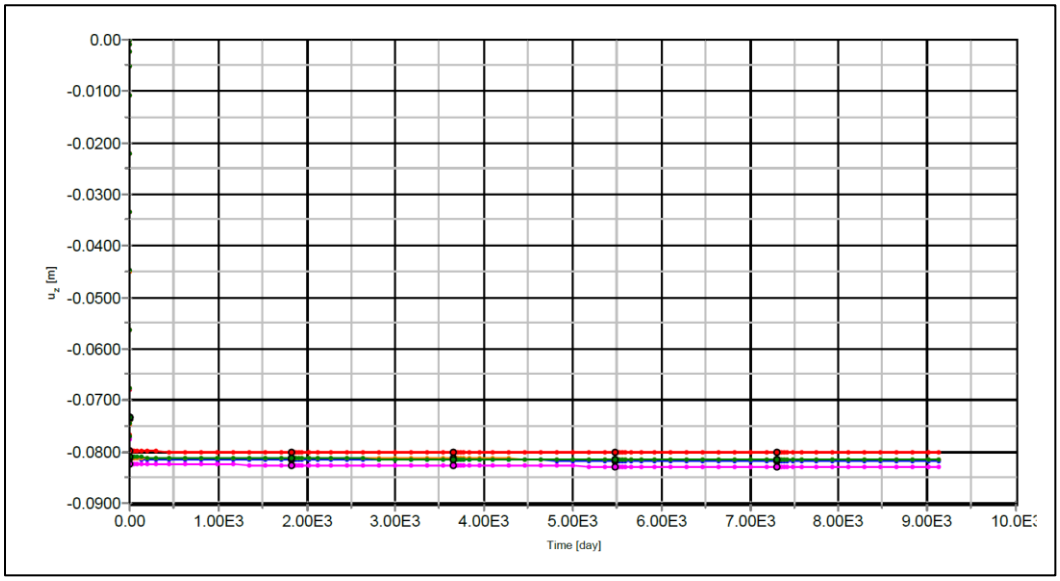


Figure 4-8: *Case 1 settlement vs time*

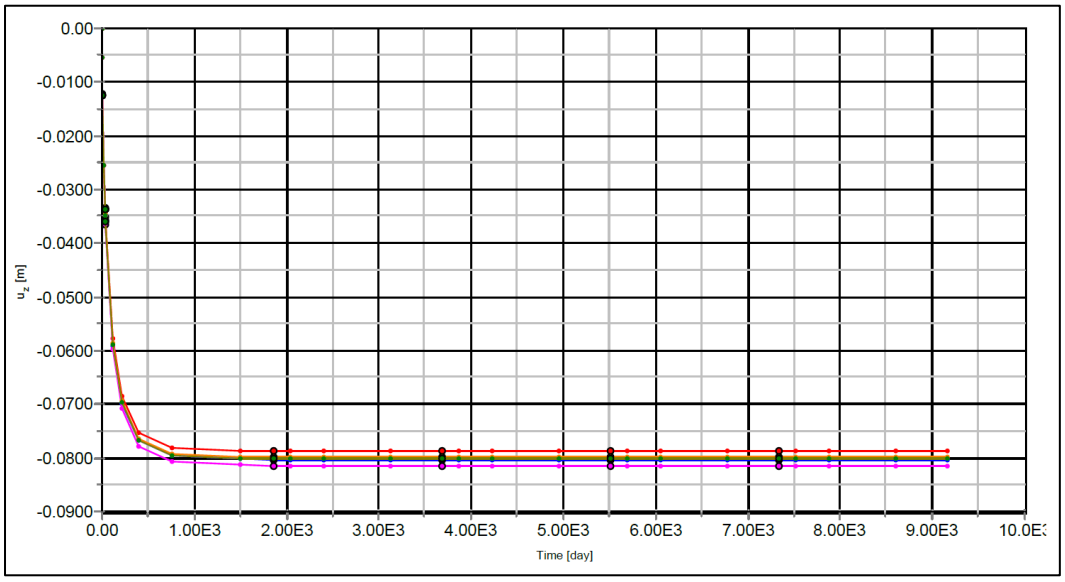


Figure 4-9: *Case 2 settlement vs time*

These settlement curves reiterate the vertical displacement results discussed previously. For further clarity on the foundation tilt behaviour graphs distinguishing between calculation phases were generated. For the purposes of this project, short-term settlement will be defined as the calculation Phases 1 and 2 (0-2 days) for Case 1, and Phases 1-3 (0-32 days) for Case 2. Long-term displacement will consist of Phases 3-7 (2-9,125 days) for Case 1, and Phases 4-8 (32-9,157 days) for Case 2. This time discrepancy was to allow a 30-day consolidation period for the clay layers in Case 2.

4.2.1 Short Term Settlement

The short term settlement-time curve for Case 1 is shown in Figure 4-10. It is clear from this curve that for the sandy soil profile the majority of the settlement occurs during the first day when the foundation is activated, compared to the second day when the load is activated. It can also be observed that during Phase 1 the foundation points vertically displace equally to 73.5mm, with no variance between points. This is in line with expectations as the foundation load on the soil is symmetrical and uniform. Conversely, throughout Phase 2 (Activate loads) the settlement varies from point to point. This is because the turbine loads, inclusive of a vertical load, horizontal load, and overturning moment, are not symmetrical through the center of the foundation. This then causes the foundation to tilt during this phase. The development of the tilt will be shown in greater detail in Figure 4-12.

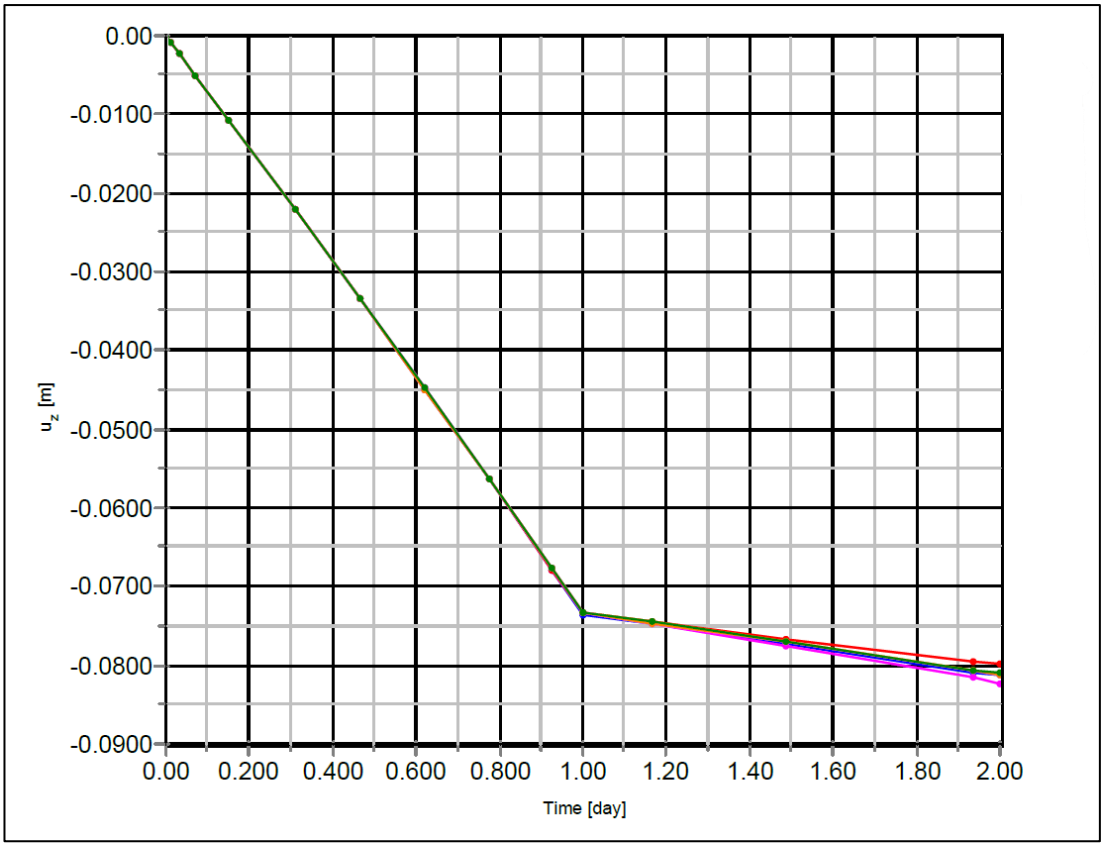


Figure 4-10: *Case 1 (sand) short term settlement-time curve*

The short-term settlement curve of Case 2 is shown in Figure 4-11. This curve demonstrates the vertical displacement of the foundation points over time. The black outlined points signify the start of each new phase. This settlement curve differs hugely from the Case 1 curve shown in Figure 4-10. Firstly, the total settlement at the end of the short-term phases is in the 35-40mm range for Case 2, compared to the 75-85mm range in Case 1. It can also be observed that the majority of the short-term settlement in Case 2 occurs during the 30-day consolidation phase, rather than immediately after the foundation is activated, as is the case in Case 1. One similarity between the two cases is that the displacement of the foundation points is relatively uniform until the turbine load is activated. In Figure 4-11, although the settlement in Phase 3 (Activate loads), from time 30-31 days is relatively small compared to other phases, there is variation between the foundation points at the end of this phase. A standalone settlement-time curve of this phase can be seen in Figure 4-13 in order to observe the occurrence of tilt in greater detail.

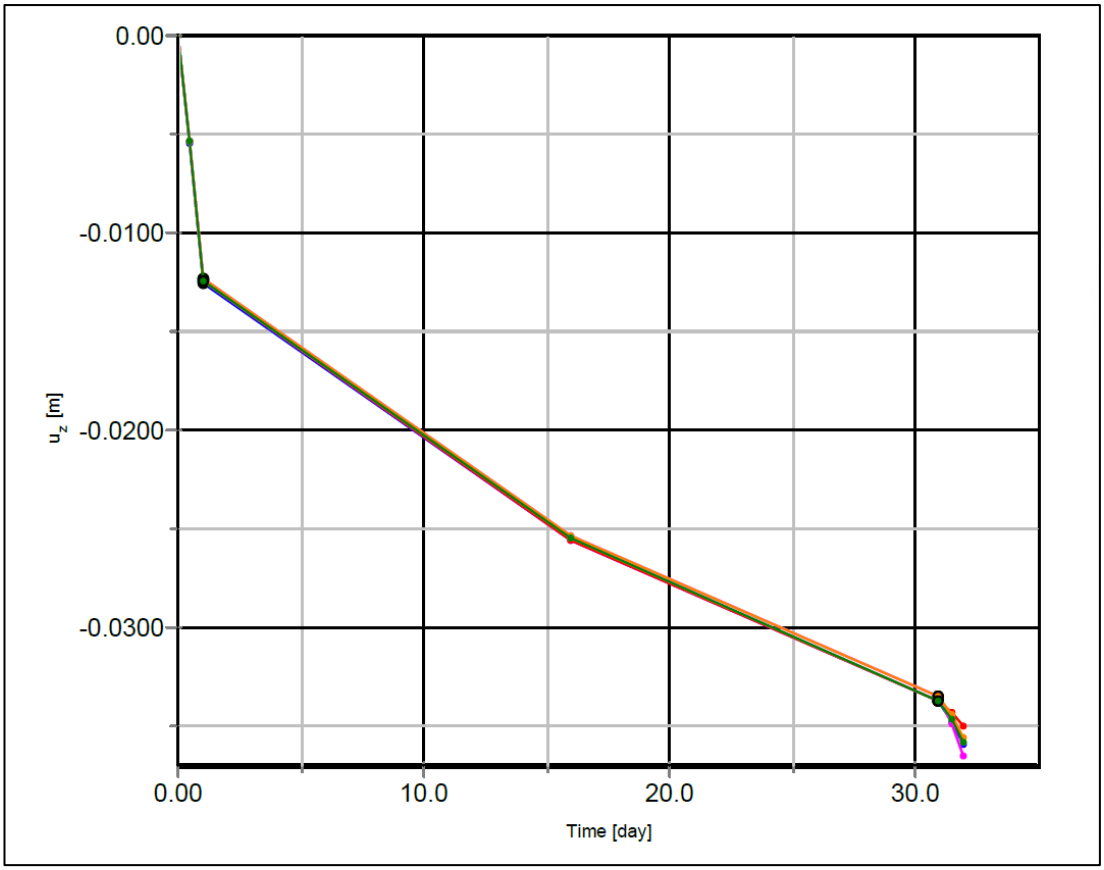


Figure 4-11: *Case 2 (clay) short term settlement-time curve*

The Activate Load phase is the first instance of significant tilt in both Case 1 and Case 2. These phases are presented standalone in Figure 4-12 (Case 1) and Figure 4-13 (Case 2) for greater clarity. In Case 1 it can be observed that at the beginning of Phase 2 (Activate loads) the foundation points are clustered closely together at around u_z = -73.5mm. The order from least to most settlement at this point is (58,50,0), (50,58,0), (50,42,0), (42,50,0), and (50,50,0). Almost immediately at the beginning of Phase 2, these points interchange as the effect of the turbine load is applied. Foundation point (58,50,0) goes from least to most displaced within 0.25 days while, conversely, point (42,50,0) experiences the least amount of displacement in this time ending up with a total settlement 80mm compared to an 82.3mm settlement for point (58,50,0). Points (50,42,0) and (50,58,50) quickly converge with a final short-term settlement of 81.1mm, midway between the extremity points. It is interesting to note how immediate the order of the points is re-established following turbine load activation for the sandy soil model. At the end of the Load Activate phase, the foundation points in order of least to most displaced is (42,50,0), (50,58,0), (50,42,0), (50,50,0), and (58,50,0).

Again, this is the expected outcome based on the load direction applied to the foundation (shown in Figure 3-1). Clearly, the risk of tilt lies between points (42,50,0) and (58,50,0).

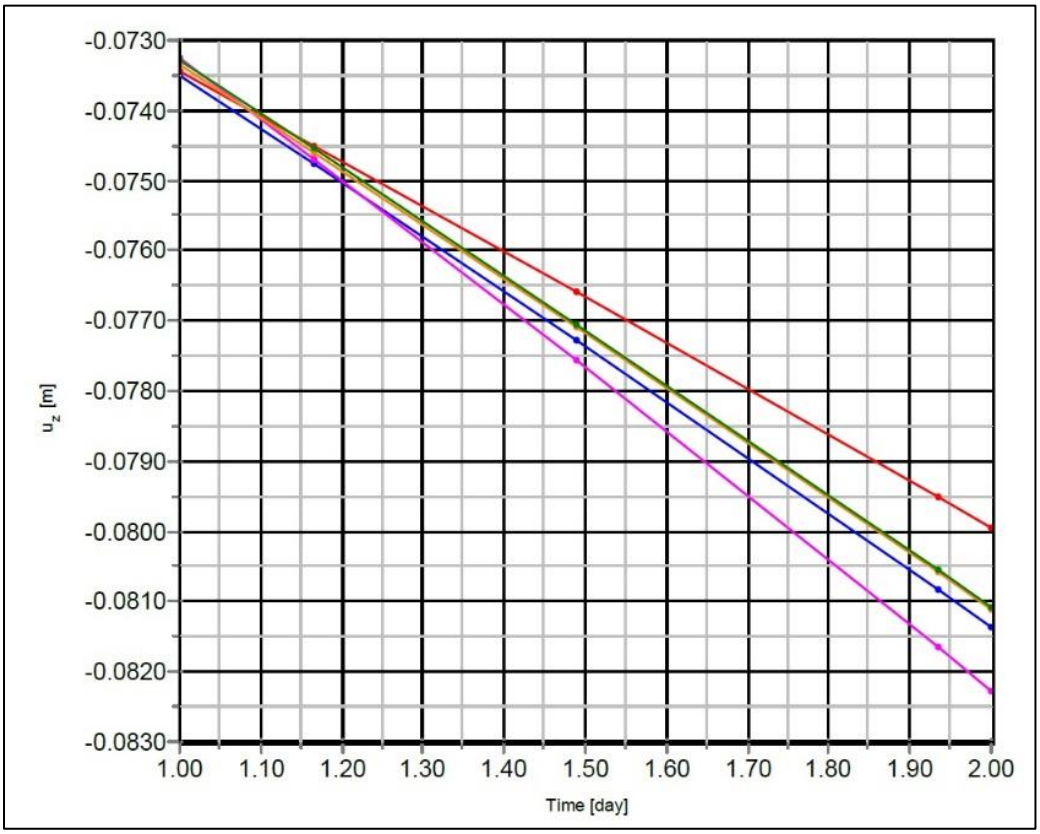


Figure 4-12: *Case 1 (sand). Phase 2: Activate loads settlement-time curve*

Figure 4-13 displays the Activate load phase for Case 2. Similarly to Case 1, the points at the start of this phase are clustered within 0.5mm and have a displacement order of (58,50,0), (50,42,0), (50,58,0), (42,50,0), (50,50,0) from least to most displaced. This starting order is different from the one seen in Case 1; however, the ending order is very similar with point (58,50,0) experiencing the most displacement of u_z = -36.5mm, (42,50,0) experiencing the least displacement of -35mm, and the centre point (50,50,0) being the second most displaced foundation point. One difference in the foundation point order is that in Case 2, point (50,58,0) has a greater final displacement than (50,42,0). Again, the risk of tilt in this phase is between points (42,50,0) and (58,50,0).

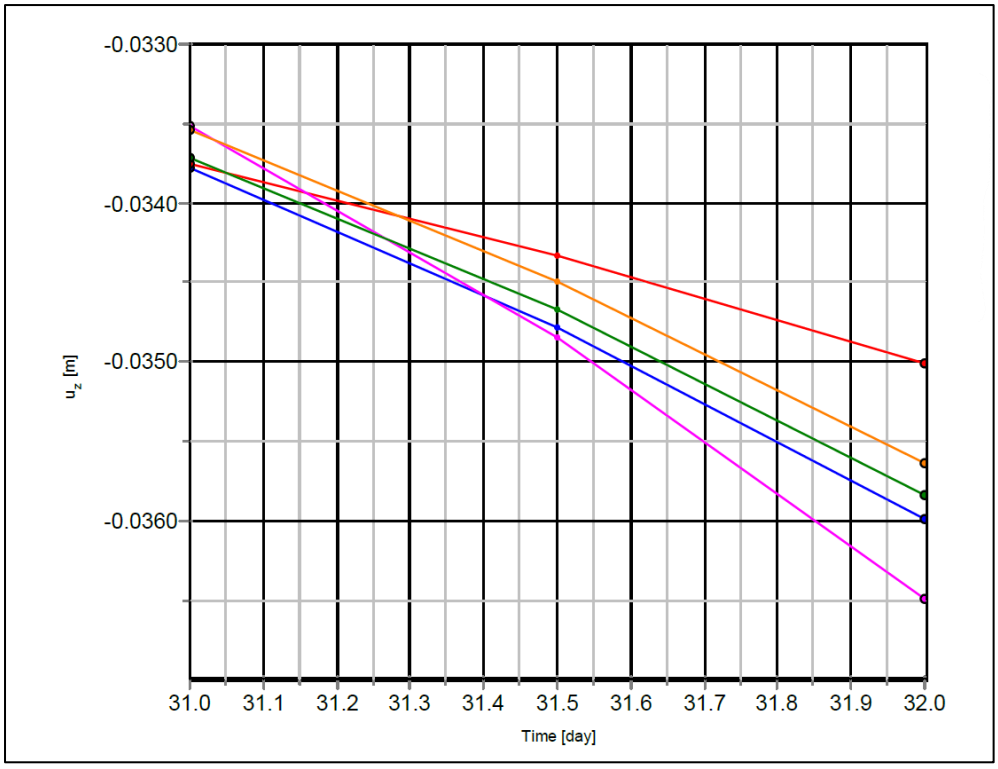


Figure 4-13: *Case 2 (clay). Phase 3: Activate loads settlement-time curve*

Comparing the Activate load phases in the two cases shows that overall, there is less displacement overall in Case 2 than in Case 1. Looking specifically at point (58,50,0) which has the most displacement in most cases, it increases from u_z = -33.5mm to u_z = -36.5mm in Case 2, giving an overall settlement of only 3mm. This is much less than in Case 1 where point (58,50,0) goes from u_z = -73.3mm to u_z = -82.3mm, giving a settlement change of 9mm. It is interesting that, for this point, the settlement in Case 2 is three times the settlement in Case 1. Another difference between the two cases is that in Case 1 the settlement increases linearly throughout the duration of the phase, whereas the same is not true for Case 2 where the rate of settlement increases at t = 31.5 days.

It is also worth noting that although the turbine load includes an overturning moment, there is absolutely no uplift for any foundation points. The vertical displacement is continuously in the downwards direction for both cases. This shows that the downwards vertical load due to the combined buoyant weights of the GBF and the turbine more than compensates for the risk of overturning which is in accordance with the overturning check completed in Chapter 3.

Overall, the short-term settlement shows that while the Activate loading phase did not provoke as much settlement as the Activate foundation phase and, for Case 2 only, the 30-day consolidation phase, it did produce differential settlement between the foundation points. So far, the points of most and least settlement are (58,50,0) and (42,50,0) respectively. Therefore, these points will be used to determine whether the GBF remains within the tolerable tilt of 0.25^{o} during the turbine serviceability lifetime. Prior to this, the long-term settlement results are presented.

4.2.2 Long Term Settlement

The long-term settlement of the GBF constitutes the 25-year period following the Activate loads phase. The settlement-time curves for Case 1 and Case 2 are shown in Figures 4-14 and 4-15 respectively. For Case 1 the time duration is 2 – 9,127 days, and for Case 2 the time duration is 32 – 9,157 days. The beginning of each new 5-year phase is marked with an outlined dot.

In Figure 4-14 it can be observed that there is continuous yet diminutive settlement during the 25-year serviceability life of the turbine. It is also evident that the amount of settlement occurring decreases over time, in that there is more settlement in Phase 3 (Year 1-5) than the ensuing phases. There are different rates of settlement between the foundation points also, for instance point (58,50,0) experiences greater displacement than any other point while point (42,50,0) experiences the least displacement which indicates that the foundations experiences continuous tilting. Points (50,42,0) and (50,58,0) interchange during Phase 3 with the latter experiencing greater settlement than the former. The settlement that occurs during these phases though are almost negligible when compared to the immediate settlement that takes place in Phases 1 (Activate foundation) and 2 (Activate load).

Figure 4-15 shows a vastly different long-term settlement-time curve for Case 2. Here, the vertical displacement of all points increases from the 35-37mm range to about 80mm during Phase 4 (Year 1-5). This phase accounts for the largest amount of settlement in Case 2. In the following phases the settlement remains constant, unlike in Case 1 where there are slight increases during every phase. Overall, each foundation point in Case 1 had a greater final vertical displacement than their counterparts in Case 2, although only by a small margin in each case. Although the final settlement of the

foundation points are all in the 80-83mm range, these curves emphasise the contrast between settlement behaviours of sand and of clay.

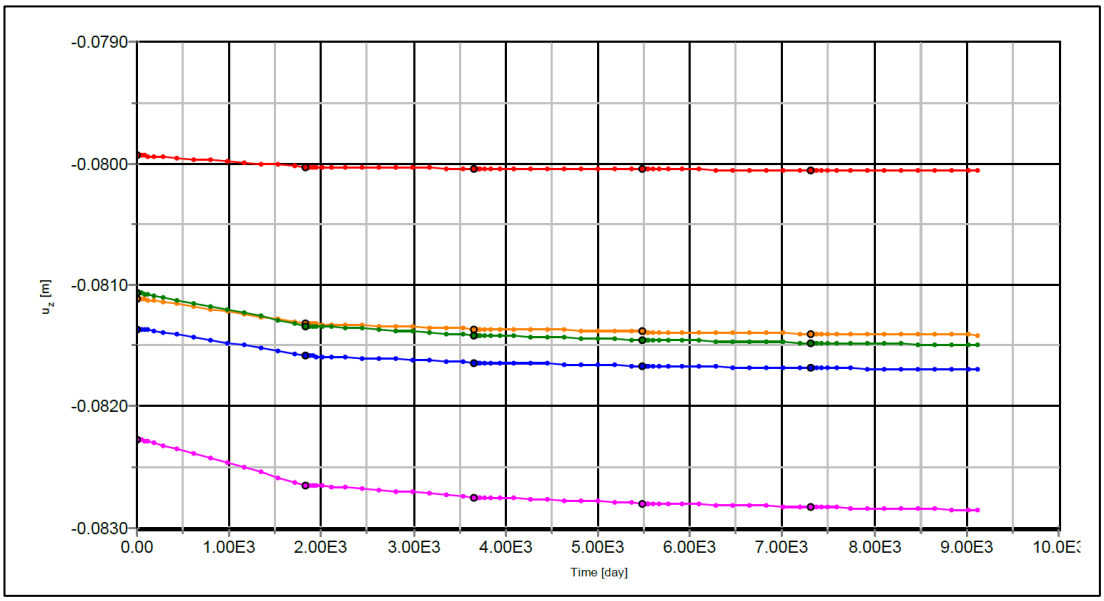


Figure 4-14: *Case 1 (sand). Phases 3-7 settlement-time curve*

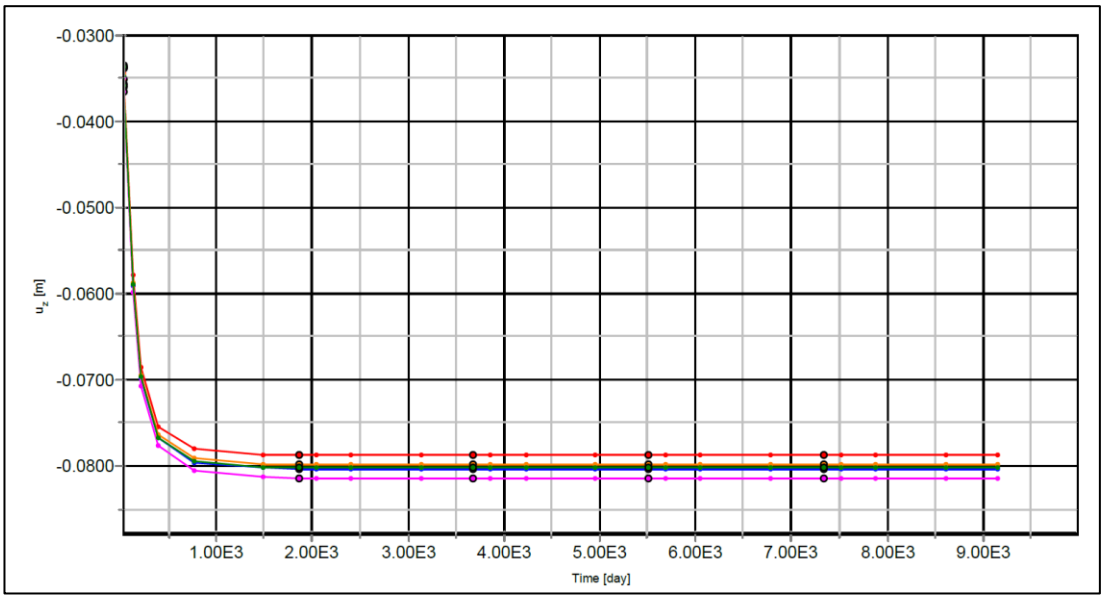


Figure 4-15: *Case 2 (clay). Phases 4-8 settlement-time curve*

From the settlement-time curves in Figures 4-12, 4-13, 4-14, and 4-15 it is obvious that foundation tilt does occur in both Case 1 and Case 2. The points of interest are (42,50,0) and (58,50,0) which one would intuitively expect based on the direction of

the applied loading. The offshore turbine tilt tolerance is 0.25° which, for a GBF of 16m width, gives a maximum differential settlement (ΔS_{max}) of 70mm. Tables 4-4 and 4-5 show the maximum and minimum settlement at each phase following the initiation of tilt, and subsequently the differential settlement at each phase. In Case 1 the different settlement increases in every phase, albeit very slightly during the latter phases. The final differential settlement is the largest with there being a 2.79mm difference between points (42,50,0) and (58,50,0). This is well within the 70mm allowable differential settlement threshold. In Case 2 the greatest differential settlement is 2.68mm occurring in Phase 4, which decreases slightly as point (42,50) settles a further 0.01mm in Phase 5. Following this there is no further change in the differential settlement. The final tilt in Case 2 is 2.67mm, which, again, is much lower than the tolerable limit. It is interesting to note here how the final differential settlement for both Case 1 and Case 2 is very similar, with just a 0.12mm difference between them.

Table 4-4: *Case 1 (sand) differential settlement calculation*

Phase	**Minimum settlement S_{min} (mm)**	**Point**	**Maximum settlement S_{max} (mm)**	**Point**	**Differential settlement ΔS (mm)**
2: Activate loads	-79.93	(42,50,0)	-82.27	(58,50,0)	2.34
3: Year 1-5	-80.03	(42,50,0)	-82.65	(58,50,0)	2.62
4: Year 6-10	-80.04	(42,50,0)	-82.75	(58,50,0)	2.71
5: Year 11-15	-80.05	(42,50,0)	-82.80	(58,50,0)	2.75
6: Year 16-20	-80.05	(42,50,0)	-82.83	(58,50,0)	2.78
7: Year 21-25	-80.06	(42,50,0)	-82.85	(58,50,0)	2.79

Table 4-5: *Case 2 (clay) differential settlement calculation*

Phase	Minimum settlement S_{min} (mm)	Point	Maximum settlement S_{max} (mm)	Point	Differential settlement ΔS (mm)
3: Activate loads	-35.02	(42,50,0)	-36.49	(58,50,0)	1.47
4: Year 1-5	-78.72	(42,50,0)	-81.40	(58,50,0)	2.68
5: Year 6-10	-78.73	(42,50,0)	-81.40	(58,50,0)	2.67
6: Year 11-15	-78.73	(42,50,0)	-81.40	(58,50,0)	2.67
7: Year 16-20	-78.73	(42,50,0)	-81.40	(58,50,0)	2.67
8: Year 21-25	-78.73	(42,50,0)	-81.40	(58,50,0)	2.67

Considering that the differential settlement for both cases was twenty times less than the threshold of 70mm, it was interesting to derive at what load would the gravity-based foundation tilt beyond the tolerable level. Therefore, using the Case 1 sand model, the turbine loading was doubled, tripled and so forth until the threshold was breached. All other aspects of the Case 1 analysis remained unchanged except for the magnitude of the point load and moment. Furthermore, only the short-term displacements were computed (i.e., Phase 1: Activate foundation, and Phase 2: Activate loads) in order to reduce computation time. This was suitable for Case 1 due to the fact that the vast majority of the displacement took place during these phases and not during the long-term analysis.

Figure 4-16 displays a bar chart showing the differential displacement associated with the increasing loads as well as a broken red line denoting the 70mm threshold. The leftmost bar represents the unchanged 1.5MW turbine loads where $\Delta S = 2.3$mm, while the rightmost bar shows the 1.5MW turbine loads multiplied by 13, where $\Delta S = 75.5$mm. The latter load case is the only one which surpasses the ΔS_{max}. This indicates that for this specific GBF on sand, the load would have to be increased by thirteen times before tilt becomes a hazard to serviceability.

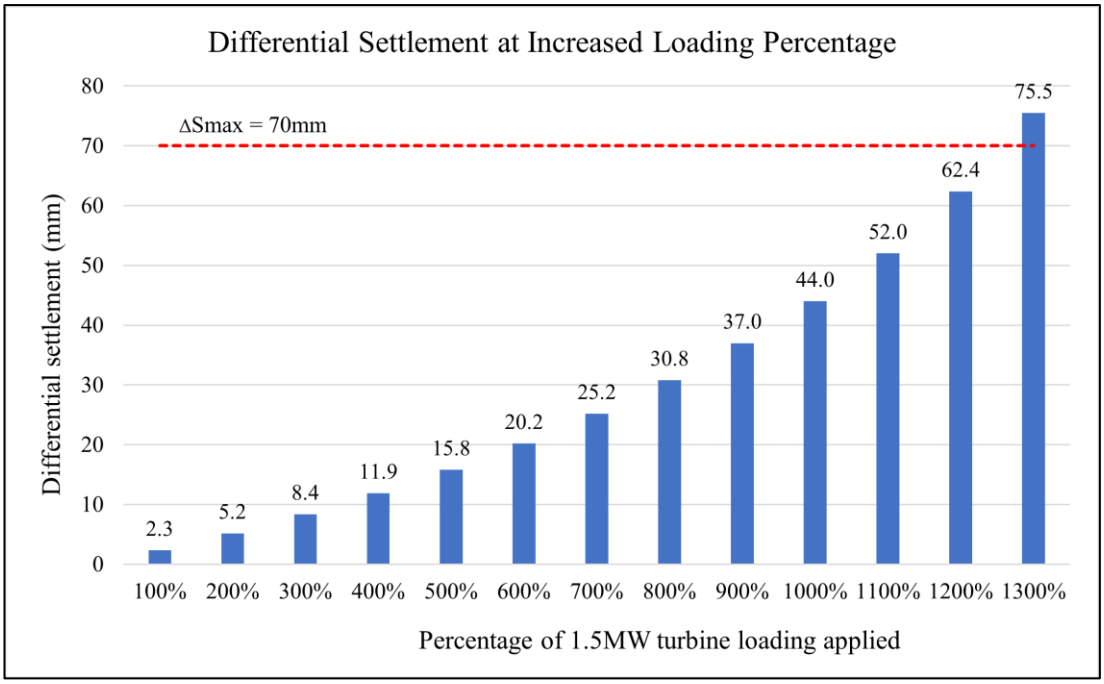


Figure 4-16: *Bar chart displaying the differential settlement results associated with increased turbine loads to determine at what load level would the tilt threshold become unsatisfactory*

4.3 Discussion

In this chapter the feasibility of reusing concrete gravity-based foundations was studied in the context of geotechnical hazards. The design and sizing of concrete GBFs are largely dependent on the design environment, namely, geotechnical parameters and design loads. Firstly, using design methods recommended by global standard agencies, a GBF was designed using real-world geotechnical data for a drained sandy soil profile, and turbine loads based on the AR1500 tidal turbine specifications. Following this, a 3D Plaxis model of this scenario, hereafter referred to as Case 1, was analysed in order to examine the displacement patterns of the soil. Subsequently, a second Plaxis model was created, named Case 2, consisting of two clay soil layers overtopping base sand layers. This model was used to contrast the settlement and tilt of the GBF atop a clayey soil to the sandy environment for which it was initially designed in order to examine the practicality of reusing the GBF in a different geotechnical environment. The results of these analyses were presented in Section 4.2 and will be discussed in this section.

The maximum overall settlement for Case 1 and Case 2 was 82.85mm and 81.40mm, respectively. Although it is evident that the sand experienced more settlement than the

clay, there was a mere difference of 1.45mm between the sandy soil settlement and the clayey soil settlement, demonstrating that, in this specific design, the soil type had little bearing on the vertical displacement of the soil. This is probably because, in order to make a fair comparison, the clayey soil layers selected for Case 2 closely matched the stiffness of the sandy layers they replaced from Case 1, and soil stiffness is a major factor that affects the extent to which shallow foundations settle. Overall, an 81-83mm settlement over a 16m wide foundation does not pose a risk of ultimate limit state violation.

Although there was little difference in the final settlement figures between the two cases, the settlement behaviour of the soils varied significantly. In Case 1, the soil beneath the GBF experienced extensive settlement immediately following GBF placement and load application and continued to undergo minor settlement throughout the serviceability life of the turbine. In contrast, the clayey soil did not vertically displace to the same extent instantaneously following activation of the foundation and turbine loads. Instead, the clay compressed more slowly over time due to the process of consolidation, where soil compression occurs as the excess pore water pressure dissipates slowly over time. Overall, the GBF reached final settlement 5 years after the turbine loads were applied. This would also be longer if there had not been a 30-day consolidation period between activating the foundation and activating the load. This demonstrates a major difference between the two soil profiles, and one that needs to be accounted for in real-world scenarios as offshore turbines are greatly dependent on exact placement for optimal energy conversion. It was also found during this study that the consolidation period of 30-days did not allow enough time for the excess pore water pressure to fully dissipate in the clay soil layers. Therefore, during the turbine activation phase and subsequent five-year phase, the consolidation process for the Activate Foundation phase was ongoing.

Another geotechnical hazard facing reused GBFs is the issue of tilt. Offshore turbines are allotted an allowable tilt of 0.25^{o} to ensure horizontal axis turbines remain in operational range (Smith, Hytiris and Mickovski, 2015). For a 16m wide foundation, this resulted in a maximum allowable differential settlement of 70mm. For the loading conditions described the foundation point with maximum settlement was (58,50,0), while the foundation point that experienced the least settlement was (42,50,0). In Case 1 the final differential settlement between these points was 2.79mm, while Case 2

sustained only 2.67mm of differential settlement. Evidentially, the sandy soil in Case 1 permitted greater tilt than the clay, although the disparity between the two cases was only 0.12mm. Considering the span of this foundation is 16m this is a negligible difference. Again, the final differential settlement results between the sand soil profile and the clay soil profile are extremely similar, indicating that the geotechnical hazards of soil subsidence and tilt are not a barrier to reusing concrete GBFs in these circumstances.

As the final differential settlement for both cases were less than 4% the allowable differential settlement of 70mm, further analysis was completed with increased loading parameters to determine at what loading capacity would the tilt become unacceptable. The results of this analysis indicated that 1300% of the 1.5MW turbine loads would be required to surpass the tolerable tilt level. This is an extremely large discrepancy between the design load and the tolerable load. This indicates that the GBF design may be over-conservative. Over-conservatism occurs as a result of the prescribed design methodology. Firstly, during the design stage there were numerous load and resistance factors applied as per the LRFD method. These factors mainly influence the ultimate limit state checks, namely, the bearing capacity, sliding, and overturning. The actual foundation size was determined using the eccentricity of the loading, i.e., the overturning moment divided by the vertical downwards load. According to the designated design methodology, the minimum allowable radius was then six times the eccentricity. This is a considerable multiplication factor, resulting in a relatively large foundation radius. Furthermore, as the question of this research is the feasibility of reuse, it is worthwhile to examine how the foundation reacted to an increased turbine load. It is well documented in the wind turbine industry that turbines have evolved to be larger and more powerful over time. It is reasonable to suggest that a similar progression could occur in the tidal turbine industry, and indeed has already begun. Therefore, should a concrete GBF be reused following a 25-year deployment period it is logical to assume that it would be required to support a more powerful turbine. Consequently, the over-conservatism of the GBF design methodology could potentially be a positive for reusability.

Overall, this study evaluated the feasibility of reusing concrete gravity-based foundations in the tidal industry with regards to geotechnical hazards, namely, settlement and tilt. It is evident from the results and subsequent discussion that a GBF

designed for deployment in Case 1 sandy soil conditions could also operate in Case 2 clayey soil conditions with no risk of excessive settlement or differential displacement. This indicates that it is indeed feasible to reuse concrete gravity-based foundation within the stipulations that both the loading conditions and the soil stiffnesses remain the same. The geotechnical data taken from marine renewable energy sites in offshore Netherlands are comparable to geotechnical conditions likely to be encountered at a tidal energy site, as it was of extreme importance in the study to use geotechnical parameters from real-world deployment sites. Additionally, the offshore Nertherlands data would not affect the extreme loading case in the design as, per the ultimate limit state recommendations from DNVGL-ST-0164, the extreme load was calculated from the rated operational velocity in the AR1500 brochure. However, tidal turbines may be placed on a variety of seabed sites; therefore, it would be important in future work to include a variety of site conditions as is recommended in Section 6.4. Further study could be completed using varying loading conditions and decreasing soil stiffness, as well as different geotechnical environments outside of sand and clay. In addition to feasibility of reuse, the results of the analysis demonstrated remarkable results with regards to the discrepancy between the allowable settlement and tilt tolerance and the actual settlement and tilt tolerance. This raises questions about the conservatism of the design, however further analysis would be required prior to discussing this thoroughly.

CHAPTER 5

BARRIER 2: DEGRADATION OF GBF

5. Barrier 2: Degradation of GBF

The second barrier to concrete GBF reuse is concrete degradation. Corrosion of rebar steel in concrete leads to a myriad of issues, namely, concrete cracking, delamination, and spalling as well as being detrimental to load-carrying capacity (Neville, 1995; Qiu *et al.*, 2021; Rossi *et al.*, 2021). Corrosion is caused by the ingress of chlorides, water, and oxygen into concrete. Therefore, concrete GBFs would not be reusable should these contaminants exceed the concentration threshold at which corrosion could occur.

From a review of the literature, it is clear that concrete GBFs that are saturated due to long-term submersion are not at risk of corrosion as, although there is water and chlorides present in the environment, there is a paucity of oxygen at the steel-concrete interface (Neville, 1995). However, in the case of reusing concrete GBFs in the tidal industry, a GBF would most likely be placed on a dry dock following decommissioning prior to reuse or relocation. As the concrete dries out, oxygen would ingress into the concrete. To illustrate the issue with this, the concentration and saturation levels of each of the three corroding components are shown throughout the life cycle of a concrete GBF in Figure 5-1, where the pre-deployment and post decommissioning stages are in a dry dock environment and the deployment period is in a fully submerged environment.

Consequently, when studying the feasibility of reusing reinforced concrete following long-term immersion in seawater, it is important to look at, firstly, whether the chloride threshold surpasses critical levels and thus compromises the protective passive layer around the reinforcement steel, and, secondly, at what saturation level can oxygen start to ingress into concrete following decommissioning. These issues are investigated in Sections 5.1 and 5.2, respectively.

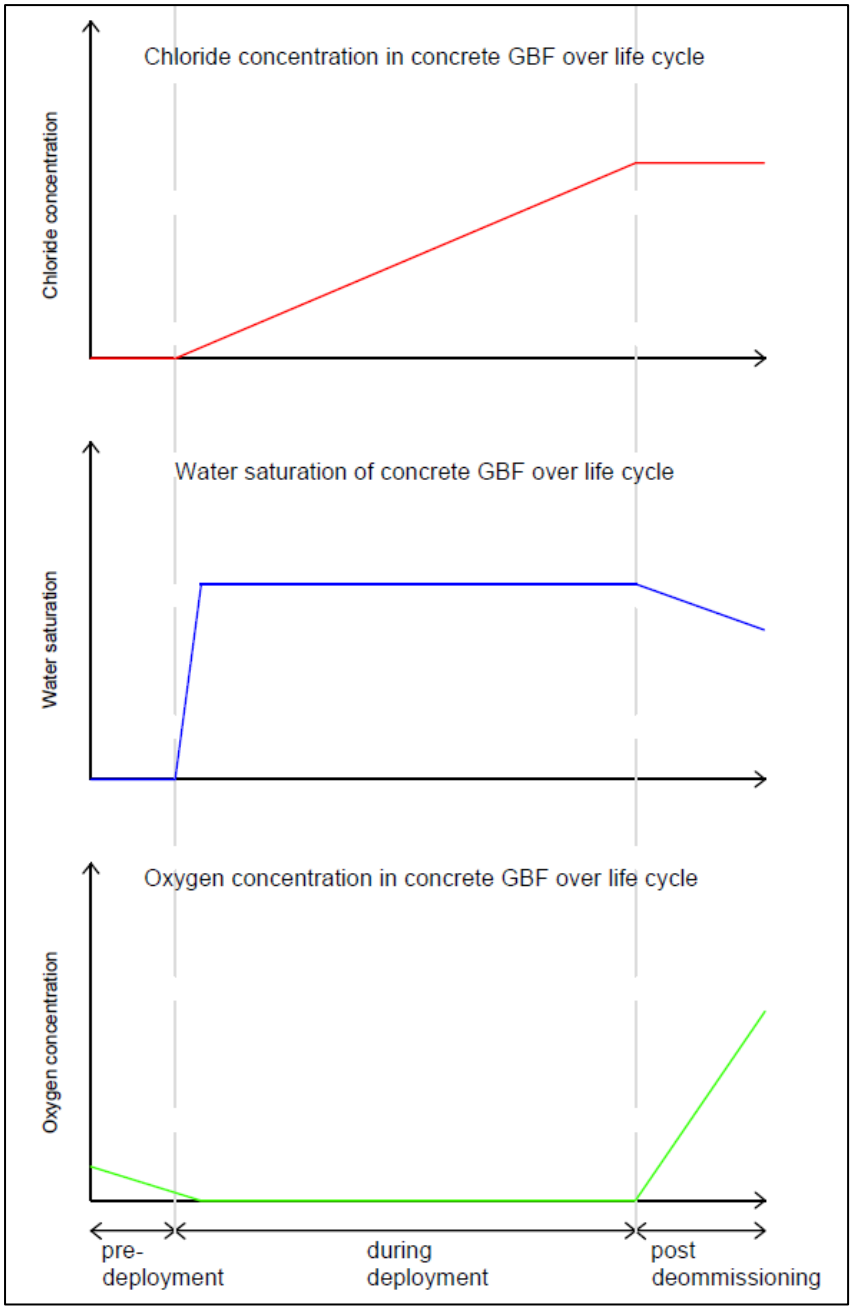


Figure 5-1: *The varying concentrations of contaminants in the concrete over the life cycle of the GBF*

5.1 Chloride Ingress

This section outlines the methodology and results of a chloride ion ingression analysis in order to determine if the chloride levels in the concrete GBF surpass the allowable threshold following a 25-year deployment period, and subsequently, whether the protective passive layer around the reinforcement steel is damaged. This analysis is critical with regards to the feasibility of reusing concrete GBFs as a compromised

passive layer leaves the steel at high risk of corrosion once oxygen becomes available, which could render the concrete unsuitable for reuse.

5.1.1 Methodology

Model Selection

In mathematical modelling, Fick's second law of diffusion (Eq. (5-1)) has been widely used to quantify chloride diffusion in the literature (Collepardi, Marcialis and Turriziani, 1972; Wu *et al.*, 2016; Cai *et al.*, 2020), and often serves as a basis for other mathematical models (Löfgren *et al.*, 2016). As determined in the literature review, diffusion is the governing transport mechanism of chloride ions in concrete in submerged environments (Shakouri and Trejo, 2018). Therefore, Fick's second law of diffusion was deemed a suitable mathematical model to use for the prediction of chloride ingress into the concrete GBF in this study.

$$\frac{\partial C}{\partial t} = D\frac{\partial^2 C}{\partial x^2}$$

(5-1)

The analytical solution to Fick's second law presents the chloride concentration as a function of depth and time, assuming constant surface chloride concentration and apparent diffusion coefficient (Sun, Liang and Chang, 2012), as shown in Eq. (5-2):

$$C(x,t) = C_s\left[1 - erf\left(\frac{x}{2\sqrt{tD_{app}}}\right)\right]$$

(5-2)

where C (% by weight of cement) is the chloride concentration, C_s (% by weight of cement) is the surface chloride concentration, x (m) is the depth, t (s) is the exposure time period, D_{app} (m^2/s) is the apparent diffusion coefficient, and erf is Cranks error solution. Depassivation occurs once the chloride content at the location of the steel reinforcement (C(x,t)) surpasses a critical chloride threshold (C_{crit}) (Khitab, Anwar and Arshad, 2017).

Parameter Development

For the case-study GBF, x, the depth below the concrete surface, was 50mm, as this is the required concrete cover for exposure class XS2 (EN1992-1-1, 2004; DNVGL-ST-0126, 2018). The time, t, was taken as 25 years as per the 25-year serviceability life

of tidal turbines, and by extension, the amount of time the foundation would be in-situ (Lande-Sudall, Stallard and Stansby, 2019). In order to obtain values for the surface chloride concentration, C_s, the apparent diffusion coefficient, D_{app}, and the critical chloride concentration, C_{crit}, it was necessary to consult the available literature in this area. Several studies have been dedicated to the characterisation of these key service life parameters using experimental methods.

Long-term exposure field tests have been used to determine the chloride ingress parameters, namely, the apparent diffusion coefficient and the surface chloride concentration. Luping (2003) conducted a comprehensive study measuring the chloride ingress into a diverse range of concrete specimens with differing water-binder ratios, cement products and compressive strengths over a 10-year interval, under varying environmental and exposure conditions. The resulting chloride concentration curve was fitted using Fick's second law of diffusion. This study found that D_{app} and C_s are time-dependent parameters, with C_s increasing for the first five years of exposure and remaining constant thereafter. Fick's second law was also employed during a Starrs *et al.* (2008) chloride profiling study which examined nine concrete pier-stems and three exposure zones over an 8-year period. A 7-year study of chloride ingress was conducted by Nanukuttan *et al.* (2008). Again, this study used Fick's second law for nonlinear regression curve-fitting considering different exposure conditions The main disadvantage of long-term exposure to the natural environment is the extensive periods of time and resources required to conduct such experiments. Therefore, in-lab chloride ingress tests have been developed to reduce experimentation time.

The 90-day salt ponding test is a long-term experimental method of measuring chloride penetration into concrete, in which Fick's second law would be fitted to the results in order to obtain numerical values for D_{app} and C_s (McGrath and Hooton, 1999). However, the effects of sorption and wicking, as well as other chloride transport mechanisms, may influence the experimental results (Stanish, Hooton and Thomas, 1997). To overcome some of these issues, bulk diffusion tests, namely, Nordtest NT Build 433 (NT Build 433, 1995) and ASTM C1556 (ASTM C1556, 2016), were developed. As diffusion is the dominant transport mechanism in saturated concrete, bulk diffusion tests only allow the transport of chlorides by diffusion (Stanish and Thomas, 2003). Recently, Al-Sodani *et al.* (2021) used the NT Build 433 bulk

diffusion method to determine the effect of temperature on the apparent diffusion coefficient using field specimens in a natural environment for comparative purposes.

It is clear from the literature that there are myriad experimental techniques for obtaining the chloride ingression parameters, D_{app} and C_s. For the purposes of this study the data procured from natural exposure techniques were deemed highly reliable as they are used for validation of more modern, short-term ingress measurement techniques (Al-Sodani *et al.*, 2021). The design standards recommend that offshore renewable energy concrete support structures in XS2 exposure class meet certain requirements, including a minimum compressive strength of C35/45, and a maximum water-to-cement ratio of 0.45 (DNVGL-ST-0126, 2018). Therefore, the values of D_{app} and C_s used in the ingress analysis herein originated from three long-term field studies of OPC concrete that met these criteria with the full details described in Table 5-1.

Table 5-1: *Values for the surface chloride concentration and apparent diffusion coefficient from the literature*

Surface chloride concentration C_s	**Apparent diffusion coefficient D_{app}**	**Water to binder ratio w/b**	**Compressive strength**	**Exposure period**	**Source**
% by weight cement	m^2/s x 10^{-12}	-	MPa	Years	-
5.82	2.90	0.4	63	8	(Starrs *et al.*, 2008)
5.10	3.13	0.4	66	7	(Nanukuttan *et al.*, 2008)
2.15	1.44	0.4	67	10	(Luping, 2003)

Methods of determining the critical chloride concentration C_{crit}, vary widely in the literature, with a broad range of values documented (Löfgren *et al.*, 2016). Angst *et al.* (2009) outlined various experimental methods that have been utilised to establish the critical chloride threshold, namely, linear polarisation resistance measurements (LPR), steel potential, electrochemical impedance spectroscopy (EIS), and weight loss. However, these methods rely on a certain level of active corrosion which occurs after depassivation. In order to overcome these limitations, Käthler *et al.* (2019) created a novel, open-access database to collect and store critical chloride contents in

concrete. A novel experimental method for determining C_{crit} that also addresses the previous experimental limitations, was recently proposed by Fakhri, Fishman and Ranade (2020). This method utilises a linear relationship between chloride content and corrosion pit-depth to find the critical chloride concentration. There is some disagreement amongst experts with regards to the best way to present critical chloride levels but generally total chloride content expressed relative to the weight of cement is widely accepted (Glass and Buenfeld, 1997). A durability study by Luping and Löfgren (2016) estimated a critical chloride threshold as 1% (by mass of cement) for CEM 1 concrete structures under a marine environment. Nanukuttan *et al.* (2008) suggested a value of 0.5% (by weight of cement), citing the tidal environment as justification for the reduced figure. As the value of C_{crit} is subject to debate amongst experts, the chloride ingress analysis in this study considered both lower and upper C_{crit} values of 0.5% (by weight cement) and 1% (by weight cement) respectively, for a more comprehensive analysis.

MATLAB Analysis

As discussed above, the chloride ingress analysis was completed using Fick's second law of diffusion in conjunction with relevant values for C_s, D_{app} and C_{crit}. MATLAB software was used to determine whether Fick's diffusion equation (Equation 5-2) satisfied Equation 5-3 for any of the selected ingress parameters from the literature. Please refer to Appendix F to view the MATLAB code. The results of this analysis are presented in the following section. For concrete GBF reuse to remain a possibility, the chloride concentration at the steel surface must remain below the critical chloride concentration, C_{crit}. That is to say, Equation 5-3 must be satisfied for x = 50mm and t = 25 years:

$$C(x,t) < C_{crit} \qquad (5\text{-}3)$$

Hydrostatic Pressure

Additionally, recent studies have found that the diffusion behaviour of concrete may be greatly impacted by hydrostatic pressure. Experimental results found that the diffusion coefficient under 0 MPa conditions is just 18.2% of the diffusion coefficient under 0.3MPa conditions (Liu and Jiang, 2021), which are conducive with a 30m water depth, conditions representative of GBF for tidal turbines. Therefore, an additional

analysis was completed with the D_{app} values modified to account for hydrostatic pressure. These values are presented in Table 5-2 with '(P)' to denote that the data has been modified to account for pressure. Similarly to the original values, this data underwent chloride ingress analysis to determine if the chloride concentration surpassed critical levels, making reuse impractical.

Table 5-2: *Modified values for surface chloride concentration and apparent diffusion coefficient accounting for hydrostatic pressure*

Name	**Surface chloride concentration C_s**	**Modified apparent diffusion coefficient D_{app}**
	% by weight cement	$m^2/s \times 10^{-12}$
Starrs (P)	5.82	15.93
Nanukuttan (P)	5.10	17.20
Luping (P)	2.15	7.91

5.1.2 Results and Discussion

The results and discussion of the chloride ingress analysis are presented in this section. Figure 5-2 shows a graph consisting of three chloride concentration profiles based on the values from Table 5-1 following a 25-year submersion period. The 50mm concrete cover depth is represented by a dot-dash black line, while the lower and upper critical chloride thresholds of 0.5% (by weight cement) and 1% (by weight cement) are represented by a dashed red line and a dotted red line, respectively.

It can be seen from Figure 5-2 that the Starrs, Nanukuttan and Luping parameters result in chloride concentrations at the reinforcement depth of 2.675% (by weight cement), 2.431% (by weight cement), and 0.632% (by weight cement) respectively. Clearly, all three chloride profiles are greater than the lower C_{crit} threshold of 0.5% (by weight cement) at the 50mm concrete cover depth. This indicates that the protective passive barrier would be compromised, and thus, there is a high risk of corrosion occurring which would render the concrete unsuitable for reuse. Although the Luping dataset does not surpass the critical chloride threshold for the less conservative C_{crit} value of 1% (by weight cement), two of the three selected datasets still greatly exceed the upper C_{crit} threshold, and this, coupled with the fact that all three datasets exceed the lower

C_{crit} threshold, indicates that this analysis does not support the feasibility of reusing concrete GBFs due to the high risk of corrosion once oxygen becomes available.

Figure 5-2 also shows that the Luping parameters (solid green line) result in significantly less chloride concentrations for all depths when compared to the Starrs (solid purple line) and the Nanukuttan (solid blue line) parameters. There may be myriad reasons for the discrepancy here. Both Starrs and Nanukuttan parameters were taken from exposure sites in Northeast Scotland, while Luping parameters were taken from the Träslövsläge field site in Sweden. This could explain the similarities between the Starrs and Nanukuttan parameters. It may also be the case that the conditions in the Träslövsläge field site could be less hostile. It is also true that the compressive strength of the Luping concrete is greater than the other two datasets as shown in Table 5-1, although the variation is minimal.

The overall results indicate that the OPC concrete is not conducive to the concept of reuse, with all three concrete samples surpassing the critical chloride concentration. Studies have shown that a mix of 40% OPC + 60% GGBS replacement has greater durability in the marine environment than a 100% OPC concrete (Ryan and O'Connor, 2014; Otieno, Beushausen and Alexander, 2016). Further studies would need to be conducted on this topic in the context of reuse, however a concrete mix of GGBS and OPC could make for a more practical, reusable GBF for tidal turbines.

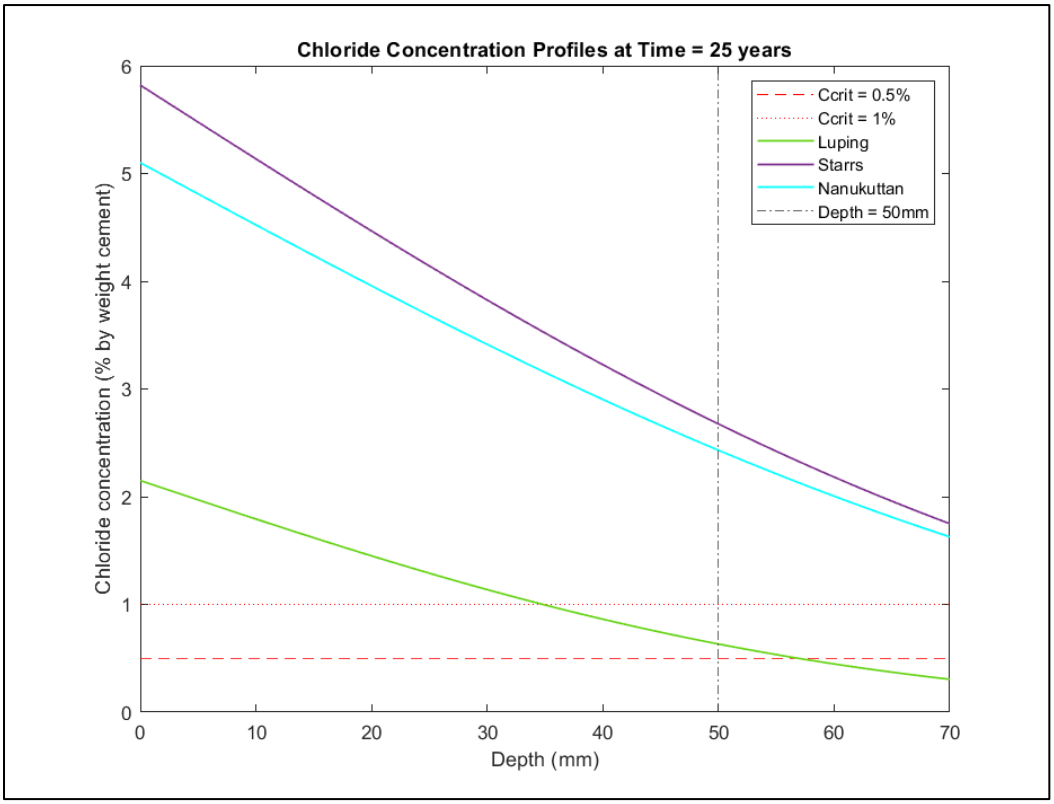


Figure 5-2: *Chloride concentration profiles comparing three sets of long-term exposure chloride ingress parameters after 25 years. These profiles were developed in MATLAB using Fick's second law of diffusion.*

Figure 5-3 shows the three chloride profiles modified for a 30MPa water pressure that corresponds with 30m of water (please refer to Table 5-2 for the key chloride ingress parameters). For ease of understanding the line types and colours correspond with Figure 5-2. As with the results from the unmodified datasets, the chloride profiles from the modified datasets do not indicate that reuse of concrete GBFs is feasible as the chloride concentration at the depth of reinforcement exceeds both the lower and upper critical chloride threshold in modified chloride profiles. Once again, the Luping (P) parameters are much lower than either the Starrs (P) or Nanukuttan (P) parameters, however, the modified D_{app} coupled with the unchanged surface chloride concentration results in much flatter curves than the unmodified profiles.

It is clear from a comparison of both graphs that the final chloride concentrations under hydrostatic pressure are significantly higher than the results that do not take 30m of water pressure into account. Table 5-3 presents a side-by-side comparison of the final results from both analyses for greater clarity. The increase in chloride concentration due to hydrostatic pressure is 1.704%, 1.452%, and 1.024% for the Starrs, Nanukuttan,

and Luping datasets, respectively. In a field where the chloride threshold value is typically less than or equal to 1%, this is a significant increase. This shows the need for further investigation on the effects of hydrostatic pressure on chloride ingress, as it is a relatively new field of study.

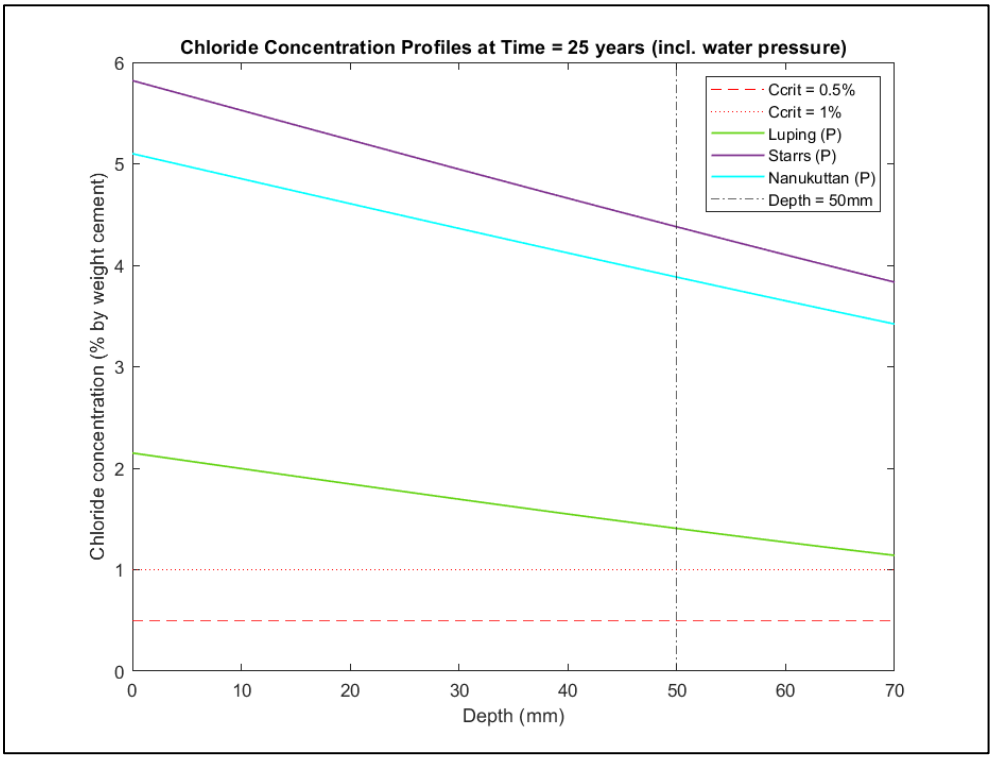


Figure 5-3: *Chloride concentration profiles comparing three sets of long-term exposure chloride ingress parameters after 25 years with modified parameters to account for water pressure*

Table 5-3: *Comparison of modified and unmodified chloride concentration values at a depth of 50mm and a time of 25 years*

Data source	**Chloride Concentration at Depth = 50mm and Time =25 years (% by weight cement)**	
	Water pressure not included (Figure 5-2)	Water pressure included (P) (Figure 5-3)
Starrs	2.675	4.379
Nanukuttan	2.431	3.883
Luping	0.632	1.407

Overall, the results from the unmodified datasets demonstrated that it would not be practicable to reuse and redeploy the concrete GBF as the chloride concentration level indicates that the passive layer would be compromised and thus, there would be high risk of corrosion should sufficient levels of oxygen and water reach the steel surface. The calculation and modelling of chloride profiles modified to account for water pressure reiterated this finding with even higher levels of chloride at the steel-concrete interface, but further study is required into how hydrostatic pressure affects chloride ingress into concrete in general.

5.2 Oxygen Availability and Water Saturation Degree

Aside from chlorides, the presence of water and oxygen are required for corrosion. The literature clearly states that structures in the submerged zone are typically at low risk of corrosion as moisture-filled concrete pores block the transport of oxygen (Hussain and Ishida, 2010). However, in a scenario of reuse, where concrete GBFs would be extracted from the seabed following decommissioning of the tidal turbine, they would likely be placed on a dry dock prior to a second deployment. This would put the concrete GBF at risk of corrosion due to the renewed availability of oxygen in chloride-contaminated concrete. Therefore, it is necessary to investigate the availability and transport of oxygen and water and examine the inter-relationship between them. The modelling of oxygen availability as a function of water saturation degree is a complex subject, which was deemed beyond the feasible scope of this MSc research project. This section does however conduct an initial investigation into this novel GBF consideration through assembly and presentation of oxygen availability methods and findings from the literature that may be used for future work on the feasibility of reusing concrete GBFs.

5.2.1 Oxygen Transport

Firstly, the transport of oxygen is of significance in the study of corrosion, particularly in this instance where risk of corrosion is dependent on the transport of oxygen through newly decommissioned drying concrete. Fick's second law, formed of Fick's first law and the mass conservation principle, is commonly used to investigate oxygen diffusion in concrete. Equations 5-4 and 5-5, sourced from Khatami, Hajilar and Shafei (2021), describe the diffusion of oxygen through concrete:

$$J_{O_2} = -D_{O_2} \nabla C_{O_2}$$

(5-4)

$$\frac{\partial C_{O_2}}{\partial t} + div(J_{O_2}) = 0$$

(5-5)

where J_{O2} is the flux of oxygen (kg/m^2.s), D_{O2} is the oxygen diffusion coefficient, and C_{O2} is the dissolved oxygen concentration in the concrete's pore solution.

Due to the complexity of boundary conditions, time dependence, and various geometries that need to be accounted for, researchers have developed state-of-the-art numerical frameworks to solve the partial differential equation and model the diffusion of oxygen through concrete. Such numerical frameworks include finite element analysis and cellular automation computational frameworks (Hussain, Ishida and Wasim, 2012; Khatami, Hajilar and Shafei, 2021; Yu *et al.*, 2021).

5.2.2 Oxygen Availability as a Function of Water Saturation Degree

It is widely accepted that the oxygen diffusivity of concrete is significantly affected by saturation degree as moisture-blocked pores prevent gaseous oxygen ingression (Yoon, 2018). Therefore, rather than calculating the diffusion of oxygen into concrete, many researchers sought to determine at what saturation state is concrete at low risk of corrosion. There is variation in the results, which range from lows of 90% saturation (Huet *et al.*, 2007) to 100% saturation (Hussain, 2011). A moisture state comparable with the long-term submersion of tidal turbine GBFs was characterised by Raupach (1996b) as 'long-term wetting'. Raupach states that "wetting is characterised as long-term if the effects of water penetration results in oxygen deprivation at the steel surface". For this moisture condition it was found that the corrosion rate rises to its initial pre-wetting value after the wetting stage indicating that there is no long-lasting oxygen deprivation at the steel surface following long periods of submersion. However, this conclusion is in contrast to a more recent study which found that submerged concrete specimen's experience reduced porosity and connectivity and subsequently reduced oxygen permeability due to a reactivation of the processes of curing and hydration (Hussain and Ishida, 2010).

In general, there appears to be little agreement on both the behaviour of concrete following long periods of submersion, and the exact level of saturation at which oxygen can ingress into chloride-contaminated concrete and cause corrosion. Findings do indicate, however, that the range at which chloride-contaminated concrete is at low risk of corrosion is from 90% to 100% saturation. Therefore, it is entirely possible that a modified concrete drying model could be utilised to determine how long a GBF could be allowed to stay on a dry dock following decommissioning before the saturation levels drop below this range where risk of corrosion rises and makes reuse infeasible.

5.2.3 Concrete Drying Models

The movement of moisture in concrete has long been studied due to the process of, and issues caused by, concrete drying and drying shrinkage. Concrete contracts and develops cracks as a result of drying shrinkage, which is caused by the loss of capillary water from the cement mixture that has dried and hardened (Awoyera, Babalola and Aluko, 2022). Many studies are therefore dedicated to the drying rate of porous materials (Courtois, Taillade and Placko, 2020; Kinda *et al.*, 2022) and thus, although not intended for such, can provide insights into the rate of drying of saturated GBF while sitting on a dry dock after decommissioning.

One of the first concrete drying models, upon which many other studies are based, was presented by Bažant and Najjar (1971), in which drying is defined by the moisture diffusivity at constant temperature. The diffusion problem of drying was found to be nonlinear as the diffusion coefficient must be treated as a function of pore relative humidity. More recently, it has been reasoned that concrete drying not only depends on temperature, humidity and air flow, but also the hydration process and subsequent changes in the material properties during this process; factors which are ignored by the earlier simplistic models (Sekki and Karvinen, 2017). These factors are accounted for by Sekki and Karvinen (2017) in the following partial differential equation system that describes heat and moisture transport in concrete (Equation 5-6 and Equation 5-7):

$$\rho C_p \frac{\partial T}{\partial t} = \nabla \cdot \left[k \nabla \mathrm{T} + L_v \delta_p \nabla(\phi p_{sat})\right] + Q$$

(5-6)

$$\xi \frac{\partial \phi}{\partial t} = \nabla \cdot \left[\xi D_w \nabla \phi + \delta_p \nabla (\phi p_{sat})\right] + S$$

(5-7)

where ρ is the density (kg/m^3), Cp is the specific heat capacity (J/kgK), T is the temperature (K), t is the time (s), k is the thermal conductivity (W/mK), L_v is the latent heat evaporation (J/kg), δ_p is the water permeability (s), p_{sat} is the saturation pressure (Pa), Q is the heat source (J/kg), ξ = dw/dϕ is the moisture storage capacity (kg/m^3), w is the water content (kg/m^3), D_w is the liquid water diffusion coefficient (m^2/s), and S is the moisture sink (kg/m^{3}s). This partial differential system was solved by the authors using finite element analysis under the boundary conditions of convective heat and moisture flux (Sekki and Karvinen, 2017).

Kamran and Sarkar (2019) outline the importance of investigating drying processes that commence from a completely saturated state, calling unsaturation the process of extended drying following exposure to moisture. An experimental investigation into the drying processes of saturated concrete revealed that there are two stages to the drying process (Šelih and Bremner, 1996). While the diffusion process and coefficient of diffusion, affected by the moisture content, are often used to describe the entire drying process of concrete, it was found that this only applied to the later stages of drying where moisture movement is primarily driven by diffusion, and concentration gradients cause water vapour and bound water to move towards the concrete surface. In fact, the experiment demonstrated that free liquid water was present in the concrete pores indicated by a constant drying rate when drying commenced and moisture contents were high. During this earlier stage, the flux of water was more rapid than during later drying stages, due to capillary forces and pressure gradients. It is therefore recommended that a Darcy-type equation be used to describe the drying process in the early stages, while the diffusion equation can continue to be used for the late stage of drying (Šelih and Bremner, 1996).

The Darcy equation is again referred to by Holmes (2009) when referring to the principle flow mechanisms in concrete, namely permeability, sorption and diffusion. Darcy's law can be applied to any fluid moving through a porous medium, as demonstrated in Equation 5-8, where v is the apparent velocity of flow (m/s), k is the intrinsic permeability (m^2), η is the dynamic viscosity of the fluid (Ns/m^2), and dp/dL

is the pressure gradient in the direction of flow. Equation 5-10 expands on the relationship between k and K, where K is the permeability (m/s), ρ is the density of the fluid (kg/m^2), g is the acceleration due to gravity (m^2/s).

$$v = -\frac{k}{\eta}\frac{dp}{dL} \quad (5\text{-}8)$$

$$k = \frac{K\eta}{\rho g} \quad (5\text{-}9)$$

However, it has also been reported that conventional moisture transport models including Darcy's law and Fick's law cannot capture anomalous moisture movement in concrete structures, and mathematical models based on phenomenological and mechanistic approaches have been developed to describe moisture transport (Zhang and Angst, 2020). Zhang and Angst (2020) used a finite differential method to solve a time-/saturation-dependent permeability/diffusivity model to correctly capture anomalies in moisture transport. Again, the complexities of these models surpass the scope of an MSc research project but form a basis for future work in this area.

5.2.4 Summary

In Section 5.1 it was found that the chloride concentration profiles indicated that the protective passive at the steel-concrete interface was damaged. However, corrosion does not occur without the presence of water and oxygen, and concrete under submersion is at very low risk of corrosion, even past the critical chloride threshold, due to a paucity of oxygen at the steel-concrete interface. Therefore, it was imperative to investigate the risk of corrosion of a concrete GBF in a dry-dock environment following decommissioning, assuming that the critical chloride threshold has been breached and the passive layer compromised.

The work described in Section 5.2 aimed to address this area of study but found that the complexities of modelling oxygen ingress as a function of water saturation degree surpassed the feasible scope of an MSc project. Consequently, the section focussed on compiling and presenting the relevant equations, methodologies, and findings from the literature which pertain to the topic of reuse that will be useful for future work. It

was found that water saturation level would have to drop below a range of 90%-100% for oxygen ingress to initiate. From these findings it could be possible to ascertain how long a concrete GBF of certain geometry could be placed on a dry dock in between deployment periods before the saturation levels decrease enough for oxygen to ingress and cause corrosion. In theory, a concrete GBF could be at low risk of corrosion for limited time-periods under the correct drying circumstances, making reuse possible. Diffusion equations are mainly used in literature to model the movement of moisture in concrete; however, it was found that in the first stage of drying, which is most relevant to this work, a Darcy-type equation may be more suitable due to the presence of free liquid water in the concrete pores that move due to capillary forces and pressure gradients. A time-dependent numerical model based on Darcy's law that would account for drying environment, changes to the concrete pore-structure during submersion and oxygen diffusion would be required for this analysis to correctly ascertain whether corrosion would a limiting factor to the reuse of a concrete GBF. This area promises to be a very interesting topic for future work.

CHAPTER 6

CONCLUSIONS

6. Conclusions

6.1 Introduction

This thesis set out to examine the feasibility of reusing concrete gravity-based foundations in the tidal energy sector. Novel concrete GBF developers assert that their foundations may be reused, relocated, or redeployed following decommissioning (Vici Ventus, 2010; Jackson, Duff and Taylor, 2012). Concrete manufacturing contributes to both the carbon intensive cement making process, which has proven to be a top contributor to worldwide CO_2 emissions, and C&D (construction and demolition) waste (Xia, Ding and Xiao, 2020; Benhelal, Shamsaei and Rashid, 2021; Brito and Kurda, 2021). Therefore, the advantages, should it be practical to reuse concrete GBFs in the offshore environment, include reduced carbon emissions due to concrete structure construction, as well as a decrease in the amount of C&D waste going to landfill. Considering there has never been a more urgent need to prioritise environmental responsibility, specifically in offshore renewable energy applications, these advantages would further elevate the sustainability of the tidal turbine industry.

However, during a review of the available literature, it appeared, to the best of the author's knowledge, that the practicalities of reusing or relocating concrete GBFs following decommissioning have yet to be studied. Therefore, this research posed, and attempted to answer, the question of whether reuse and relocation is feasible with regards to two potential barriers to reuse, namely geotechnical hazards and concrete degradation. Prior to conducting analysis into the barriers to reuse, it was necessary to design a representative concrete gravity-based foundation using recommended design guidelines and the Selkie F&M design tool. This foundation design was based on real-world environmental parameters including realistic geotechnical profiles and loading data from the AR1500 tidal turbine. Following this, the concrete GBF underwent analyses to determine the practicality of reuse, first in a geotechnical context and secondly in a concrete deterioration context. The conclusions from these analyses are detailed in Section 6.2 and Section 6.3 respectively.

6.2 Conclusions from Geotechnical Analysis

For the geotechnical analysis, Plaxis 3D software, a tool that utilises finite element method, was used to calculate the settlement patterns and tilt of the concrete GBF over

a period of 25 years on a sandy soil profile, for which it was designed, and a contrasting clayey soil profile to measure the feasibility of relocation to a different soil type. The main findings from this analysis are:

- Both the total settlement and tilt on both soil profiles were significantly less than the allowable total settlement and tilt.
- These results support the possibility of relocating concrete GBFs to alternative deployment sites.
- The total settlement and tilt for both soil profiles were similar, although the settlement behaviour over time differed which would need to be accounted for in a relocation scenario.

Furthermore, the results of this research show that the design methodologies for offshore turbine GBFs support much larger loads than the design load and, therefore, it could be possible to tailor the design methodologies in two ways. Firstly, the conservative design could be curtailed meaning less concrete would be required. This would have positive implications both economically and environmentally. Secondly, the design could purposefully target reuse using long-term planning for potentially greater turbine loads, should the turbines increase in size and power in the future, much like the trajectory of the offshore wind turbine industry. Again, premeditating reuse would reduce future expenditure and the carbon load associated with building tidal turbine foundations.

6.3 Conclusions from Concrete Degradation Analysis

Concrete degradation due to corrosion was examined as the second barrier to reusing tidal turbine GBFs. Corrosion cannot occur if the passive layer surrounding the steel at the steel-concrete interface remains intact. This passive layer is damaged if the critical chloride concentration is breached. Therefore, a mathematical model based on Fick's second law of diffusion was utilised to determine if the level of chlorides at the steel-concrete interface surpassed the critical chloride concentration following 25 years of submersion. To do this, three sets of chloride ingress parameters were taken from literature to be used in the model. All three datasets were from OPC based concrete and complied with the maximum water-binder ratio and minimum compressive strength required for tidal turbine GBFs. There were upper and lower

thresholds for the C_{crit} parameter in this study as there is much uncertainty associated with the precise value of the critical chloride level. The results of the chloride ingress modelling found that:

- The results from the chloride ingress modelling showed that all three datasets exceeded the critical chloride concentration at the steel-concrete interface.
- This indicates that the protective passive barrier would be compromised, putting the concrete at high risk of corrosion should oxygen become available at the steel surface.
- The chloride concentration levels resulting from the datasets modified for hydrostatic pressure were relatively high compared to the unmodified sets, demonstrating the significance of considering hydrostatic pressure in future work.

As corrosion requires the presence of oxygen and water as well as chlorides, the availability of oxygen and water were examined in the reuse scenario of placing a chloride contaminated GBF on a dry dock while awaiting redeployment. The complexities of the relationship between oxygen availability and water saturation degree meant modelling it surpassed the feasible scope of this MSc research project, however an initial investigation into the novel scenario of GBF reuse found that oxygen can begin to ingress into concrete of 90-100% saturation and a drying model based on Darcy's equation could be developed in future work to determine how long chloride-contaminated concrete could stay on a dry dock before water levels reduce enough for oxygen ingression, creating an optimal environment for corrosion at the steel-concrete interface.

6.4 Overall Recommendations and Future Work

Overall, the geotechnical analysis indicates that it is indeed feasible to reuse or relocate the concrete GBF in this study. Subsequent research steps could include the analysis of soil profiles with varying stiffness to validate this for a variety of soil cases. One could also consider the conservatism of the current recommended design methodologies for offshore gravity-based foundations. The analysis of increasing turbine loading parameters could also be pertinent to the study of GBF reuse, which would align with the study of conservatism. Furthermore, both the GBF design and

the geotechnical analysis utilised constant operational loads rather than accounting for cyclic loads. Due to the competitive nature of the tidal industry, there is an understandable reluctance within the industry to disclose detailed loading information for confidentiality purposes. However, the operational turbine loads are cited as the governing extreme loads in design standards (please refer to Section 3.2.2) ensuring that the GBF was designed according to the extreme load case as is common practice. It is worth noting however, that cyclical loading conditions may influence soil compression and consolidation behaviour in both Case 1 and Case 2. Future work could investigate this more thoroughly should cyclical loading data become accessible. In this study, the discrepancy between the resulting settlements and tilt from the constant load source and the allowable settlement and tilt that the exclusion of cyclical loading would not affect the findings.

In contrast, the chloride ingress analysis results did not support the possibility of reuse due to the high risk of corrosion following the destruction of the passive layer, although further research would be required to determine how long a concrete GBF could be situated on a dry dock prior to the propagation of corrosion. The development of a time-dependent numerical drying model based on Darcy's law that accounts for oxygen diffusion as well as changes to the concrete pore-structure during submersion could therefore be included in future work. Should such a model be developed and validated it is technically possible that a chloride contaminated concrete GBF could be reused following an allowable period on a dry-dock, although in a practical application this is unlikely to happen. The use of GGBS as a partial substitute for OPC in concrete could be one option to increase the durability, and thus, the reusability of concrete GBFs, with studies showing an increased performance in offshore applications (Ryan and O'Connor, 2014). A wet-dock storage option could also be explored for concrete GBFs, to maintain a saturated state and, consequently, inhibit oxygen ingress which would protect the concrete from corrosion.

In general, there is immense opportunity to conduct future study in the field of GBF concrete reuse for offshore tidal energy converters due to the relevancy of the research and the lack of existing studies in this area. The feasibility of reusing and relocating concrete GBFs raises many other research questions not touched on in this thesis such as the effect of turbine evolution, increases in extreme loading incidents due to climate change, ecological impact on the seabed, and ocean acidification. In broader terms,

concrete in all offshore applications could benefit from the advantages of reuse and thus this area provides ample opportunities for future work.

REFERENCES

Abdullah, G.M.S. (2022) ‘Using Plaxis 2D finite element modeling to assess bearing capacity of Sultana’s soil in Najran Region, Kingdom of Saudi Arabia’, *Materials Today: Proceedings*, 49, pp. 2679–2687. Available at: https://doi.org/10.1016/j.matpr.2021.09.051.

Adesina, A. (2020) ‘Recent advances in the concrete industry to reduce its carbon dioxide emissions’, *Environmental Challenges*, 1, p. 100004. Available at: https://doi.org/10.1016/j.envc.2020.100004.

Al-Sodani, K.A.A. *et al.* (2021) ‘Chloride diffusion models for Type I and fly ash cement concrete exposed to field and laboratory conditions’, *Marine Structures*, 76, p. 102900. Available at: https://doi.org/10.1016/j.marstruc.2020.102900.

Al-Sodani, K.A.A. *et al.* (2022) ‘Chloride diffusion models for plain and blended cement concretes exposed to laboratory and atmospheric marine conditions’, *Journal of Materials Research and Technology*, 17, pp. 125–138. Available at: https://doi.org/10.1016/j.jmrt.2021.12.136.

Angst, U. *et al.* (2009) ‘Critical chloride content in reinforced concrete — A review’, *Cement and Concrete Research*, 39(12), pp. 1122–1138. Available at: https://doi.org/10.1016/j.cemconres.2009.08.006.

ASTM C1202 (2010) ‘Standard test method for electrical indication of concrete’s ability to resist chloride ion penetration’, *American Society for Testing and Materials*, 04.02, p. 6. Available at: https://doi.org/10.1520/C1202-05.

ASTM C1556 (2016) ‘Standard Test Method for Determining the Apparent Chloride Diffusion Coefficient of Cementatious Mixtures by Bulk Diffusion’, *American Society for Testing and Materials*, 04.02, p. 7. Available at: https://doi.org/10.1520/C1556-11AR16.

Atlantis Resources (2016) ‘AR1500 Tidal Turbine Brochure’. Atlantis Resources. Available at: https://simecatlantis.com/wp-content/uploads/2016/08/AR1500-Brochure-Final-1.pdf (Accessed: 13 October 2021).

Attari, Y., Prendergast, L. and Gavin, K. (2016) ‘Performance Testing of a Novel Gravity Base Foundation for Offshore Wind’, in. Available at: https://doi.org/10.13140/RG.2.1.2606.3604.

Awoyera, P.O., Babalola, O.E. and Aluko, O.G. (2022) ‘7 - The use of slags in recycled aggregate concrete’, in P.O. Awoyera, C. Thomas, and M.S. Kirgiz (eds) *The Structural Integrity of Recycled Aggregate Concrete Produced with Fillers and Pozzolans*. Woodhead Publishing (Woodhead Publishing Series in Civil and Structural Engineering), pp. 145–170. Available at: https://doi.org/10.1016/B978-0-12-824105-9.00009-3.

Bailey, H. *et al.* (2010) ‘Assessing underwater noise levels during pile-driving at an offshore windfarm and its potential effects on marine mammals’, *Marine Pollution Bulletin*, 60(6), pp. 888–897. Available at: https://doi.org/10.1016/j.marpolbul.2010.01.003.

Balestra, C.E.T., Reichert, T.A. and Savaris, G. (2019) 'Contribution for durability studies based on chloride profiles analysis of real marine structures in different marine aggressive zones', *Construction and Building Materials*, 206, pp. 140–150. Available at: https://doi.org/10.1016/j.conbuildmat.2019.02.067.

BAM (2017) *Blyth Offshore Demontrator Wind Farm Project: First Gravity Base Foundation lowered onto sea bed | Koninklijke BAM Groep / Royal BAM Group*. Available at: https://www.bam.com/en/press/press-releases/2017/8/blyth-offshore-demontrator-wind-farm-project-first-gravity-base (Accessed: 2 June 2021).

BAM (2018) *Gravity Base Foundation for Blyth | BAM Infrastructure Netherlands*. Available at: https://www.baminfra.nl/projecten/gravity-base-foundation-for-blyth (Accessed: 13 December 2021).

Bažant, Z.P. (1979) 'Physical Model For Steel Corrosion in Concrete Sea Structures - Theory', *ASCE J Struct Div*, 105(6), pp. 1137–1153.

Bažant, Z.P. and Najjar, L.J. (1971) 'Drying of concrete as a nonlinear diffusion problem', *Cement and Concrete Research*, 1(5), pp. 461–473. Available at: https://doi.org/10.1016/0008-8846(71)90054-8.

Benhelal, E., Shamsaei, E. and Rashid, M.I. (2021) 'Challenges against CO2 abatement strategies in cement industry: A review', *Journal of Environmental Sciences*, 104, pp. 84–101. Available at: https://doi.org/10.1016/j.jes.2020.11.020.

Bentley (2022) 'Plaxis3D CE V22.01: 0 - General info'. Bentley. Available at: https://communities.bentley.com/products/geotech-analysis/w/plaxis-soilvision-wiki/46137/manuals---plaxis.

Bentley, R.W. (2002) 'Global oil & gas depletion: an overview', *Energy Policy*, 30(3), pp. 189–205. Available at: https://doi.org/10.1016/S0301-4215(01)00144-6.

Breeze, P. (2019) 'Chapter 9 - Tidal Barrage Power Plants', in P. Breeze (ed.) *Power Generation Technologies (Third Edition)*. Third Edition. Newnes, pp. 203–217. Available at: https://doi.org/10.1016/B978-0-08-102631-1.00009-2.

Brito, J. de and Kurda, R. (2021) 'The past and future of sustainable concrete: A critical review and new strategies on cement-based materials', *Journal of Cleaner Production*, 281, p. 123558. Available at: https://doi.org/10.1016/j.jclepro.2020.123558.

Bull, A.S. and Love, M.S. (2019) 'Worldwide oil and gas platform decommissioning: A review of practices and reefing options', *Ocean & Coastal Management*, 168, pp. 274–306. Available at: https://doi.org/10.1016/j.ocecoaman.2018.10.024.

Burić, M. *et al.* (2021) 'A numerical investigation of tidal current energy resource potential in a sea strait', *Energy*, 234, p. 121241. Available at: https://doi.org/10.1016/j.energy.2021.121241.

Cai, R. *et al.* (2020) 'Prediction of surface chloride concentration of marine concrete using ensemble machine learning', *Cement and Concrete Research*, 136, p. 106164. Available at: https://doi.org/10.1016/j.cemconres.2020.106164.

Capobianco, N. *et al.* (2021) 'Toward a Sustainable Decommissioning of Offshore Platforms in the Oil and Gas Industry: A PESTLE Analysis', *Sustainability*, 13, p. 6266. Available at: https://doi.org/10.3390/su13116266.

Chen, D. *et al.* (2020) 'Static and dynamic loading behavior of a hybrid foundation for offshore wind turbines', *Marine Structures*, 71, p. 102727. Available at: https://doi.org/10.1016/j.marstruc.2020.102727.

Cochet, C. and Lambert, M. (2017) 'The Rance Tidal Power Plant Model', p. 7.

Collepardi, M., Marcialis, A. and Turriziani, R. (1972) 'Penetration of Chloride Ions into Cement Pastes and Concretes', *Journal of the American Ceramic Society*, 55(10), pp. 534–535. Available at: https://doi.org/10.1111/j.1151-2916.1972.tb13424.x.

Courtois, A., Taillade, F. and Placko, D. (2020) 'Some considerations on the benefit of measuring concrete moisture to predict long term structural behaviour', *Construction and Building Materials*, 265, p. 120283. Available at: https://doi.org/10.1016/j.conbuildmat.2020.120283.

Dai, K. *et al.* (2015) 'Environmental issues associated with wind energy – A review', *Renewable Energy*, 75, pp. 911–921. Available at: https://doi.org/10.1016/j.renene.2014.10.074.

Dai, R. and Zhang, J. (2017) 'Green process innovation and differentiated pricing strategies with environmental concerns of South-North markets', *Transportation Research Part E: Logistics and Transportation Review*, 98, pp. 132–150. Available at: https://doi.org/10.1016/j.tre.2016.12.009.

Das, B. and Sivakugan, N. (2007) 'Settlements of shallow foundations on granular soil - An overview', *International Journal of Geotechnical Engineering*, 1, pp. 19–29. Available at: https://doi.org/10.3328/IJGE.2007.01.01.19-29.

Das, B.M. and Sobhan, K. (2016) 'Chapter 11: Compressibility of Soil', in *Principles of Geotechical Engineering*. 9th Edition.

Ding, H. *et al.* (2015) 'Model tests on the bearing capacity of wide-shallow composite bucket foundations for offshore wind turbines in clay', *Ocean Engineering*, 103, pp. 114–122. Available at: https://doi.org/10.1016/j.oceaneng.2015.04.068.

DNVGL-ST-0126 (2018) 'DNVGL Standard: Support Structures for Wind Turbines'. DNVGL Standard.

DNVGL-ST-0164 (2015) 'DNVGL Standard: Tidal Turbines'. DNVGL Standard.

DNV-OSS-312 (2008) 'DNV Offshore Service Specification: Certification of Tidal and Wave Energy Converters'. DNV Offshore Service Specification.

Doherty, P. and Gavin, K. (2011) ‘Shaft Capacity of Open-Ended Piles in Clay’, *Journal of Geotechnical and Geoenvironmental Engineering*, 137(11), pp. 1090–1102. Available at: https://doi.org/10.1061/(ASCE)GT.1943-5606.0000528.

EMEC (2021) ‘Tidal clients : EMEC: European Marine Energy Centre’. Available at: https://www.emec.org.uk/about-us/our-tidal-clients/ (Accessed: 10 December 2021).

EN 206-1 (2000) ‘Concrete - Part 1: Specification, performance, production and conformity’. CEN.

EN1992-1-1 (2004) ‘Eurocode 2: Design of Concrete Structures - Part 1-1: General rules and rules for buildings’. European Commission.

Ersdal, G. and Hörnlund, E. (2008) ‘Assessment of Offshore Structures for Life Extension’, in *Proceedings of the International Conference on Offshore Mechanics and Arctic Engineering - OMAE*. Available at: https://doi.org/10.1115/OMAE2008-57451.

Esteban, M.D. *et al.* (2015) ‘Gravity based support structures for offshore wind turbine generators: Review of the installation process’, *Ocean Engineering*, 110, pp. 281–291. Available at: https://doi.org/10.1016/j.oceaneng.2015.10.033.

Esteban, M.D., López-Gutiérrez, J.-S. and Negro, V. (2019) ‘Gravity-Based Foundations in the Offshore Wind Sector’, *Journal of Marine Science and Engineering*, 7(3). Available at: https://doi.org/10.3390/jmse7030064.

European Commission (2017) *Attitudes of European citizens towards the environment: report.* LU: Publications Office. Available at: https://data.europa.eu/doi/10.2779/84809 (Accessed: 15 October 2020).

Faizi, K. *et al.* (2019) ‘Investigating the monotonic behaviour of hybrid tripod suction bucket foundations for offshore wind towers in sand’, *Applied Ocean Research*, 89, pp. 176–187. Available at: https://doi.org/10.1016/j.apor.2019.05.018.

Fakhri, H., Fishman, K.L. and Ranade, R. (2020) ‘A novel experimental method to determine the critical chloride content in cement-based composites’, *Construction and Building Materials*, 263, p. 120101. Available at: https://doi.org/10.1016/j.conbuildmat.2020.120101.

Fowler, A. *et al.* (2018) ‘Environmental benefits of leaving offshore infrastructure in the ocean’, *Frontiers in Ecology and the Environment*, 16. Available at: https://doi.org/10.1002/fee.1827.

Frid, C. *et al.* (2012) ‘The environmental interactions of tidal and wave energy generation devices’, *Environmental Impact Assessment Review*, 32(1), pp. 133–139. Available at: https://doi.org/10.1016/j.eiar.2011.06.002.

Fu, C. *et al.* (2021) ‘Bond degradation of non-uniformly corroded steel rebars in concrete’, *Engineering Structures*, 226, p. 111392. Available at: https://doi.org/10.1016/j.engstruct.2020.111392.

Fugro (2020) ‘Geotechnical Parameters Hollandse Kust (west) Wind Farm Zone’. Netherlands Enterprise Agency. Available at: https://offshorewind.rvo.nl/file/view/55040691/Report+-+Geotechnical+Parameters+HKW+-+Fugro (Accessed: 15 June 2021).

Futai, M.M., Haigh, S.K. and Madabhushi, G.S.P. (2021) ‘Comparison of the dynamic responses of monopiles and gravity base foundations for offshore wind turbines in sand using centrifuge modelling’, *Soils and Foundations*, 61(1), pp. 50–63. Available at: https://doi.org/10.1016/j.sandf.2020.10.009.

Galbraith, D. and Sharp, J. (2007) *Recommendations for design life extension regulations*. POS-DK06-195-R02. Poseidon. Available at: https://www.ptil.no/contentassets/24974571fd8442bea4c21d3679d93a8e/posdk06134r02revr02.pdf.

Glass, G.K. and Buenfeld, N.R. (1997) ‘The presentation of the chloride threshold level for corrosion of steel in concrete’, *Corrosion Science*, 39(5), pp. 1001–1013. Available at: https://doi.org/10.1016/S0010-938X(97)00009-7.

Government of Ireland (2021) ‘Climate Action Plan 2021’. Available at: https://www.gov.ie/en/publication/6223e-climate-action-plan-2021/ (Accessed: 21 September 2022).

Goyal, A. *et al.* (2018) ‘A Review of Corrosion and Protection of Steel in Concrete’, *ARABIAN JOURNAL FOR SCIENCE AND ENGINEERING*, pp. 1–21. Available at: https://doi.org/10.1007/s13369-018-3303-2.

Guillou, N., Chapalain, G. and Neill, S.P. (2016) ‘The influence of waves on the tidal kinetic energy resource at a tidal stream energy site’, *Applied Energy*, 180, pp. 402–415. Available at: https://doi.org/10.1016/j.apenergy.2016.07.070.

Han, Y. *et al.* (2018) ‘Experimental Study on Gravity Anchor for Optimum Design of Shear Key’, in, p. V009T10A007. Available at: https://doi.org/10.1115/OMAE2018-78390.

Heath, J. *et al.* (2014) ‘Specific requirements for MRE foundation analysis, DTOcean Deliverable 4.2’, *DTO_WP4_SNL_D4.2* [Preprint]. Available at: http://www.dtoceanplus.eu/About-DTOceanPlus/History.

Hernandez C, O.M. *et al.* (2021) ‘Environmental impacts of offshore wind installation, operation and maintenance, and decommissioning activities: A case study of Brazil’, *Renewable and Sustainable Energy Reviews*, 144, p. 110994. Available at: https://doi.org/10.1016/j.rser.2021.110994.

Holmes, N. (2009) *Moisture movement in concrete during drying*. University of Dublin, Trinity College. Available at: https://arrow.tudublin.ie/cgi/viewcontent.cgi?article=1031&context=engschcivoth.

Huet, B. *et al.* (2007) ‘Steel corrosion in concrete: Determinist modeling of cathodic reaction as a function of water saturation degree’, *Corrosion Science*, 49(4), pp. 1918–1932. Available at: https://doi.org/10.1016/j.corsci.2006.10.005.

Hussain, R.R. (2011) ‘Effect of moisture variation on oxygen consumption rate of corroding steel in chloride contaminated concrete’, *Cement and Concrete Composites*, 33(1), pp. 154–161. Available at: https://doi.org/10.1016/j.cemconcomp.2010.09.014.

Hussain, R.R. and Ishida, T. (2010) ‘Influence of connectivity of concrete pores and associated diffusion of oxygen on corrosion of steel under high humidity’, *Construction and Building Materials*, 24(6), pp. 1014–1019. Available at: https://doi.org/10.1016/j.conbuildmat.2009.11.017.

Hussain, R.R., Ishida, T. and Wasim, W. (2012) ‘Oxygen Transport and Corrosion of Steel in Concrete under Varying Concrete Cover, w/c, and Moisture’, *ACI Materials Journal*, 109(1), pp. 3–10.

Ikhennicheu, M. *et al.* (2020) ‘Review of the state of the art of mooring and anchoring design, technical challenges and identification of relevent DLCs’. Zenodo. Available at: https://doi.org/10.5281/zenodo.4056096.

Intergovernmental Panel on Climate Change (ed.) (2015) ‘Energy Systems’, in *Climate Change 2014: Mitigation of Climate Change: Working Group III Contribution to the IPCC Fifth Assessment Report*. Cambridge: Cambridge University Press, pp. 511–598. Available at: https://doi.org/10.1017/CBO9781107415416.013.

Itasca (2015) ‘FLAC 8 Basics: An introduction to FLAC8 and a guide to its practical application in geotechnical engineering’. First Edition, Revision 01 (FLAC Version 8.0). Available at: http://itasca-downloads.s3.amazonaws.com/documents/software/manuals/FLAC8Basics.pdf.

Jackson, G., Duff, C. and Taylor, I. (2012) ‘Gravitas Offshore’. ARUP. Available at: https://www.arup.com/-/media/arup/files/publications/g/gravitas_brochure_final_press_quality2.pdf (Accessed: 13 December 2021).

Jones, C. and Hammond, G. (2008) ‘Embodied energy and carbon in construction materials’, *Proceedings of The Ice - Energy*, 161, pp. 87–98. Available at: https://doi.org/10.1680/ener.2008.161.2.87.

Ju, X. *et al.* (2021) ‘Prediction of chloride concentration with elevation in concrete exposed to cyclic drying-wetting conditions in marine environments’, *Construction and Building Materials*, 278, p. 122370. Available at: https://doi.org/10.1016/j.conbuildmat.2021.122370.

Kamran, M. and Sarkar, K. (2019) ‘A Short Review of Experimental Approaches for the Estimation of Drying Diffusivity of Porous Building Materials’. Available at: https://doi.org/10.13140/RG.2.2.19045.86247.

Käthler, C.B. *et al.* (2019) ‘A novel approach to systematically collect critical chloride contents in concrete in an open access data base’, *Data in Brief*, 27, p. 104675. Available at: https://doi.org/10.1016/j.dib.2019.104675.

Khatami, D., Hajilar, S. and Shafei, B. (2021) 'Investigation of oxygen diffusion and corrosion potential in steel-reinforced concrete through a cellular automaton framework', *Corrosion Science*, 187, p. 109496. Available at: https://doi.org/10.1016/j.corsci.2021.109496.

Khitab, A., Anwar, W. and Arshad, M. (2017) 'Predictive Models of Chloride Penetration in concrete: An Overview', *MUST Journal of Engineering and Applied Sciences*, 1, pp. 1–14. Available at: https://doi.org/10.22496/mjeas20170103.

Kim, H.-G. and Kim, B.-J. (2018) 'Feasibility study of new hybrid piled concrete foundation for offshore wind turbine', *Applied Ocean Research*, 76, pp. 11–21. Available at: https://doi.org/10.1016/j.apor.2018.04.005.

Kinda, J. *et al.* (2022) 'Experimental and numerical investigation of drying rate impact on moisture loss, exchange coefficient and drying shrinkage of cement paste', *Construction and Building Materials*, 330, p. 127099. Available at: https://doi.org/10.1016/j.conbuildmat.2022.127099.

Kumar, S., Toan, C. and Vahedifard, F. (2021) 'Poisson's Ratio Characteristic Curve of Unsaturated Soils', *Journal of Geotechnical and Geoenvironmental Engineering*, 147, p. 04020149. Available at: https://doi.org/10.1061/(ASCE)GT.1943-5606.0002424.

Lakhal, S.Y., Khan, M.I. and Islam, M.R. (2009) 'An "Olympic" framework for a green decommissioning of an offshore oil platform', *Ocean & Coastal Management*, 52(2), pp. 113–123. Available at: https://doi.org/10.1016/j.ocecoaman.2008.10.007.

Lande-Sudall, D., Stallard, T. and Stansby, P. (2019) 'Co-located deployment of offshore wind turbines with tidal stream turbine arrays for improved cost of electricity generation', *Renewable and Sustainable Energy Reviews*, 104, pp. 492–503. Available at: https://doi.org/10.1016/j.rser.2019.01.035.

Lempriere, M. (2017) *Full circle: decommissioning the first ever offshore windfarm*, *Power Technology*. Available at: https://www.power-technology.com/features/full-circle-decommissioning-first-ever-offshore-windfarm/ (Accessed: 22 February 2022).

Leporini, M. *et al.* (2019) 'Reconversion of offshore oil and gas platforms into renewable energy sites production: Assessment of different scenarios', *Renewable Energy*, 135, pp. 1121–1132. Available at: https://doi.org/10.1016/j.renene.2018.12.073.

Li, D., Wang, X. and Li, L. (2019) 'An analytical solution for chloride diffusion in concrete with considering binding effect', *Ocean Engineering*, 191, p. 106549. Available at: https://doi.org/10.1016/j.oceaneng.2019.106549.

Li, X., Zeng, X. and Wang, X. (2020) 'Feasibility study of monopile-friction wheel-bucket hybrid foundation for offshore wind turbine', *Ocean Engineering*, 204, p. 107276. Available at: https://doi.org/10.1016/j.oceaneng.2020.107276.

Lian, J. *et al.* (2021) 'An experimental investigation on long-term performance of the wide-shallow bucket foundation model for offshore wind turbine in saturated sand',

Ocean Engineering, 228, p. 108921. Available at: https://doi.org/10.1016/j.oceaneng.2021.108921.

LimitState Ltd (2021) 'LimitState:GEO Manual Version 3.6.0'. LimitState Ltd. Available at: http://acad.limitstate.com/files/pdf/geo/GEO_Manual.pdf.

Liu, H. and Jiang, L. (2021) 'Influence of Hydrostatic Pressure and Cationic Type on the Diffusion Behavior of Chloride in Concrete', *Materials*, 14, p. 2851. Available at: https://doi.org/10.3390/ma14112851.

Liu, Q. *et al.* (2020) 'Prediction of Chloride Distribution for Offshore Concrete Based on Statistical Analysis', *Materials*, 13(1). Available at: https://doi.org/10.3390/ma13010174.

Löfgren, I. *et al.* (2016) 'Predicting Chloride Induced Depassiviation and Minimum Concrete Cover with Different Binders', in. *Materials, Systems and Structures in Civil Engineering 2016*, Lyngby, Denmark.

Luping, T. (2003) *Chloride ingress in concrete exposed to marine environment - field data up to 10 years exposure*. (SP Rapport, ISSN 0284-5172 ; 2003:16).

Luping, T. and Löfgren, I. (2016) *Evaluation of Durability of Concrete with Mineral Additions with regard to ChlorideInduced Corrosion*. 2016–4. Sweden: Chalmers University of Technology. Available at: https://publications.lib.chalmers.se/records/fulltext/241518/local_241518.pdf.

Luxcey, N. *et al.* (2020) 'Advanced Design Tools for Ocean Energy Systems Innovation, Development and Deployment: Deliverable 5.6: Station Keeping Tools – alpha version'. DTOceanPLus. Available at: https://www.dtoceanplus.eu/Publications/Deliverables/Deliverable-D5.6-Station-keeping-tools-alpha-version.

Ma, H. and Yang, J. (2020) 'A novel hybrid monopile foundation for offshore wind turbines', *Ocean Engineering*, 198, p. 106963. Available at: https://doi.org/10.1016/j.oceaneng.2020.106963.

Macdonald, D.D. *et al.* (2021) 'Corrosion of rebar in concrete. Part IV. On the theoretical basis of the chloride threshold', *Corrosion Science*, 185, p. 109460. Available at: https://doi.org/10.1016/j.corsci.2021.109460.

Margheritini, L. *et al.* (2020) 'Development of an Eco-Sustainable Solution for the Second Life of Decommissioned Oil and Gas Platforms: The Mineral Accretion Technology', *Sustainability*, 12, p. 3742. Available at: https://doi.org/10.3390/su12093742.

Mathern, A., von der Haar, C. and Marx, S. (2021) 'Concrete Support Structures for Offshore Wind Turbines: Current Status, Challenges, and Future Trends', *Energies*, 14(7). Available at: https://doi.org/10.3390/en14071995.

McAuliffe, F.D. and Norbeck, J.A. (2017) 'Driving Cost Reductions in Offshore Wind', in.

McGrath, P.F. and Hooton, R.D. (1999) ‘Re-evaluation of the AASHTO T259 90-day salt ponding test’, *Cement and Concrete Research*, 29(8), pp. 1239–1248. Available at: https://doi.org/10.1016/S0008-8846(99)00058-7.

McKenna, R., D’Andrea, M. and González, M.G. (2021) ‘Analysing long-term opportunities for offshore energy system integration in the Danish North Sea’, *Advances in Applied Energy*, 4, p. 100067. Available at: https://doi.org/10.1016/j.adapen.2021.100067.

Melchers, R.E. and Beck, A.T. (2017) ‘Measures of Structural Reliability’, in *Structural Reliability Analysis and Prediction*. John Wiley & Sons, Ltd, pp. 1–29. Available at: https://doi.org/10.1002/9781119266105.ch1.

Mendi, V., Rao, S. and Seelam, J. (2016) ‘Tidal Energy: A Review’, in. Available at: https://www.researchgate.net/publication/310795127_Tidal_Energy_A_Review.

Mendoza, E. *et al.* (2019) ‘A framework to evaluate the environmental impact of OCEAN energy devices’, *Renewable and Sustainable Energy Reviews*, 112, pp. 440–449. Available at: https://doi.org/10.1016/j.rser.2019.05.060.

Mestres, M. *et al.* (2016) ‘Analysis of the optimal deployment location for tidal energy converters in the mesotidal Ria de Vigo (NW Spain)’, *Energy*, 115, pp. 1179–1187. Available at: https://doi.org/10.1016/j.energy.2016.06.055.

MeyGen (2020) ‘MeyGen Subsea Hub Decomissioning Programme’. Available at: https://simecatlantis.com/wp-content/uploads/2020/03/Subsea-Hub-Decom_Prog_v2.0.pdf (Accessed: 30 August 2021).

MeyGen (2021) *MeyGen | Tidal Projects, SIMEC Atlantis Energy*. Available at: http://simecatlantis.com/projects/meygen/ (Accessed: 30 August 2021).

Ming, J., Wu, M. and Shi, J. (2021) ‘Passive film modification by concrete carbonation: Re-visiting a corrosion-resistant steel with Cr and Mo’, *Cement and Concrete Composites*, 123, p. 104178. Available at: https://doi.org/10.1016/j.cemconcomp.2021.104178.

Mofor, L., Goldsmith, J. and Jones, F. (2014) ‘Ocean Energy: Technology Readiness, Patents, Deployments Status and Outlook’. IRENA. Available at: https://www.irena.org/-/media/Files/IRENA/Agency/Publication/2014/IRENA_Ocean_Energy_report_2014.pdf.

Mueller, M. and Jeffrey, H. (2008) ‘UKERC Marine (Wave and Tidal Current) Renewable Energy Technology Roadmap’. Uk Eenergy Research Centre. Available at: https://d2e1qxpsswcpgz.cloudfront.net/uploads/2020/03/ukerc-marine-wave-and-tidal-current-renewable-energy-technology-roadmap.pdf.

Nachtane, M. *et al.* (2020) ‘A review on the technologies, design considerations and numerical models of tidal current turbines’, *Renewable Energy*, 157, pp. 1274–1288. Available at: https://doi.org/10.1016/j.renene.2020.04.155.

Naderi, E. and Hataf, N. (2014) ‘Model testing and numerical investigation of interference effect of closely spaced ring and circular footings on reinforced sand’, *Geotextiles and Geomembranes*, 42(3), pp. 191–200. Available at: https://doi.org/10.1016/j.geotexmem.2013.12.010.

Najimi, M., Ghafoori, N. and Nikoo, M. (2019) ‘Modeling chloride penetration in self-consolidating concrete using artificial neural network combined with artificial bee colony algorithm’, *Journal of Building Engineering*, 22, pp. 216–226. Available at: https://doi.org/10.1016/j.jobe.2018.12.013.

Nanukuttan, S. *et al.* (2008) ‘Full-scale marine exposure tests on treated and untreated concretes-initial 7-year results’, *ACI Materials Journal*, 105, pp. 81–87.

Neill, S.P. and Hashemi, M.R. (2018) ‘Chapter 3 - Tidal Energy’, in S.P. Neill and M.R. Hashemi (eds) *Fundamentals of Ocean Renewable Energy*. Academic Press (E-Business Solutions), pp. 47–81. Available at: https://doi.org/10.1016/B978-0-12-810448-4.00003-3.

Netherlands Enterprise Agency (2021) ‘Data - Geotechnical Parameters HKW - Fugro’. Available at: https://offshorewind.rvo.nl/file/view/55040846/Data+-+Geotechnical+Parameters+HKW+-+Fugro (Accessed: 15 May 2021).

Neville, A. (1995) ‘Chloride attack of reinforced concrete: an overview’, *Materials and Structures*, 28(63). Available at: https://doi.org/10.1007/BF02473172.

NI 603 DT R01 E (2015) ‘Bureau Veritas Guidance Note: Current and Tidal Turbines’. Bureau Veritas.

NT Build 433 (1995) ‘Nordtest Method, Hardened Concrete: Accelerated Chloride Penetration’. Nordtest. Available at: http://nordtest.info/images/documents/nt-methods/building/NT%20build%20443_Concrete,%20hardened_Accelerated%20chloride%20penetration_Nordtest%20Method.pdf.

NT Build 492 (1999) ‘Nordtest Method, Concrete, Mortar and Cement-Based Repair Materials: Chloride Migration Coefficient from Non-Steady State Migration Experiments’. Nordtest. Available at: https://salmanco.com/wp-content/uploads/2018/10/NT-Build-492.pdf.

Oasys Ltd (2014) ‘Safe Oasys GEO Suite for Windows Version 19.1’.

O’Rourke, F., Boyle, F. and Reynolds, A. (2010) ‘Tidal current energy resource assessment in Ireland: Current status and future update’, *Renewable and Sustainable Energy Reviews*, 14(9), pp. 3206–3212. Available at: https://doi.org/10.1016/j.rser.2010.07.039.

Otieno, M., Beushausen, H. and Alexander, M. (2016) ‘Chloride-induced corrosion of steel in cracked concrete – Part I: Experimental studies under accelerated and natural marine environments’, *Cement and Concrete Research*, 79, pp. 373–385. Available at: https://doi.org/10.1016/j.cemconres.2015.08.009.

Owen, A. (2020) ‘17 - Tidal Current Energy: Origins and Challenges’, in T.M. Letcher (ed.) *Future Energy (Third Edition)*. Third Edition. Elsevier, pp. 357–374. Available at: https://doi.org/10.1016/B978-0-08-102886-5.00017-7.

PCCI (2009) ‘Wave and Current Energy Generating Devices Criteria and Standards’. MMS Contract No. M08PC20032. Available at: http://large.stanford.edu/courses/2011/ph240/yan1/docs/AA.pdf.

Peire, K., Nonnneman, H. and Bosschem, E. (2009) ‘Gravity Base Foundations for the Thornton Bank Offshore Wind Farm’. Available at: https://www.iadc-dredging.com/wp-content/uploads/2017/02/article-gravity-base-foundations-for-the-thornton-bank-offshore-wind-farm-115-3.pdf (Accessed: 14 December 2021).

PlaCE (2019) *The PlaCE Project, Bluegrowth PlaCE*. Available at: https://bluegrowth-place.eu/?page_id=2 (Accessed: 23 February 2022).

Qiu, J. *et al.* (2021) ‘An SMFL-based non-destructive quantification method for the localized corrosion cross-sectional area of rebar’, *Corrosion Science*, 192, p. 109793. Available at: https://doi.org/10.1016/j.corsci.2021.109793.

Radhakrishnan, N. and Reese, L.C. (1970) ‘A Review of Applications of the Finite Element Method of Analysis to Problems in Soil and Rock Mechanics’, *Soils and Foundations*, 10(3), pp. 95–112. Available at: https://doi.org/10.3208/sandf1960.10.3_95.

Rajgor, G. (2016) ‘Tidal developments power forward’, *Renewable Energy Focus*, 17(4), pp. 147–149. Available at: https://doi.org/10.1016/j.ref.2016.06.006.

Raoux, A. *et al.* (2020) ‘Isotopic analyses, a good tool to validate models in the context of Marine Renewable Energy development and cumulative impacts’, *Estuarine, Coastal and Shelf Science*, 237, p. 106690. Available at: https://doi.org/10.1016/j.ecss.2020.106690.

Raupach, M. (1996a) ‘Investigations on the influence of oxygen on corrosion of steel in concrete - Part 2’, *Materials and Structures/Materiaux et Constructions*, 29(4), pp. 226–232. Available at: https://doi.org/10.1007/bf02485944.

Raupach, M. (1996b) ‘Investigations on the influence of oxygen on corrosion of steel in concrete—Part I’, *Materials and Structures/Materiaux et Constructions*, 29, pp. 174–184. Available at: https://doi.org/10.1007/BF02486163.

Rossi, E. *et al.* (2021) ‘Analysis of naturally-generated corrosion products due to chlorides in 20-year old reinforced concrete: An elastic modulus-mineralogy characterization’, *Corrosion Science*, 184, p. 109356. Available at: https://doi.org/10.1016/j.corsci.2021.109356.

Russell, K. (2020) *Enhances Design of Offshore Wind Energy Gravity Based Structure Foundations*. Trinity College Dublin. Available at: http://hdl.handle.net/2262/93738 (Accessed: 13 December 2021).

Ryan, P. and O'Connor, A. (2014) 'Examination of Self-Compacting Concrete Options for Marine Bridge Applications', *Journal of Bridge Engineering*, 19. Available at: https://doi.org/10.1061/(ASCE)BE.1943-5592.0000541.

Sabella (2018) *D10, Sabella*. Available at: https://www.sabella.bzh/en/projects/d10 (Accessed: 30 August 2021).

Šavija, B. and Schlangen, E. (2012) 'Chloride ingress in cracked concrete- a literature review', in C. Andrade and J. Gulikers (eds) *Advances in Modeling Concrete Service Life*. Dordrecht: Springer Netherlands, pp. 133–142. Available at: https://doi.org/10.1007/978-94-007-2703-8_14.

Seatower (no date) *Seatower - innovative foundations for offshore wind, seatower*. Available at: http://seatower.com/ (Accessed: 14 December 2021).

Segura, E. *et al.* (2017) 'Techno-economic challenges of tidal energy conversion systems: Current status and trends', *Renewable and Sustainable Energy Reviews*, 77, pp. 536–550. Available at: https://doi.org/10.1016/j.rser.2017.04.054.

Sekki, P. and Karvinen, T. (2017) 'Numerical simulation and measurements of drying of Finnish concrete grades', *Energy Procedia*, 132, pp. 729–734. Available at: https://doi.org/10.1016/j.egypro.2017.10.015.

Šelih, J. and Bremner, T.W. (1996) 'Drying of saturated lightweight concrete: an experimental investigation', *Materials and Structures*, 29, pp. 401–405. Available at: https://doi.org/10.1007/BF02485989.

Shakouri, M. and Trejo, D. (2018) 'A study of the factors affecting the surface chloride maximum phenomenon in submerged concrete samples', *Cement and Concrete Composites*, 94, pp. 181–190. Available at: https://doi.org/10.1016/j.cemconcomp.2018.09.006.

Shi, X. *et al.* (2012) 'Durability of steel reinforced concrete in chloride environments: An overview', *Construction and Building Materials*, 30, pp. 125–138. Available at: https://doi.org/10.1016/j.conbuildmat.2011.12.038.

Shiekh Elsouk, M.N., Santa Cruz, A. and Guillou, S.S. (2018) 'Review on the characterization and selection of the advanced materials for tidal turbines blades', in. *7th International Conference on Ocean Energy*, Cherbourg, France.

Simonsen, K. and Niclasen, B.A. (2021) 'Analysis of the energy potential of tidal streams on the Faroe Shelf', *Renewable Energy*, 163, pp. 836–844. Available at: https://doi.org/10.1016/j.renene.2020.08.123.

Slama, M. *et al.* (2021) 'Turbine design dependency to turbulence: An experimental study of three scaled tidal turbines', *Ocean Engineering*, 234, p. 109035. Available at: https://doi.org/10.1016/j.oceaneng.2021.109035.

Smith, G. *et al.* (2016) *Assessment of Offshore Wind Farm Decommissioning Requirements*. 800785-CAMO-R-06. DNVGL. Available at: https://files.ontario.ca/assessment_of_offshore_wind_farm_decommissioning_requirements.pdf.

Smith, M. (2009) ‘ABAQUS/Standard User’s Manual, Version 6.9’. Dassault Systèmes Simulia Corp.

Smith, P., Hytiris, N. and Mickovski, S. (2015) ‘Comparison of settlement calculation methods for the design of a gravity base foundation in deep water’, in *Proceedings of the XVI ECSMGE Geotechnical Engineering for Infrastructure and Development*. ICE Publishing, pp. 1327–1332. Available at: https://doi.org/10.1680/ecsmge.60678.

Sound and Sea Technology (2009) *Advanced Anchoring and Mooring Study*. Technical Report, p. 192.

Stanish, K., Hooton, D. and Thomas, M. (1997) ‘Testing the Chloride Penetration Resistance of Concrete: A Literature Review’.

Stanish, K. and Thomas, M. (2003) ‘The use of bulk diffusion tests to establish time-dependent concrete chloride diffusion coefficients’, *Cement and Concrete Research*, 33(1), pp. 55–62. Available at: https://doi.org/10.1016/S0008-8846(02)00925-0.

Starling, M. and Scott, A. (2009) ‘Foundations and moorings for tidal stream systems’, *A report by BMT Cordah on behalf of Carbon Trust, London, UK* [Preprint]. Available at: https://prod-drupal-files.storage.googleapis.com/documents/resource/public/Accelerating%20marine%20energy%20-%20Foundations%20%26amp%3B%20Moorings%20For%20Tidal%20Stream%20Systems%20-%20REPORT.pdf (Accessed: 14 December 2021).

Starrs, G. *et al.* (2008) ‘Performance of concrete in XS1, XS2 and XS3 environments’, *Magazine of Concrete Research - MAG CONCR RES*, 60, pp. 261–270. Available at: https://doi.org/10.1680/macr.2008.60.4.261.

Subramanian, S., Khan, Q. and Ku, T. (2020) ‘Effect of sand on the stiffness characteristics of cement-stabilized clay’, *Construction and Building Materials*, 264, p. 120192. Available at: https://doi.org/10.1016/j.conbuildmat.2020.120192.

Sun, Y.-M., Liang, M.-T. and Chang, T.-P. (2012) ‘Time/depth dependent diffusion and chemical reaction model of chloride transportation in concrete’, *Applied Mathematical Modelling*, 36(3), pp. 1114–1122. Available at: https://doi.org/10.1016/j.apm.2011.07.053.

Sunday, K. and Brennan, F. (2021) ‘A review of offshore wind monopiles structural design achievements and challenges’, *Ocean Engineering*, 235, p. 109409. Available at: https://doi.org/10.1016/j.oceaneng.2021.109409.

Techera, E.J. and Chandler, J. (2015) ‘Offshore installations, decommissioning and artificial reefs: Do current legal frameworks best serve the marine environment?’, *Marine Policy*, 59, pp. 53–60. Available at: https://doi.org/10.1016/j.marpol.2015.04.021.

Thomsen, J. (2017) *Mooring Solutions for Large Wave Energy Converters*. PhD Thesis.

Topham, E. *et al.* (2019) 'Recycling offshore wind farms at decommissioning stage', *Energy Policy*, 129, pp. 698–709. Available at: https://doi.org/10.1016/j.enpol.2019.01.072.

Topham, E. and McMillan, D. (2017) 'Sustainable decommissioning of an offshore wind farm', *Renewable Energy*, 102, pp. 470–480. Available at: https://doi.org/10.1016/j.renene.2016.10.066.

Topper, M.B.R., Olson, S.S. and Roberts, J.D. (2020) 'Techno-Economic Modelling of Tidal Energy Converter Arrays in the Tacoma Narrows', *Journal of Marine Science and Engineering*, 8(9). Available at: https://doi.org/10.3390/jmse8090646.

Trojnar, K. (2021) 'Simplified design of new hybrid monopile foundations for offshore wind turbines', *Ocean Engineering*, 219, p. 108046. Available at: https://doi.org/10.1016/j.oceaneng.2020.108046.

Uihlein, A. and Magagna, D. (2016) 'Wave and tidal current energy – A review of the current state of research beyond technology', *Renewable and Sustainable Energy Reviews*, 58, pp. 1070–1081. Available at: https://doi.org/10.1016/j.rser.2015.12.284.

United Nations (2020) 'The Sustainable Development Goals Report 2020'. Available at: https://unstats.un.org/sdgs/report/2020/The-Sustainable-Development-Goals-Report-2020.pdf.

United Nations, Department of Economic and Social Affairs, and Population Division (2019) *World population prospects Highlights, 2019 revision Highlights, 2019 revision*.

Vici Ventus (2010) 'Offshore Wind Turbines: Concrete Foundations'. Vici Ventus Technology AS. Available at: https://viciventus.no/global/upload/3sPPQ/files/GBF_product_sheet_231111.pdf (Accessed: 14 December 2021).

Wang, X. *et al.* (2018) 'Feasibility study of offshore wind turbines with hybrid monopile foundation based on centrifuge modeling', *Applied Energy*, 209, pp. 127–139. Available at: https://doi.org/10.1016/j.apenergy.2017.10.107.

Wani, F., Dong, J. and Polinder, H. (2020) 'Tidal Turbine Generators', in *Advances in Modelling and Control of Wind and Hydrogenerators*. Available at: https://doi.org/10.5772/intechopen.90433.

Weller, S. *et al.* (2015) 'Reducing Reliability Uncertainties for Marine Renewable Energy', *Journal of Marine Science and Engineering*, 3, pp. 1349–1361. Available at: https://doi.org/10.3390/jmse3041349.

Weller, S., Hardwick, J. and Johanning, L. (2014) 'DTOcean Deliverable 4.1: A comprehensive assessment of the applicability of available and proposed offshore mooring and foundation technologies and design tools for array application', p. 68.

Weller, S.D. *et al.* (2018) 'Verification of a rapid mooring and foundation design tool', *Proceedings of the Institution of Mechanical Engineers, Part M: Journal of*

Engineering for the Maritime Environment, 232(1), pp. 116–129. Available at: https://doi.org/10.1177/1475090217721064.

Weston, D. (2015) *Seatower gravity-base foundation installed*. Available at: https://www.windpowermonthly.com/article/1333039?utm_source=website&utm_medium=social (Accessed: 14 December 2021).

Whitehouse, R., Sutherland, J. and Harris, J. (2011) 'Evaluating scour at marine gravity foundations', *Proceedings of the ICE - Maritime Engineering*, 164, pp. 143–157. Available at: https://doi.org/10.1680/maen.2011.164.4.143.

Wu, J. *et al.* (2016) 'Transport model of chloride ions in concrete under loads and drying-wetting cycles', *Construction and Building Materials*, 112, pp. 733–738. Available at: https://doi.org/10.1016/j.conbuildmat.2016.02.167.

Xia, B., Ding, T. and Xiao, J. (2020) 'Life cycle assessment of concrete structures with reuse and recycling strategies: A novel framework and case study', *Waste Management*, 105, pp. 268–278. Available at: https://doi.org/10.1016/j.wasman.2020.02.015.

Xia, J. *et al.* (2019) 'Numerical simulation of steel corrosion in chloride contaminated concrete', *Construction and Building Materials*, 228, p. 116745. Available at: https://doi.org/10.1016/j.conbuildmat.2019.116745.

Xu, Y. and Jin, R. (2018) 'Measurement of reinforcement corrosion in concrete adopting ultrasonic tests and artificial neural network', *Construction and Building Materials*, 177, pp. 125–133. Available at: https://doi.org/10.1016/j.conbuildmat.2018.05.124.

Yoon, I.-S. (2018) 'Comprehensive Approach to Calculate Oxygen Diffusivity of Cementitious Materials Considering Carbonation', *International Journal of Concrete Structures and Materials*, 12. Available at: https://doi.org/10.1186/s40069-018-0242-y.

Yu, Y. *et al.* (2021) 'An integrated framework for modelling time-dependent corrosion propagation in offshore concrete structures', *Engineering Structures*, 228, p. 111482. Available at: https://doi.org/10.1016/j.engstruct.2020.111482.

Yu, Z. *et al.* (2015) 'Accelerated simulation of chloride ingress into concrete under drying–wetting alternation condition chloride environment', *Construction and Building Materials*, 93, pp. 205–213. Available at: https://doi.org/10.1016/j.conbuildmat.2015.05.090.

Zagonari, F. (2021) 'Decommissioning vs. reusing offshore gas platforms within ethical decision-making for sustainable development: Theoretical framework with application to the Adriatic Sea', *Ocean & Coastal Management*, 199, p. 105409. Available at: https://doi.org/10.1016/j.ocecoaman.2020.105409.

Zhang, Z. and Angst, U. (2020) 'Modeling Anomalous Moisture Transport in Cement-Based Materials with Kinetic Permeability', *International Journal of Molecular Sciences*, 21, p. 837. Available at: https://doi.org/10.3390/ijms21030837.

Zhou, Z. *et al.* (2017) 'Developments in large marine current turbine technologies – A review', *Renewable and Sustainable Energy Reviews*, 71, pp. 852–858. Available at: https://doi.org/10.1016/j.rser.2016.12.113.

Appendices

Appendix A

Guidelines, Specifications, and Standards Relevant to the Design of Tidal Turbine Support Structures

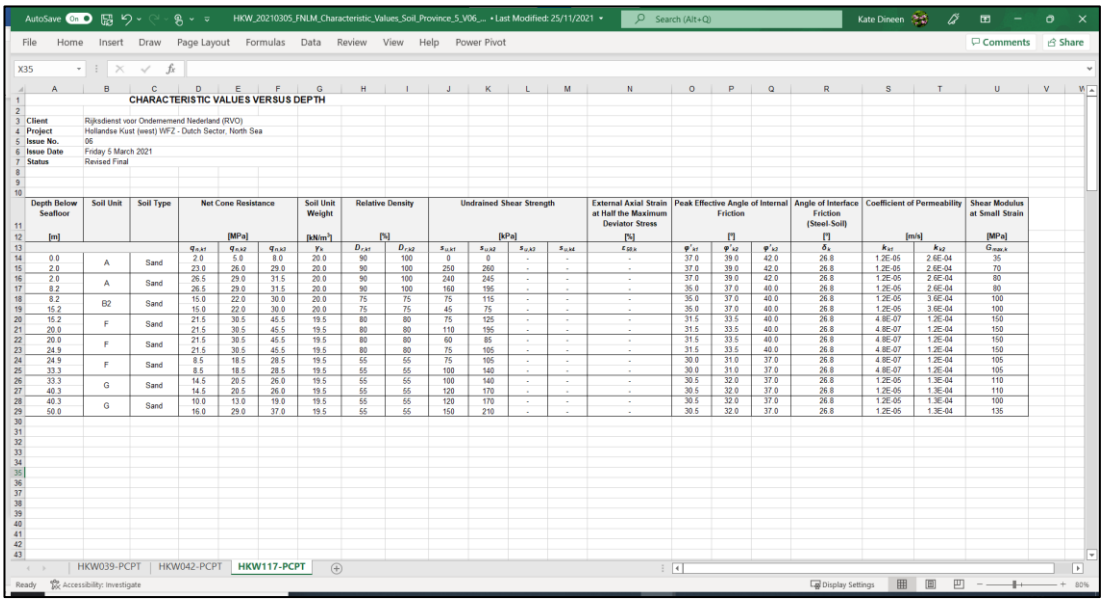
Title	Identifier	Current version
Det Norske Veritas & Germanischer Lloyd		
1. DNVGL Offshore Service Specification: Certification of Tidal and Wave Energy Converters	DNV-OSS-312	October 2008
2. DNVGL Service Specification: Certification of Tidal Turbines and Arrays	DNVGL-SE-0163	October 2015
3. DNVGL Standard: Tidal Turbines	DNVGL-ST-0164	October 2015
4. DNVGL Recommended Practice: Modelling and Analysis of Marine Operations	DNVGL-RP-N103	July 2017
5. DNVGL Standard: Offshore Concrete Structures	DNVGL-ST-C502	February 2018
6. DNVGL Standard: Support Structures for Wind Turbines	DNVGL-ST-0126	July 2018
7. DNVGL Offshore Standard: Design of Offshore Steel Structures, general (LRFD Method)	DNVGL-OS-C101	July 2019
8. DNVGL Recommended Practice: Fatigue Design of Offshore Steel Structures	DNVGL-RP-C203	September 2019
9. DNVGL Recommended Practice: Structural Design Against Accidental Loads	DNVGL-RP-C204	September 2019
10. DNVGL Offshore Standard: Position Mooring	DNVGL-OS-E301	July 2020
11. DNVGL Recommended Practice: Environmental Conditions and Environmental Loads	DNVGL-RP-C205	December 2020
12. ***International Organisation for Standardisation***		
13. ISO: Petroleum and Natural Gas Industries – Specific Requirements for Offshore Structures – Part 7: Stationkeeping Systems for Floating Offshore Structures and Mobile Offshore Units, 2nd Edition	ISO19901-7	May 2013
14. ISO: Petroleum and natural gas industries – Concrete offshore structures	ISO 19903:2019	2019

15. ***European Committee for Standardisation (CEN)***		
16. Eurocode 2: Design of Concrete Structures – Part 1-1: General rules and rules for buildings	EN1992-1-1	2004
17. Eurocode 7: Geotechnical Design – Part 1: General rules	EN1997-1	2004
18. Concrete – Part 1: Specification, performance, production and conformity	EN206-1	2000
19. Cement – Part 1: Composition, specifications and conformity criteria for common cements	EN197-1	2000
20. ***Other***		
21. IEC Technical Specification: Marine Energy – Wave, Tidal and Other Water Current Converters – Part 10: Assessment of Mooring System for Marine Energy Converters (MECs)	IEC TS 62600-10	March 2015
22. Bureau Veritas Guidance Note: Current and Tidal Turbines	NI 603 DT R01 E	May 2015
23. API Recommended Practice: Design and Analysis of Stationkeeping Systems for Floating Structures, 3rd Edition	API RP 2SK	October 2005
24. Standards Norway: Marine Fish Farms – Requirements for Site survey, Risk Analyses, Design, Dimensioning, Production, Installation and Operation	SN NS 9415 (E)	November 2009
25. BSI: Maritime Works Part 1-3: General – Code of Practice for Geotechnical Design	BS 6349-1-3	September 2012

Appendix B

Screenshots of Geotechnical Parameters Used in Design Calculations and Plaxis Model (Available from (Netherlands Enterprise Agency, 2021))

Sand parameters – Province 5 – HKW117

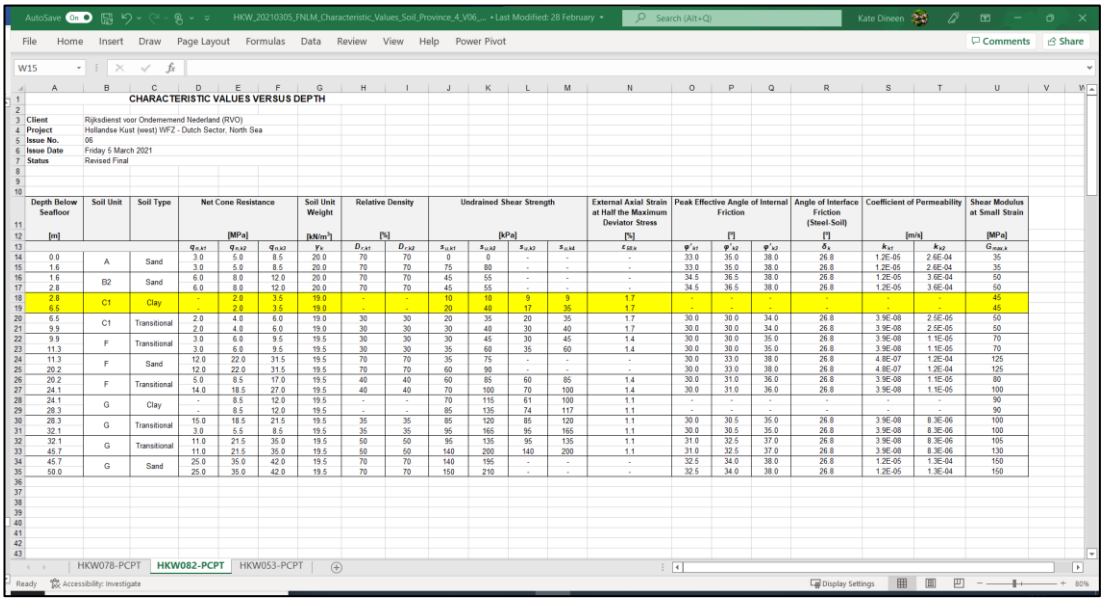


CHARACTERISTIC VALUES VERSUS DEPTH

Client	Rijksdienst voor Ondernemend Nederland (RVO)
Project	Hollandse Kust (west) WFZ - Dutch Sector, North Sea
Issue No.	06
Issue Date	Friday 5 March 2021
Status	Revised Final

Depth Below Seafloor [m]	Soil Unit	Soil Type	Net Cone Resistance [MPa]			Soil Unit Weight [kN/m³]	Relative Density [%]		Undrained Shear Strength [kPa]				External Axial Strain at Half the Maximum Deviator Stress [%]	Peak Effective Angle of Internal Friction [°]			Angle of Interface Friction (Steel-Soil) [°]	Coefficient of Permeability [m/s]		Shear Modulus at Small Strain [MPa]
			$q_{c,k1}$	$q_{c,k2}$	$q_{c,k3}$	γ_k	$D_{r,k1}$	$D_{r,k2}$	$s_{u,k1}$	$s_{u,k2}$	$s_{u,k3}$	$s_{u,k4}$	$\varepsilon_{50,k}$	φ'_{k1}	φ'_{k2}	φ'_{k3}	δ_k	k_{k1}	k_{k2}	$G_{max,k}$
0.0	A	Sand	2.0	5.0	8.0	20.0	90	100	0	0	-	-	-	37.0	39.0	42.0	26.8	1.2E-05	2.6E-04	35
2.0			23.0	26.0	29.0	20.0	90	100	250	260	-	-	-	37.0	39.0	42.0	26.8	1.2E-05	2.6E-04	70
2.0	A	Sand	26.5	29.0	31.5	20.0	90	100	240	245	-	-	-	37.0	39.0	42.0	26.8	1.2E-05	2.6E-04	80
8.2			26.5	29.0	31.5	20.0	90	100	160	195	-	-	-	35.0	37.0	40.0	26.8	1.2E-05	2.6E-04	80
8.2	B2	Sand	15.0	22.0	30.0	20.0	75	75	75	115	-	-	-	35.0	37.0	40.0	26.8	1.2E-05	3.6E-04	100
15.2			15.0	22.0	30.0	20.0	75	75	45	75	-	-	-	35.0	37.0	40.0	26.8	1.2E-05	3.6E-04	100
15.2	F	Sand	21.5	30.5	45.5	19.5	80	80	75	125	-	-	-	31.5	33.5	40.0	26.8	4.8E-07	1.2E-04	150
20.0			21.5	30.5	45.5	19.5	80	80	110	195	-	-	-	31.5	33.5	40.0	26.8	4.8E-07	1.2E-04	150
20.0	F	Sand	21.5	30.5	45.5	19.5	80	80	60	85	-	-	-	31.5	33.5	40.0	26.8	4.8E-07	1.2E-04	150
24.9			21.5	30.5	45.5	19.5	80	80	75	105	-	-	-	31.5	33.5	40.0	26.8	4.8E-07	1.2E-04	150
24.9	F	Sand	8.5	18.5	28.5	19.5	55	55	75	105	-	-	-	30.0	31.0	37.0	26.8	4.8E-07	1.2E-04	105
33.3			8.5	18.5	28.5	19.5	55	55	100	140	-	-	-	30.0	31.0	37.0	26.8	4.8E-07	1.2E-04	105
33.3	G	Sand	14.5	20.5	26.0	19.5	55	55	100	140	-	-	-	30.5	32.0	37.0	26.8	1.2E-05	1.3E-04	110
40.3			14.5	20.5	26.0	19.5	55	55	120	170	-	-	-	30.5	32.0	37.0	26.8	1.2E-05	1.3E-04	110
40.3	G	Sand	10.0	13.0	19.0	19.5	55	55	120	170	-	-	-	30.5	32.0	37.0	26.8	1.2E-05	1.3E-04	100
50.0			16.0	29.0	37.0	19.5	55	55	150	210	-	-	-	30.5	32.0	37.0	26.8	1.2E-05	1.3E-04	135

Clay_1 parameters – Province 4 – HKW082

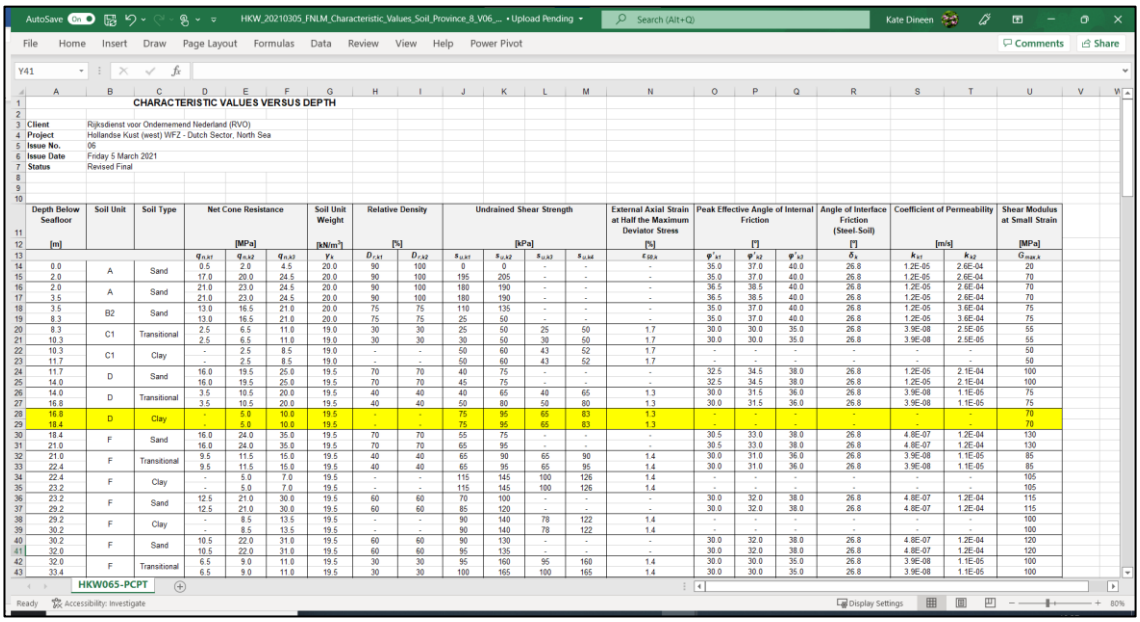


CHARACTERISTIC VALUES VERSUS DEPTH

Client	Rijksdienst voor Ondernemend Nederland (RVO)
Project	Hollandse Kust (west) WFZ - Dutch Sector, North Sea
Issue No.	06
Issue Date	Friday 5 March 2021
Status	Revised Final

Depth Below Seafloor [m]	Soil Unit	Soil Type	Net Cone Resistance [MPa]			Soil Unit Weight [kN/m³]	Relative Density [%]		Undrained Shear Strength [kPa]				External Axial Strain at Half the Maximum Deviator Stress [%]	Peak Effective Angle of Internal Friction [°]			Angle of Interface Friction (Steel-Soil) [°]	Coefficient of Permeability [m/s]		Shear Modulus at Small Strain [MPa]
			$q_{c,k1}$	$q_{c,k2}$	$q_{c,k3}$	γ_k	$D_{r,k1}$	$D_{r,k2}$	$s_{u,k1}$	$s_{u,k2}$	$s_{u,k3}$	$s_{u,k4}$	$\varepsilon_{50,k}$	φ'_{k1}	φ'_{k2}	φ'_{k3}	δ_k	k_{k1}	k_{k2}	$G_{max,k}$
0.0	A	Sand	3.0	5.0	8.5	20.0	70	70	0	0	-	-	-	33.0	35.0	38.0	26.8	1.2E-05	2.6E-04	35
1.6			3.0	5.0	8.5	20.0	70	70	75	80	-	-	-	33.0	35.0	38.0	26.8	1.2E-05	2.6E-04	35
1.6	B2	Sand	6.0	8.0	12.0	20.0	70	70	45	55	-	-	-	34.5	36.5	38.0	26.8	1.2E-05	3.6E-04	50
2.8			6.0	8.0	12.0	20.0	70	70	45	55	-	-	-	34.5	36.5	38.0	26.8	1.2E-05	3.6E-04	50
2.8	C1	Clay	-	2.0	3.5	19.0	-	-	10	10	9	9	1.7	-	-	-	-	-	-	45
6.5			-	2.0	3.5	19.0	-	-	20	40	17	35	1.7	-	-	-	-	-	-	45
6.5	C1	Transitional	2.0	4.0	6.0	19.0	30	30	20	35	20	35	1.7	30.0	30.0	34.0	26.8	3.9E-08	2.5E-05	50
9.9			2.0	4.0	6.0	19.0	30	30	30	40	30	40	1.7	30.0	30.0	34.0	26.8	3.9E-08	2.5E-05	50
9.9	F	Transitional	3.0	6.0	9.5	19.5	30	30	30	45	30	45	1.4	30.0	30.0	35.0	26.8	3.9E-08	1.1E-05	70
11.3			3.0	6.0	9.5	19.5	30	30	35	60	35	60	1.4	30.0	30.0	35.0	26.8	3.9E-08	1.1E-05	70
11.3	F	Sand	12.0	22.0	31.5	19.5	70	70	35	75	-	-	-	30.0	33.0	38.0	26.8	4.8E-07	1.2E-04	125
20.2			12.0	22.0	31.5	19.5	70	70	60	90	-	-	-	30.0	33.0	38.0	26.8	4.8E-07	1.2E-04	125
20.2	F	Transitional	5.0	8.5	17.0	19.5	40	40	60	85	60	85	1.4	30.0	31.0	36.0	26.8	3.9E-08	1.1E-05	80
24.1			14.0	18.5	27.0	19.5	40	40	70	100	70	100	1.4	30.0	31.0	36.0	26.8	3.9E-08	1.1E-05	100
24.1	G	Clay	-	8.5	12.0	19.5	-	-	70	115	61	100	1.1	-	-	-	-	-	-	90
28.3			-	8.5	12.0	19.5	-	-	85	135	74	117	1.1	-	-	-	-	-	-	90
28.3	G	Transitional	15.0	18.5	21.5	19.5	35	35	85	120	85	120	1.1	30.0	30.5	35.0	26.8	3.9E-08	8.3E-06	100
32.1			3.0	5.5	8.5	19.5	35	35	95	165	95	165	1.1	30.0	30.5	35.0	26.8	3.9E-08	8.3E-06	100
32.1	G	Transitional	11.0	21.5	35.0	19.5	50	50	95	135	95	135	1.1	31.0	32.5	37.0	26.8	3.9E-08	8.3E-06	105
45.7			11.0	21.5	35.0	19.5	50	50	140	200	140	200	1.1	31.0	32.5	37.0	26.8	3.9E-08	8.3E-06	130
45.7	G	Sand	25.0	35.0	42.0	19.5	70	70	140	195	-	-	-	32.5	34.0	38.0	26.8	1.2E-05	1.3E-04	150
50.0			25.0	35.0	42.0	19.5	70	70	150	210	-	-	-	32.5	34.0	38.0	26.8	1.2E-05	1.3E-04	150

Clay_2 parameters – Province 8 – HKW065



CHARACTERISTIC VALUES VERSUS DEPTH

Client	Rijksdienst voor Ondernemend Nederland (RVO)
Project	Hollandse Kust (west) WFZ - Dutch Sector, North Sea
Issue No.	06
Issue Date	Friday 5 March 2021
Status	Revised Final

Depth Below Seafloor [m]	Soil Unit	Soil Type	Net Cone Resistance [MPa]			Soil Unit Weight [kN/m³]	Relative Density [%]		Undrained Shear Strength [kPa]				External Axial Strain at Half the Maximum Deviator Stress [%]	Peak Effective Angle of Internal Friction [°]			Angle of Interface Friction (Steel-Soil) [°]	Coefficient of Permeability [m/s]		Shear Modulus at Small Strain [MPa]
			$q_{n,k1}$	$q_{n,k2}$	$q_{n,k3}$	γ_k	$D_{r,k1}$	$D_{r,k2}$	$s_{u,k1}$	$s_{u,k2}$	$s_{u,k3}$	$s_{u,k4}$	$\varepsilon_{50,k}$	φ'_{k1}	φ'_{k2}	φ'_{k3}	δ_k	k_{k1}	k_{k2}	$G_{max,k}$
0.0	A	Sand	0.5	2.0	4.5	20.0	90	100	0	0	-	-	-	35.0	37.0	40.0	26.8	1.2E-05	2.6E-04	20
2.0			17.0	20.0	24.5	20.0	90	100	195	205	-	-	-	35.0	37.0	40.0	26.8	1.2E-05	2.6E-04	70
2.0	A	Sand	21.0	23.0	24.5	20.0	90	100	180	190	-	-	-	36.5	38.5	40.0	26.8	1.2E-05	2.6E-04	70
3.5			21.0	23.0	24.5	20.0	90	100	180	190	-	-	-	36.5	38.5	40.0	26.8	1.2E-05	2.6E-04	70
3.5	B2	Sand	13.0	16.5	21.0	20.0	75	75	110	135	-	-	-	35.0	37.0	40.0	26.8	1.2E-05	3.6E-04	75
8.3			13.0	16.5	21.0	20.0	75	75	25	50	-	-	-	35.0	37.0	40.0	26.8	1.2E-05	3.6E-04	75
8.3	C1	Transitional	2.5	6.5	11.0	19.0	30	30	25	50	25	50	1.7	30.0	30.0	35.0	26.8	3.9E-08	2.5E-05	55
10.3			2.5	6.5	11.0	19.0	30	30	30	50	38	50	1.7	30.0	30.0	35.0	26.8	3.9E-08	2.5E-05	55
10.3	C1	Clay	-	2.5	8.5	19.0	-	-	50	60	43	52	1.7	-	-	-	-	-	-	50
11.7			-	2.5	8.5	19.0	-	-	50	60	43	52	1.7	-	-	-	-	-	-	50
11.7	D	Sand	16.0	19.5	25.0	19.5	70	70	40	75	-	-	-	32.5	34.5	38.0	26.8	1.2E-05	2.1E-04	100
14.0			16.0	19.5	25.0	19.5	70	70	45	75	-	-	-	32.5	34.5	38.0	26.8	1.2E-05	2.1E-04	100
14.0	D	Transitional	3.5	10.5	20.0	19.5	40	40	40	65	40	65	1.3	30.0	31.5	36.0	26.8	3.9E-08	1.1E-05	75
16.8			3.5	10.5	20.0	19.5	40	40	50	80	50	80	1.3	30.0	31.5	36.0	26.8	3.9E-08	1.1E-05	75
16.8	D	Clay	-	5.0	10.0	19.5	-	-	75	95	65	83	1.3	-	-	-	-	-	-	70
18.4			-	5.0	10.0	19.5	-	-	75	95	65	83	1.3	-	-	-	-	-	-	70
18.4	F	Sand	16.0	24.0	35.0	19.5	70	70	55	75	-	-	-	30.5	33.0	38.0	26.8	4.8E-07	1.2E-04	130
21.0			16.0	24.0	35.0	19.5	70	70	65	95	-	-	-	30.5	33.0	38.0	26.8	4.8E-07	1.2E-04	130
21.0	F	Transitional	9.5	11.5	15.0	19.5	40	40	65	90	65	90	1.4	30.0	31.0	36.0	26.8	3.9E-08	1.1E-05	85
22.4			9.5	11.5	15.0	19.5	40	40	65	95	65	95	1.4	30.0	31.0	36.0	26.8	3.9E-08	1.1E-05	85
22.4	F	Clay	-	5.0	7.0	19.5	-	-	115	145	100	126	1.4	-	-	-	-	-	-	105
23.2			-	5.0	7.0	19.5	-	-	115	145	100	126	1.4	-	-	-	-	-	-	105
23.2	F	Sand	12.5	21.0	30.0	19.5	60	60	70	100	-	-	-	30.0	32.0	38.0	26.8	4.8E-07	1.2E-04	115
29.2			12.5	21.0	30.0	19.5	60	60	85	120	-	-	-	30.0	32.0	38.0	26.8	4.8E-07	1.2E-04	115
29.2	F	Clay	-	8.5	13.5	19.5	-	-	90	140	78	122	1.4	-	-	-	-	-	-	100
30.2			-	8.5	13.5	19.5	-	-	90	140	78	122	1.4	-	-	-	-	-	-	100
30.2	F	Sand	10.5	22.0	31.0	19.5	60	60	90	130	-	-	-	30.0	32.0	38.0	26.8	4.8E-07	1.2E-04	120
32.0			10.5	22.0	31.0	19.5	60	60	95	135	-	-	-	30.0	32.0	38.0	26.8	4.8E-07	1.2E-04	120
32.0	F	Transitional	6.5	9.0	11.0	19.5	30	30	95	160	95	160	1.4	30.0	30.0	35.0	26.8	3.9E-08	1.1E-05	100
33.4			6.5	9.0	11.0	19.5	30	30	100	165	100	165	1.4	30.0	30.0	35.0	26.8	3.9E-08	1.1E-05	100

Appendix C

Calculation of Resultant Forces and Buoyant Weight of the Turbine

Calculation of the resultant forces:

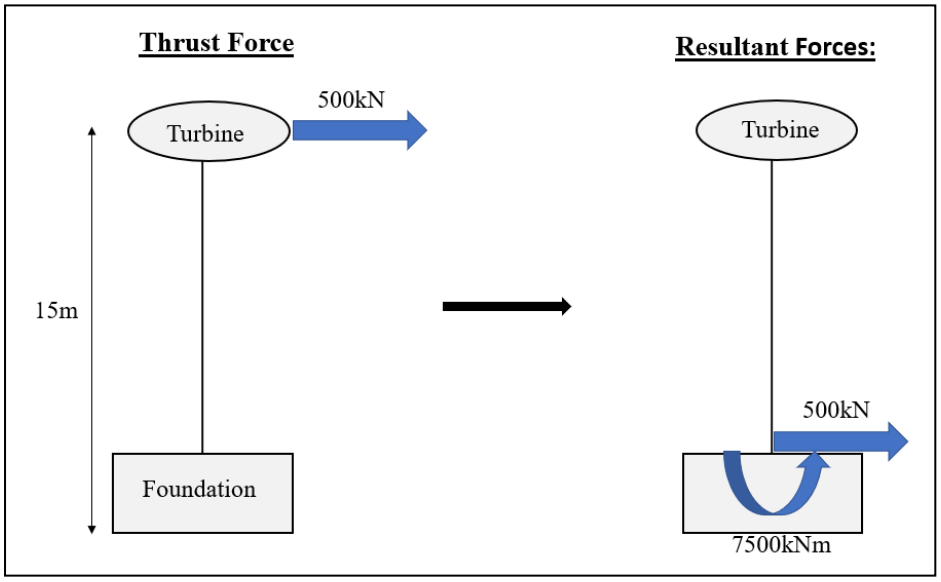
Turbine rated power = 1.5MW = 1,500kW

Turbine rated operational velocity = 3.0m/s

$$Thrust\ force = \frac{1{,}500}{3} = 500kN$$

$$Resulting\ moment = 500kN \cdot 15m = 7{,}500kNm$$

$$Resulting\ horizontal\ force = 500kN$$

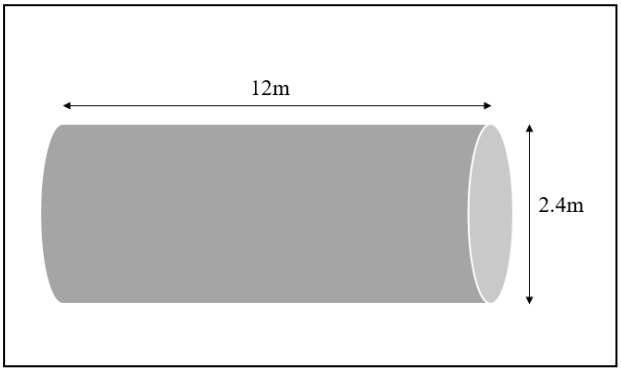


Calculation of turbine buoyant weight:

Turbine weight in air = 150T = 150,000kg = 1,470kN

Hub length = 12m

Hub diameter = 2.4m



$Hub\ Volume = \pi r^2 h = \pi(1.2^2)(12) = 54.3m^3$

Density of seawater, ρ = 1,025kg/m^3

$Buoyancy\ force = \rho V g = 1{,}025 \cdot 54.3 \cdot 9.8 = 545{,}444.N = 545kN$

$Buoyant\ weight\ of\ turbine = Turbine\ weight - Buoyancy = 1{,}470 - 545 = 925kN$

Appendix D

Concrete Gravity-Based Foundation Design Calculations

Part of Structure: Inputs			Calc. sheet No. 1
CALCULATIONS			**OUTPUT**
Device characteristics:			
Device geometry =	3.5 m	(AR1500 tidal turbine)	
Safety factors			
Safety factor for soil parameters =	1.25		
Safety factor for BC =	1.5		
Safety factor for sliding =	1.5		
Safety factor for OT =	1.5		
Soil parameters:			
Soil type:	Sand	*Drained, cohesionless*	
Friction angle of soil, φ =	39 degrees	(HKW parameters)	
$\varphi_d = \arctan\left(\frac{\tan(39)}{1.25}\right) =$	32.9	*incorporate SF*	$\varphi_d =$ 32.9 °
Cohesion, c_d =	0 kN/m^2		
$c_d = \frac{0}{1.25} =$	0 kN/m^2	*incorporate SF*	$c_d =$ 0 kN/m^2
Bulk unit weight of soil =	20 kN/m^3		
Seabed slope =	0 degrees		
Foundation characteristics			
Unit weight of concrete =	24 kN/m^3		
Provide shear-key/skirt:	NO	*No. of fins in skirt can be determined*	
Foundation embedded:	NO	*Whether the foundation is on the sea floor or embedded*	

Part of Structure: Loads	Calc. sheet No. 2
CALCULATIONS	**OUTPUT**

Mooring and structural loads

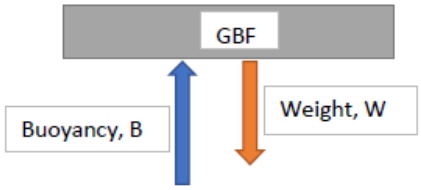
$M_{x,uls}$ = 9375 kNm (7500kNm x SF)

V_{uls} = 1156 kN *downwards* (925kN x SF)

H_{uls} = 625 kN (500kN x SF)

$V_v = Vuls + W_b$

Where W_b is the pre-sized buoyant weight of foundation



$B = \rho_{seawater} V_{GBF} g$

$W = \gamma_{conc} V_{GBF}$

assume presized thickness and radius:

where thickness = ***2.4*** *m* and radius = ***8*** m

$V_{GBF} = \pi r^2 t$

V_{GBF} = 482.549 m^3

B = 4845.52 kN

W = 11581.2 kN

$W_b = W - B$

Wb = 6735.65 kN

Part of Structure: Sizing calculations	Calc. sheet No. 3
CALCULATIONS	**OUTPUT**

Eccentricity

$e_r = \frac{M_{x,uls}}{V_V} = \frac{9375}{7891} = 1.19$ m (Vv = Vuls + Wb)

$r_{min} = MAX(6e_r, device\ r)$

Where:

$6e_r$ = 6 x 1.19 = 7.13 m

device geometry = 3.5 m

r_{min} = 7.13 m

r = 8 m *(let r = 8m > r_{min})* r = 8 m

$$A' = 2\left[r^2 arccos\left(\frac{e_r}{r}\right) - e_r\sqrt{r^2 - {e_r}^2}\right]$$

A' = 163.186 m^2

$b_e = 2(r - e)$

b_e = 13.624 m [check: be <2r, TRUE]

$$l_e = 2r\sqrt{1 - \left(1 - \frac{B'}{2r}\right)^2}$$

B' = b_e = 13.6 m

l_e = 15.8226 m

$$L' = \sqrt{A'\frac{l^e}{b_e}}$$

L' = 13.7666 m

$$B' = \frac{L'}{l_e} b_e$$

B' = 11.8537 m

Part of Structure: Bearing capacity check	Calc. sheet No. 4
CALCULATIONS	**OUTPUT**

Bearing capacity

$$\frac{Q_u}{SF} > (V_{uls,down} + W_b)(cos\beta + H_{uls,res} sin\beta)$$

Where:

$V_{uls,down}$ is the vertical oad from ULS load analysis (N)

$H_{uls,res}$ is the resultant horizontal load from ULS (N)

W_b is the foundations buoyant weight (N)

β is the seabed slope (degrees)

$Q_u = A'(q_\gamma)$ *Calc RHS of BC eqn.*

Bearing capacity stress: $q_\gamma = \gamma_b \left(\frac{B'}{2}\right) N_\gamma i_\gamma s_\gamma$

Where:

γ_b = 20 kN/m^3 *(Weight of soil)*

$$N_\gamma = 2(1 + N_q)\, tan\varphi_d \tan\left(\frac{\pi}{4} + \frac{\varphi_d}{5}\right)$$

$$N_q = \exp(\pi tan\varphi_d)\left[tan\left(\frac{\pi}{4} + \frac{\varphi_d}{2}\right)\right]^2$$

N_q = 25.894

N_γ = 43.9438

$$i_\gamma = \left(1 - \frac{H_{uls,res}}{V_{uls,down} + B'L'c_{ud}cot\varphi_d}\right)^4$$

i_γ = 0.04446

$$s_\gamma = 1 - 0.4\left(\frac{B'}{L'}\right)$$

s_γ = 0.65558

q_γ = 151.84 kN/m^2

$Q_u = A'(q_\gamma)$

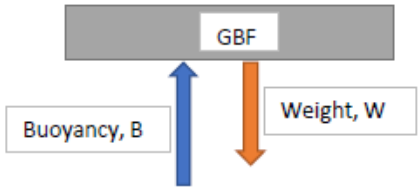
Qu = 24778.63 kN

bearing capacity check continued on following page

Part of Structure: Bearing capacity check	Calc. sheet No. 5
CALCULATIONS	**OUTPUT**

$(V_{uls,down} + W_b)(cos\beta + H_{uls,res}sin\beta)$ *Calc LHS of BC eqn.*

W_b is the foundations buoyant weight (N)



$B = \rho_{seawater} V_{GBF} g$
$W = \gamma_{conc} V_{GBF}$

$V_{GBF} = \pi r^2 t$ *where thickness =* 2.4 *m*
V_{GBF} = 482.549 m^3

B = 4845.52 kN
W = 11581.2 kN

$W_b = W - B$
W_b = 6735.65 kN

$(V_{uls,down} + W_b)(cos\beta + H_{uls,res}sin\beta)$
Vuls,down + Wb = 7891 kN

$\frac{Q_u}{SF} > (V_{uls,down} + W_b)(cos\beta + H_{uls,res}sin\beta)$

$\frac{24779}{1.5} > 7891.35$

16519.1 > 7891.35 kN TRUE

Passes bearing capacity check

Part of Structure: Sliding resistance check and overturning moment check	Calc. sheet No. 6
CALCULATIONS	**OUTPUT**

Sliding resistance

To verify the sliding resistance the lateral resistance of the foundation should be bigger than the max horizontal load that can be applied

Drained conditions:

$$\frac{H_u}{SF} > \left(V_{uls,down} + W_b\right)sin\beta + \left(H_{uls,res}cos\beta\right)$$

$$H_u = V_{uls,down}tan(\varphi_d)$$

H_u = 5112.23 kN

Seabed slope, β = 0

$\left(V_{uls,down} + W_b\right)sin\beta$ = 0

$\left(H_{uls,res}cos\beta\right)$ = 625 kN

$$\frac{H_u}{SF} > \left(H_{uls,res}cos\beta\right)$$

3408 > 625 TRUE

Passes sliding resistance check

Overturning moment

To verify the overturning moment, the stability moment of the foundation should be greater than the applied overturning moment:

$$\frac{\left(V_{uls,down} + W_b\right)cos\beta \; x \; r}{SF} > M_{uls} + \left(H_{uls,res} \; x \; z_{ap}\right)$$

z_{ap} is the vertical distance between the seabed and the application point of maximum horiontal load (m) *For AR1500,* z_{ap} = 15 m

r is the foundations radius

Wb is the foundations buoyant weight (N)

$$\frac{\left(V_{uls,down} + W_b\right)cos\beta \; x \; r}{SF} > M_{uls} + \left(H_{uls,res} \; x \; z_{ap}\right)$$

$\left(V_{uls,down} + W_b\right)cos\beta \; x \; r$ = 63130.8 kNm

$M_{uls} + \left(H_{uls,res} \; x \; z_{ap}\right)$ = 18750 kNm

$\frac{63130.8}{1.5}$ > 18750 kNm

42087.2 > 18750 kNm TRUE

Passes overturning moment check

r = 8m

t = 2.4m

Therefore, foundation radius 8m and thickness 2.4m passes required checks

Appendix E

Step-by-Step Development of Plaxis 3D Model

Project dimensions

The first step in creating a finite element model in Plaxis 3D is the specification of the model type, units, dimensions, and other general values. Generally, the soil model should be at least five times greater than the structure dimensions. As the GBF has a diameter of 16m, a conservative soil model of 100m x 100m was specified for this project.

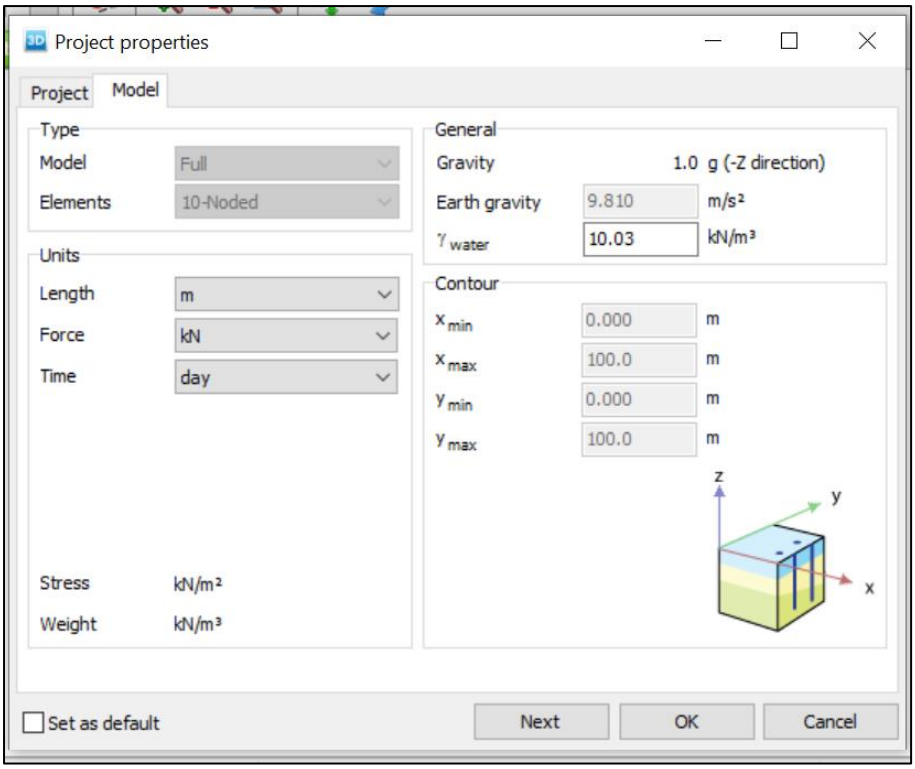


Figure A-1: *Project properties window*

Soils mode

A borehole was then created to define the soil profile. From Figure 0-2, the depth and thickness of the six sand layers were defined as well as the head of water above the seabed, which was 30m in this instance. For each soil layer, it was necessary to define the soil properties. An example of this is shown in Figures 0-3, Figure 0-4, and Figure 0-5 for Sand_1. This process was repeated for all soil layers used in this model.

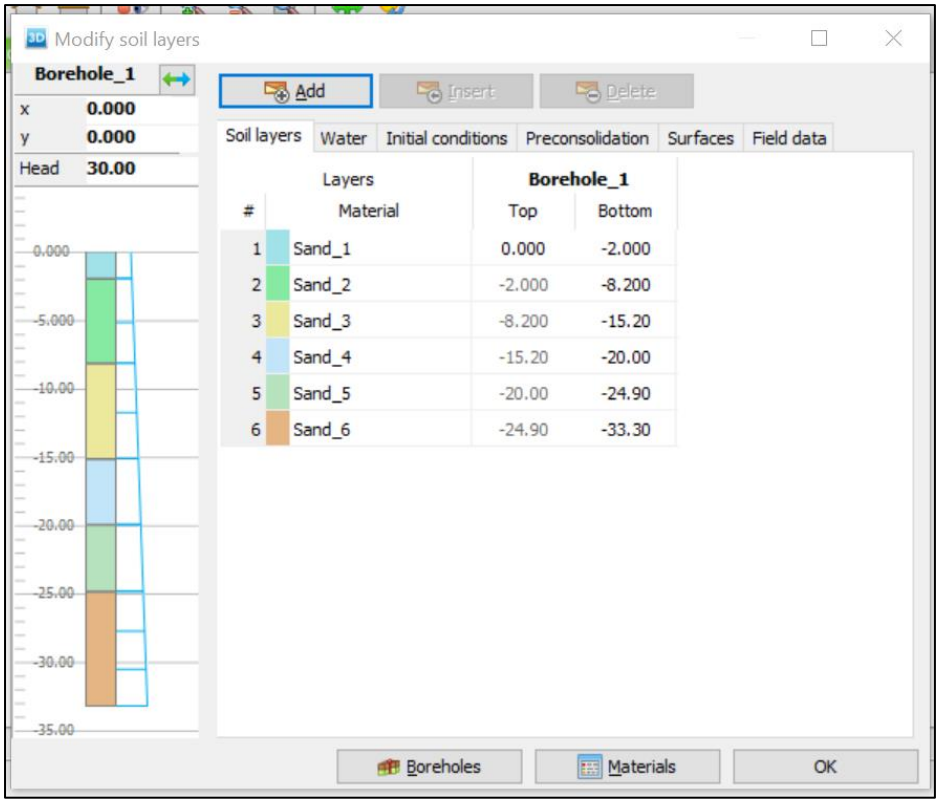


Figure A-2: *Modify soil layers window*

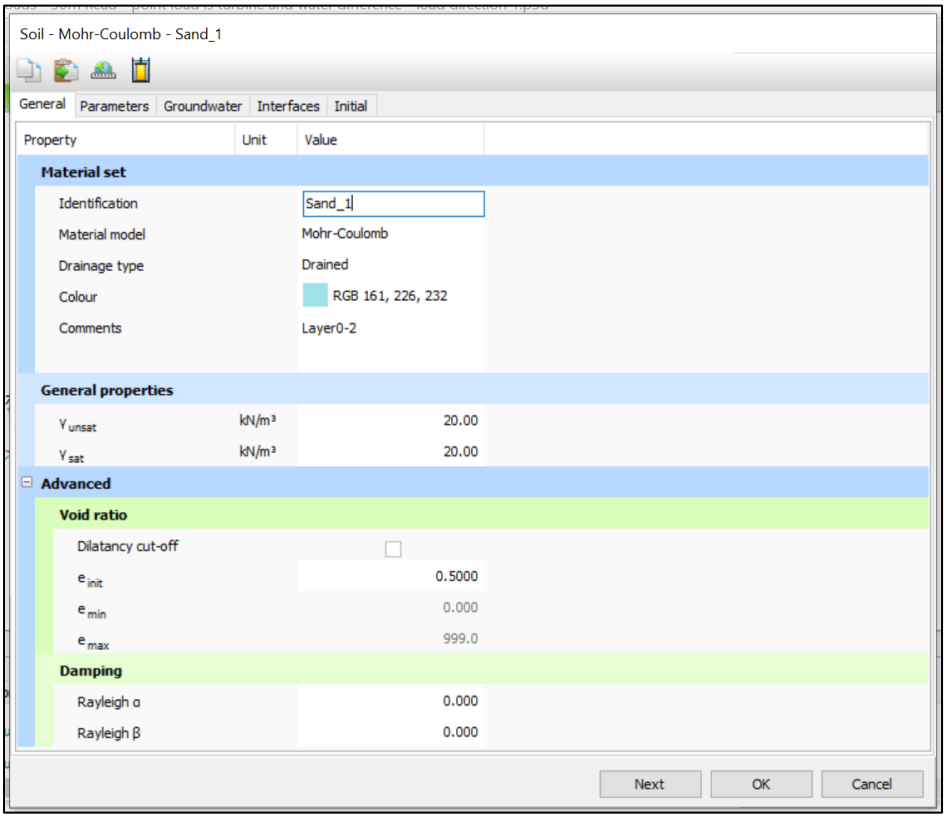


Figure A-3: *Sand_1 general soil properties*

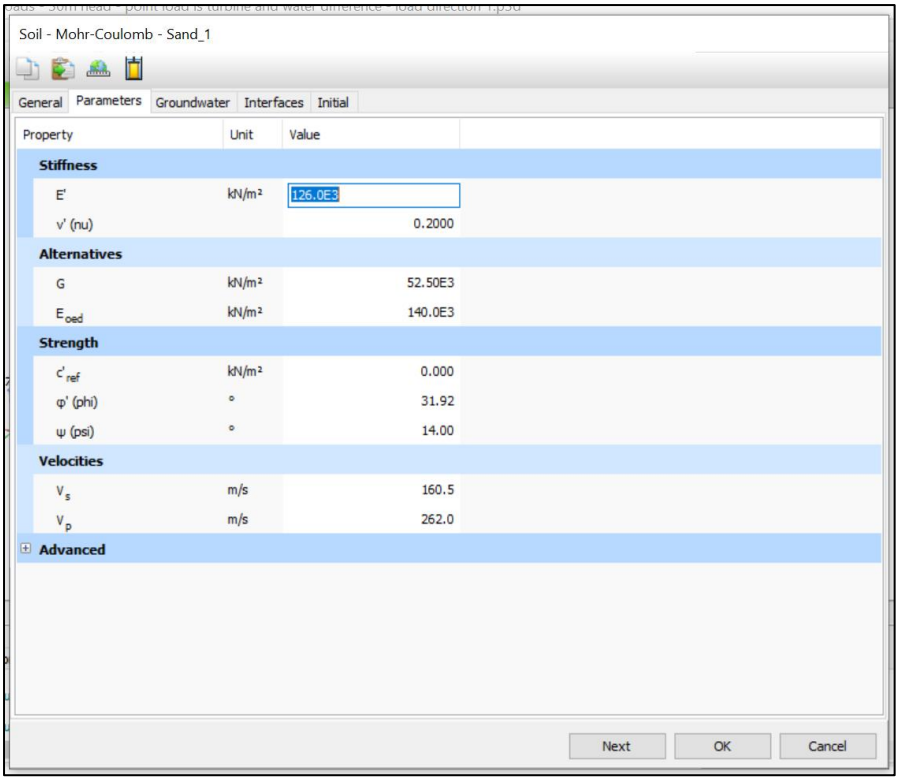


Figure A-4: *Sand_1 parameters*

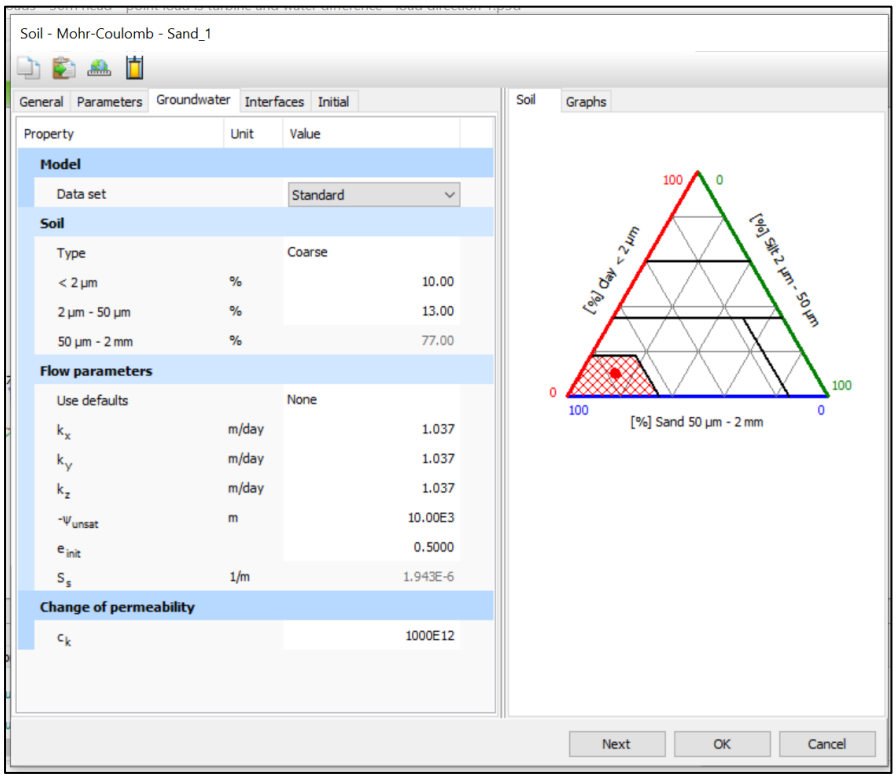


Figure A-5: *Sand_1 groundwater properties*

Structures mode

The GBF was represented by a plate in the model. The plate was created in structures mode using the polycurve feature (please see Figure 0-6). This polycurve was then used to create a plate, which had the material properties as shown in Figure 0-7.

Loading conditions were also defined in structures mode. For this model, a point load was applied to the centre of the GBF (at point 50,50,2), which incorporated the vertical load, horizontal load and moment as described in Section 3.2.2 (Figure 0-8). The final soil and structure model can be seen in Figure 0-9.

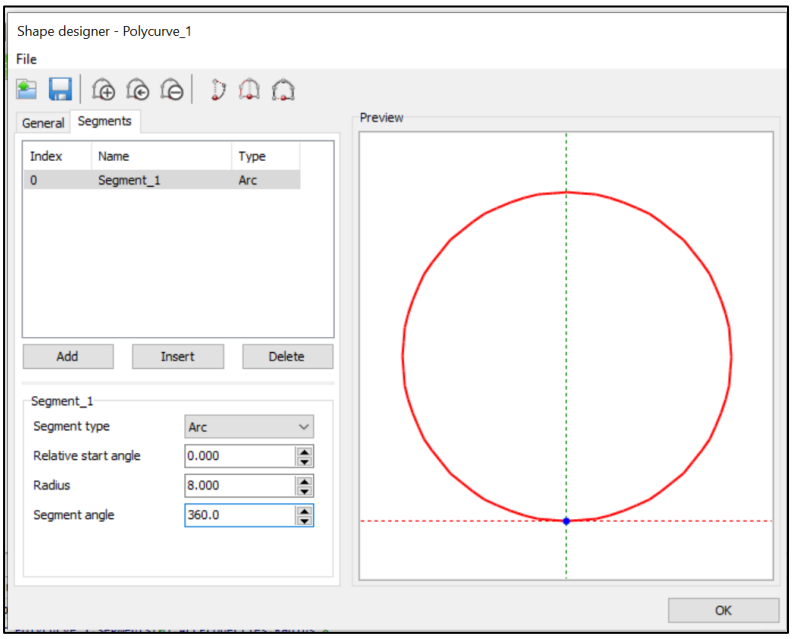


Figure A-6: *Polycurve shape designer*

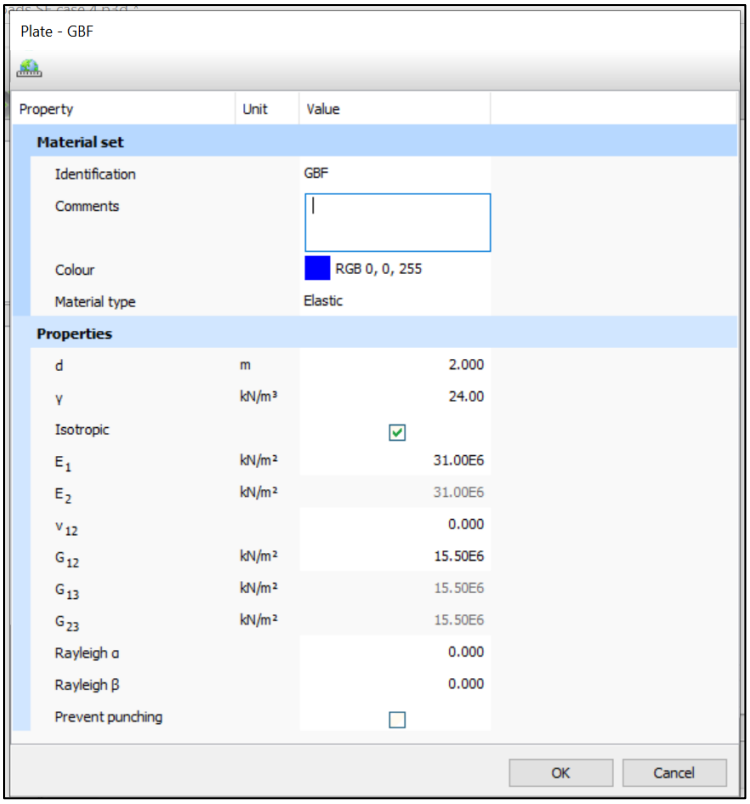


Figure A-7: *Plate properties*

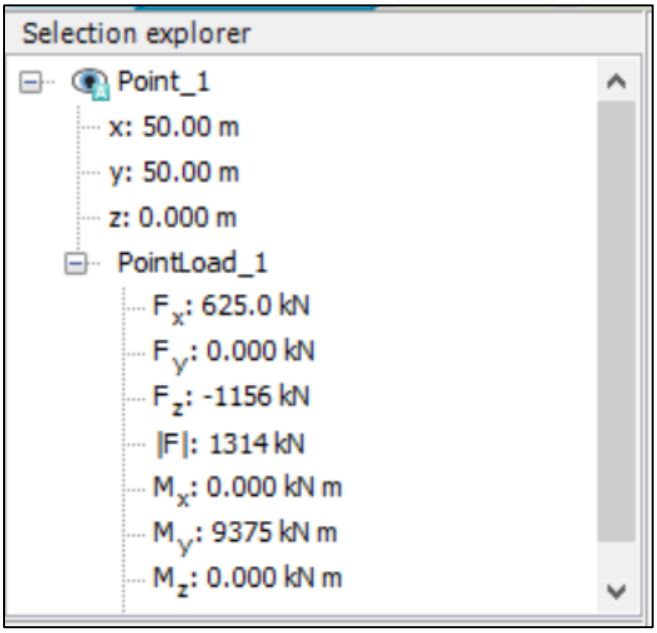


Figure A-8: *Load settings*

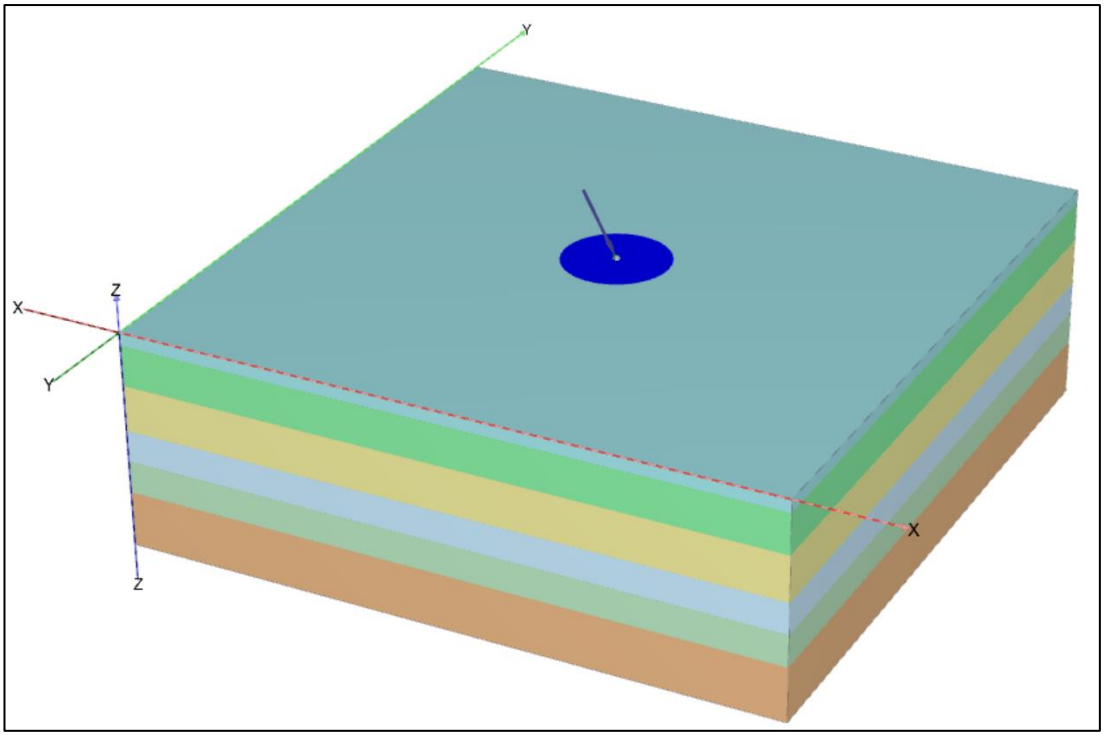


***Figure A-9**: Finalised Plaxis 3D model*

Mesh mode

Following the creation of the soil and structure model, the model is meshed to undergo finite element analysis. Plaxis 3D enables fully automatic finite element mesh generation. The mesh settings used are shown in Figure 0-10, with the generated mesh model shown in Figure 0-11.

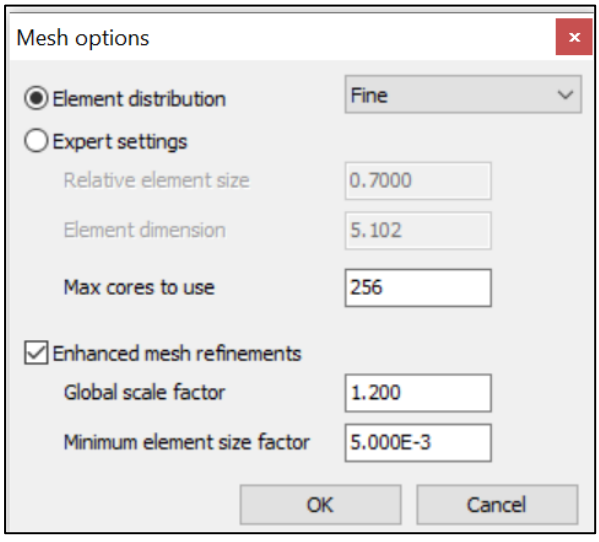


***Figure A-10:** Finite element mesh settings*

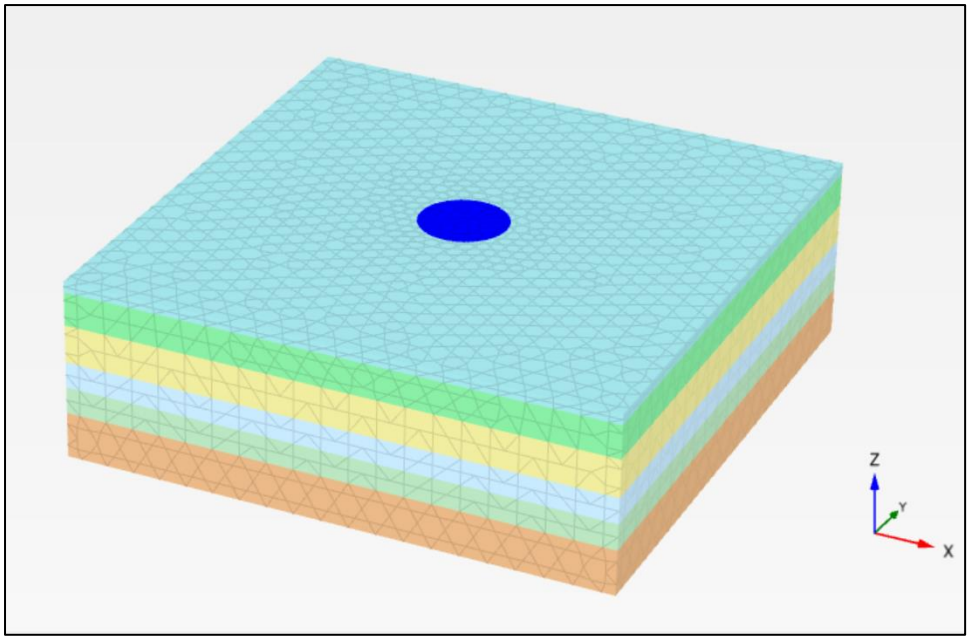


Figure A-11: *Finalised mesh model (pre-calculation)*

Staged construction mode

Calculation phases are defined in staged construction mode. The phases are outlined in Figure 0-12.

- An initial phase was defined first to calculate initial stresses, pore pressures and state parameters. There are no structural elements or loads 'active' in this phase.
- The foundation volume is activated in Phase 1 to simulate the soil-structure interaction following GBF placement on the seabed. A plastic calculation type is suitable to calculate soil deformations at this stage. These phase settings are shown in Figure 0-13.
- The placement and operation of the turbine are simulated in Phase 2 by activating the loadings on the GBF, again using a plastic analysis.
- Phases 3-7 were defined in order to calculate the long-term soil deformation with continuous loading from the GBF and the turbine. A fully coupled flow-deformation calculation type was utilised as this is a time-dependant analysis of deformation which also takes pore water pressures into account. The total turbine operational time of 25 years (9125 days) was divided into 5 year (1825

day) increments to give a greater understanding of how the soil settles over time. The settings for these phases are shown in Figure 0-14.

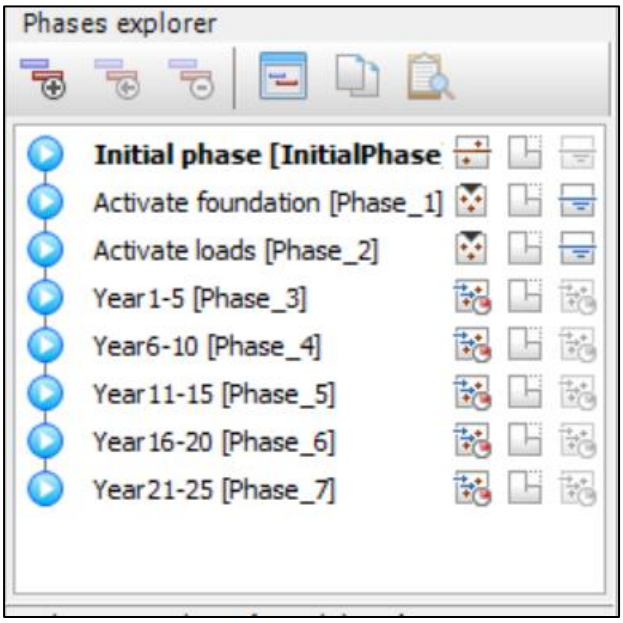


Figure A-12: *Calculation phases*

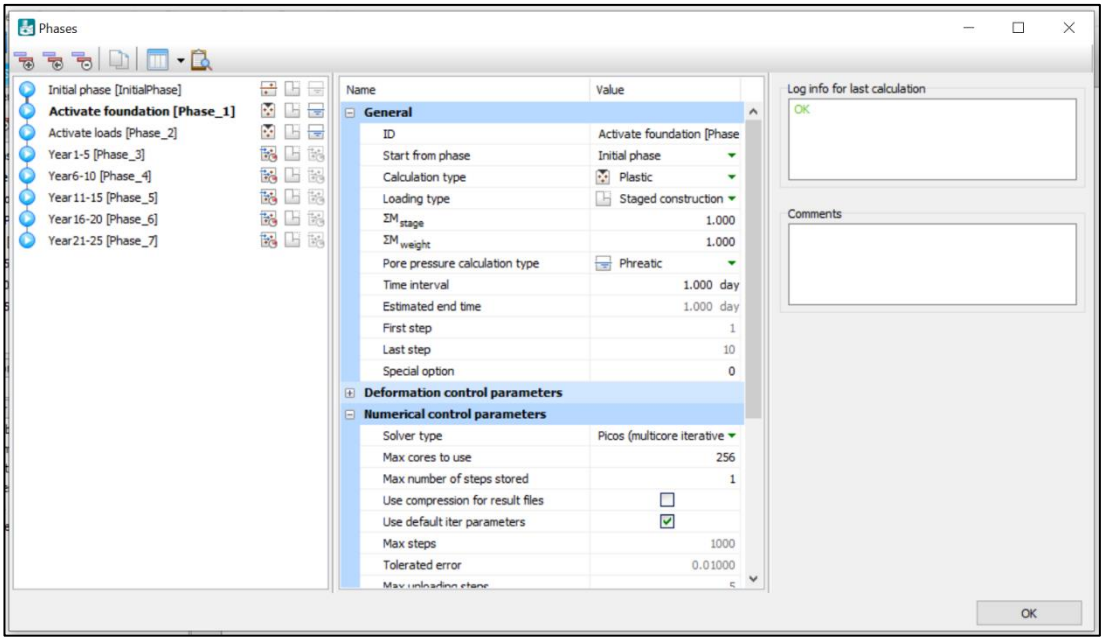


Figure A-13: *Phase 1 - Activate foundation phase settings*

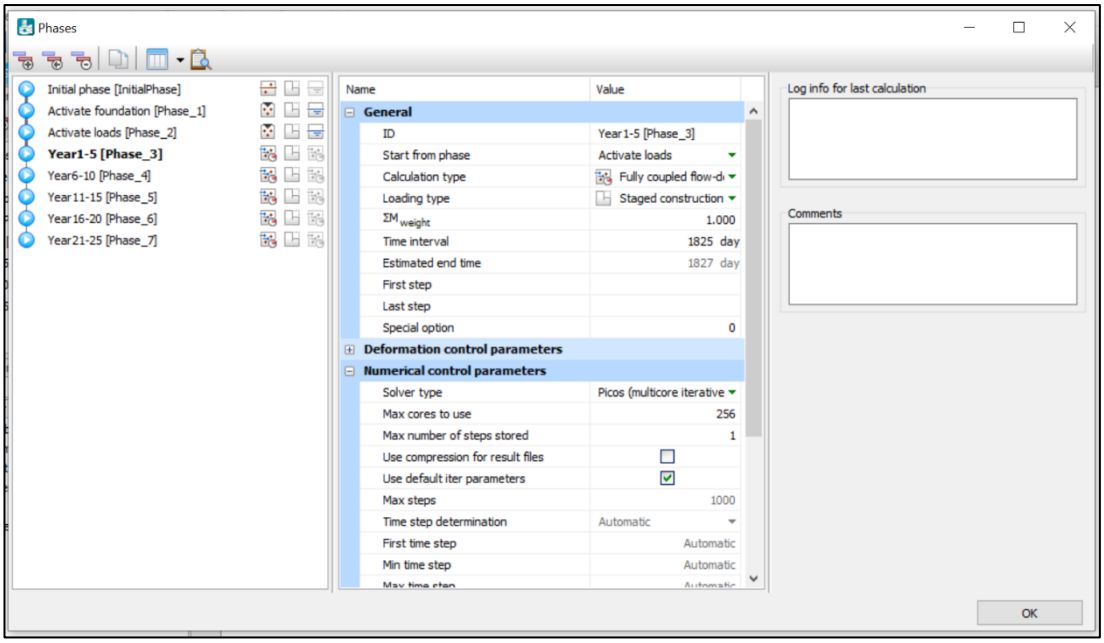


Figure A-14: *Phase 3 - Year 1-5 phase settings*

Appendix F

Chloride Concentration Profiles MATLAB Code

Editor - C:\Users\k-e-d\OneDrive\Documents\Masters\Matlab\Chloride ingress modelling.m

Chloride ingress modelling.m | Pressure30MPa.m

```
%This code plots chloride concentration profiles using parameters from
%three studies: Luping (2003) = L, Starrs (2008) = S, Nanukuttan (2008) = N
%does not include water pressure

% converting years to seconds
t_years = 25;
t_seconds = t_years*365*24*60*60;
x= (0:1:70);
C_crit = 0.5*ones(1,71);
C_crit1 = ones(1,71);

%Luping (2003) parameters
Dapp_L = 1.44*10^-12;
Cs_L = 2.15;
Cl_L = Cs_L*erfc((x/1000)/(2*sqrt(Dapp_L*t_seconds)));

%Starrs (2008) parameters
Dapp_S = 2.9*10^-12;
Cs_S = 5.82;
Cl_S = Cs_S*erfc((x/1000)/(2*sqrt(Dapp_S*t_seconds)));

%Nanukuttan (2008) parameters
Dapp_N = 3.13*10^-12;
Cs_N = 5.1;
Cl_N = Cs_N*erfc((x/1000)/(2*sqrt(Dapp_N*t_seconds)));

%Create graph with line at x = 50mm
cover = 50*ones(1,71);
plot(x,C_crit,x,C_crit1,x,Cl_L,x,Cl_S,x,Cl_N)
xline(50)
```